To the Graduate Council:

I am submitting herewith a thesis written by Daniel Frank Spond entitled "A Study of the Ferrite-Fissuring Relationship in Austenitic Stainless Steel Weld Metals." I recommend that it be accepted in partial fulfillment of the requirements for the degree of Master of Science, with a major in Metallurgical Engineering.

C. D. Lundin, Major Professor

We have read this thesis and recommend its acceptance:

Charlie R. Brooks

J. E. Spruiell

Accepted for the Council:

Hilton A. Smith
Vice Chancellor
Graduate Studies and Research

THESIS
75
S665
Cop. 2

A STUDY OF THE FERRITE-FISSURING RELATIONSHIP IN AUSTENITIC STAINLESS STEEL WELD METALS

A Thesis

Presented for the

Master of Science

Degree

The University of Tennessee

Daniel Frank Spond

December 1975

1266555

ACKNOWLEDGMENTS

The author wishes to express his sincere thanks to Dr. C. D. Lundin for his assistance, encouragement, and guidance during the course of this research program. The author would also like to thank Mr. Raymond Bellamy of The University of Tennessee staff for the preparation of many of the test specimens. Thanks are also extended to Mr. H. B. Thompson and other members of the Chemical and Metallurgical Engineering Department machine shop for the construction of several pieces of testing equipment. Special thanks are due to Mr. Bob McGill and Mr. Mike Hunter for their contributions in the scanning electron microscopy and to Miss Sylvia Goode for her assistance in the testing and evaluation of the specimens. The author also appreciates the helpful comments of Mr. W. T. DeLong of the Teledyne McKay Corporation on portions of the manuscript. The author appreciates the financial support of the Welding Research Council during the course of this investigation. Finally, the author would like to thank his wife Mary for her forbearance and support throughout his graduate program.

ABSTRACT

The Fissure Bend Test was used to measure the extent of fissuring as a function of ferrite level for eight types of stainless steel weld metal (308, 308L, 316, 316L, 309, 318, 347, and 16-8-2) deposited by the Shielded Metal-Arc (SMA) process. These weld metals were designed and fabricated to produce four different ferrite levels: 0 FN, 2 FN, 4 FN, and 6 FN with the exception that the 16-8-2 weld metal was from two commercial lots of low ferrite level.

Results of this testing show that the 347 weld metal, followed closely by the 318 weld metal, is the most prone to fissuring and that the 16-8-2 weld metal is the least sensitive to fissuring. The ferrite level needed to eliminate fissuring was determined for each weld metal type, and the eight weld metals were ranked according to their fissuring tendency.

The Ferrite Number needed for fissure elimination in each of the weld metals tested is as follows:

Weld Metal Type	Ferrite Numbers
16-8-2	0-2
316L	1 1/2
308	2
316	2 1/2
308L	3
309	4
318	5
347	6

As a result of the initial testing program, numerous well-documented specimens were available for study. Careful study of these specimens by light metallography, scanning electron microscopy, and energy dispersive x-ray techniques has revealed information as to the nature and morphology of the fissures present at low ferrite levels.

In essence the study showed:

1. The fissures occur primarily along grain boundaries in the HAZ of the previously deposited pass.
2. The fissuring tendency is enhanced by multiple thermal cycling in the HAZ.
3. The fissures are invariably more prone to form in ferrite-free areas.
4. The origin of fissures is related to a liquation mechanism.
5. The size distribution of fissures determined by light metallography at 200X reveals that the average fissure length in 308 weld metal (0.4 FN) is 0.004" and in 316 weld metal (0.4 FN) is 0.005".

The thermal distribution in the HAZ was determined for the actual welding conditions utilized in the test, and the peak temperature range in which the fissures form is discussed. The influence of weld bead sequence and the effect of multiple thermal cycling on fissuring tendency were evaluated with both SMA deposits and GTA remelting of previously deposited SMA weld metal. The multiple thermal cycle effect can produce a several-fold increase in fissuring propensity and extend the fissuring tendency to higher ferrite levels.

The fissures formed in the weld metals studied do not propagate under room temperature, slow bend conditions even when subjected to 20 percent plastic strain. The fissures merely open and thus are more easily revealed at low magnification.

The data obtained in this investigation are compared to the observations and studies by others (unpublished) for service-fabricated, heavy section weldments. A one-to-one correlation exists between the Fissure Bend Test observations and those recorded from production welds.

Since this initial utilization of the Fissure Bend Test produced such promising results, it appeared that other investigators may desire to utilize the testing method in similar studies. To preclude test proliferation without adequate initial test variable definition, a more thorough investigation of the test parameters was undertaken. This continued investigation yielded sufficient information as to the importance of variables and a standard test procedure was devised and is presented. Methods of data presentation are also suggested.

In addition to the application of the Fissure Bend Test as a screening test for use by electrode suppliers and fabricators, the test is also useful in studying the metallurgical phenomena surrounding the nature of fissuring. The test has logical extensions beyond the austenitic stainless steels and into the realm of fissuring in nickel base, cupro-nickel and other metallurgically similar alloys.

TABLE OF CONTENTS

CHAPTER		PAGE
I.	INTRODUCTION AND HISTORICAL REVIEW	1
	Theories of Hot Cracking	2
	The Question of Ferrite	6
	Measurement of Ferrite	15
	Object	17
	Organization	18
II.	THE FERRITE-FISSURING RELATIONSHIP IN AUSTENITIC STAINLESS STEEL WELD METALS	19
	Filler Metals Tested	19
	The Ferrite-Fissuring Relationship	20
III.	THE NATURE AND MORPHOLOGY OF FISSURES IN AUSTENITIC STAINLESS STEEL WELD METALS	35
	Introduction	35
	Fissuring in Austenitic Stainless Steel Weld Metals	35
	Fissure Morphology in Austenitic Stainless Steel Weld Metals	40
	General	40
	Fissure appearance and location	41
	Other discontinuities detected	55
	Fissure behavior during bend testing	62
	Fissure surface morphology and energy dispersive analysis	77

CHAPTER PAGE

Fissure sizes 81

The Influence of Thermal Cycling on Fissure Occurrence . 94

Factors Contributing to the Multiple HAZ Thermal Cycle Phenomenon 105

IV. THE FISSURE BEND TEST 107

Introduction 107

Procedure for the Conduct of the Fissure Bend Test . . . 109

General 109

Test plate preparation and fixturing 109

Welding 112

Surface preparation 114

Ferrite Number determination 115

Fissure evaluation 115

The ferrite-fissuring relationship 117

Investigation and Evaluation of the Test Variables . . . 120

Weld pad 120

Bead sequence 121

Weld pad restraint 124

Surface preparation 124

Plane of examination 126

Etching of the prepared surface 127

Bending the test specimen 128

Fissure determination 129

Ferrite 129

CHAPTER PAGE

Closure 131

V. CONCLUSIONS 134

Fissure Bend Test Results 134

Basic Fissuring Mechanisms 134

Fissure Size 135

VI. FUTURE WORK 137

LIST OF REFERENCES 138

APPENDIXES 147

Appendix A 148

Appendix B 150

Appendix C 153

VITA 157

LIST OF TABLES

TABLE		PAGE
I.	Ferrite Numbers Needed for Fissure Elimination	34
II.	Average Number of Fissures and Average Fissure Size (Based on Disc Assumption) for 308 and 316 Weld Metal as a Function of Pad Surface Preparation Technique (Measured on Bent Sample)	95
III.	Weld Metal Analyses	151
IV.	Core Wire Analyses	152

LIST OF FIGURES

FIGURE		PAGE
1.	Vertical Section of Fe-Cr-Ni System at 70 Percent Fe	8
2.	The Ferrite-Fissuring Relationship for 308 Weld Metal . . .	22
3.	The Ferrite-Fissuring Relationship for 308L Weld Metal . . .	23
4.	The Ferrite-Fissuring Relationship for 316 Weld Metal . . .	24
5.	The Ferrite-Fissuring Relationship for 316L Weld Metal . . .	25
6.	The Ferrite-Fissuring Relationship for 309 Weld Metal . . .	26
7.	The Ferrite-Fissuring Relationship for 318 Weld Metal . . .	27
8.	The Ferrite-Fissuring Relationship for 347 Weld Metal . . .	28
9.	The Ferrite-Fissuring Relationship Summary	29
10.	Light Micrograph of a Fissure Along a Grain Boundary Near an Interpass Boundary (See Arrow) in a Polished and Etched Sample of 316L Austenitic Stainless Steel Weld Metal (0.5 FN), Unbent, Transverse Section	42
11.	Light Micrograph of a Fissure Along a Grain Boundary Near an Interpass Boundary (See Arrow) in a Polished and Etched Sample of 309 Austenitic Stainless Steel Weld Metal (0.4 FN), Bent, Transverse Section	43
12.	SEM Micrograph of a Fissure Along a Grain Boundary Near an Interpass Boundary (See Arrow) in a Polished and Etched Sample of 308 Weld Metal (0.3 FN), Unbent, Transverse Section	45

FIGURE PAGE

13. Light Micrograph of a Fissure Near Two Interpass Boundaries (See Arrows) in a Polished and Etched Sample of 309 Weld Metal (0.4 FN), Bent, Transverse Section 46

14. Light Micrograph of Two Fissures (One Open to Surface) Near an Interpass Boundary (See Arrows) in a Polished and Etched Sample of 309 Weld Metal (0.4 FN), Bent, Transverse Section 48

15. Light Micrograph of Smaller Fissure in Figure 14 at 200X . . 49

16. Light Micrograph of a Fissure in a Ferrite-Free Area of 316 Weld Metal (Ave. 2.5 FN), Bent, Longitudinal, Top View Section 51

17. SEM Micrograph of Three Fissures in a Ferrite-Free Area Near an Interpass Boundary (See Arrows) in a Polished and Etched Sample of 308L Weld Metal (4.0 FN), Bent, Longitudinal, Top View Section 52

18. Light Micrograph of a Fissure in a Ferrite-Free Area in a Polished and Etched Sample of 308L Weld Metal (4.0 FN), Bent, Longitudinal, Top View Section 53

19. Light Micrograph of Grinding Tears in a Polished and Etched Sample of 308L Weld Metal (2.5 FN), Bent, Longitudinal, Top View Section 56

20. SEM Micrograph of a Surface Fissure in an As-Ground 309 Weld Metal Pad (2.8 FN), Bent, Longitudinal, Top View Section 58

FIGURE PAGE

21. SEM Micrograph of Fissure Surface (Figure 20) Showing Ductile Fracture Characteristics in a 309 Weld Metal Pad (2.8 FN), Bent, Longitudinal, Top View Section 59

22 SEM Micrograph of a Discontinuity in a 316L Weld Metal Pad (5.6 FN), Bent, Longitudinal, Top View Section 61

23. Light Micrograph of a Fissure in a Polished and Etched 308 Weld Metal Pad (0.4 FN), 1 Percent Plastic Strain, Longitudinal, Top View Section 65

24. Light Micrograph of the Same Fissure Shown in Figure 23, 4 Percent Plastic Strain 66

25. SEM Micrograph of the Same Fissure Shown in Figures 23 and 24, 20 Percent Plastic Strain 67

26. SEM Micrograph of the Tip of the Fissure Shown in Figure 25 68

27. Micrographs of a Fissure in a Polished and Etched 316 Weld Metal Pad (0.4 FN) as a Function of Bending Strain, Longitudinal, Top View Section 71

28. Light Micrograph of Two Fissures in a Polished and Etched 316 Weld Metal Pad (0.4 FN) as a Function of Bending Strain, Longitudinal, Top View Section 73

29. SEM Micrograph Showing the Predominant Type of Fissure Surface Morphology 79

30. SEM Micrograph of Secondary Fissure Surface Morphology . . . 80

31. Fissure Size Distribution for 308 Weld Metal, Milled Surface 84

FIGURE PAGE

32. Fissure Size Distribution for 308 Weld Metal, Ground Surface 85

33. Fissure Size Distribution for 308 Weld Metal, Polished and Etched Surface 86

34. Fissure Size Distribution for 316 Weld Metal, Milled Surface 87

35. Fissure Size Distribution for 316 Weld Metal, Ground Surface 88

36. Fissure Size Distribution for 316 Weld Metal, Polished and Etched Surface 89

37. SEM Micrograph of a Fissure in a Polished and Etched 16-8-2 Weld Metal Pad (1.5 FN), Bent, Longitudinal, Top View Section 93

38. Weld Pad Cross-Section Showing Bead Sequence 97

39. Portion of Weld Pad Cross-Section Showing Overlapping HAZ and its Intersection with the Prepared Pad Surface 103

40. Portion of Weld Pad Cross-Section Showing Overlapping HAZ Which Does Not Intersect Prepared Pad Surface 104

41. Photomacrograph of Fissure Bend Test Specimen (120° Included Angle) 110

42. Recommended Clamping Fixture 111

43. Fissure Bend Test Weld Pad Configuration 113

44. Recommended Grid Spacing for Ferrite Number Determination . 116

45. Fissure Bend Test Fixture 118

FIGURE PAGE

46. Data Presentation Method. Verified Fissure Count vs. Ferrite Number, Typical for Austenitic Stainless Steel Weld Metals 119

47. Weld Pad Cross-Section Showing Recommended Plane of Examination 123

48. Total Strain and Ferrite Number vs. Distance from Center of Span for Bent Sample of 16-8-2 Weld Metal 132

49. Variation of Ferrite Number with Energy Input, 316 Weld Metal, GTA Remelt 155

50. Variation of Ferrite Number with Reciprocal of Travel Speed, 316 Weld Metal, GTA Remelt 156

NOMENCLATURE

FN	=	Ferrite Number
HAZ	=	heat-affected zone
SMA	=	shielded metal-arc
GTA	=	gas tungsten-arc
GMA	=	gas metal-arc
SA	=	submerged-arc
SEM	=	scanning electron microscopy
EI	=	energy input
TS	=	travel speed
KJ	=	kilojoules
G	=	thermal gradient
R	=	growth rate
α	=	alpha
δ	=	delta
γ	=	gamma
Fe	=	iron
Ni	=	nickel
Cr	=	chromium
L	=	liquid

CHAPTER I

INTRODUCTION AND HISTORICAL REVIEW

Recently renewed interest in the ferrite-fissuring relationship in austenitic stainless steel weld metals is in large measure due to the increased utilization of nuclear power. The current energy crisis serves only to amplify the interest as a greater dependence is sure to be placed on nuclear power generation. Nuclear power systems, be they light water power reactors or the next generation breeder reactors, employ a great deal of austenitic stainless steel in their fabrication. The design and fabrication codes for nuclear reactors are very critical of the metallurgical nature of the materials used in nuclear construction. One of the goals of the code bodies is to limit the extent of microfissuring in austenitic stainless steel weld metal (1). It is felt that this can be achieved by controlling the chemical composition and thus the ferrite content of the weld metal. This has led to the establishment of one of the most controversial specifications: the level of ferrite required in the deposited austenitic stainless steel weld metal to assure freedom from microfissures. While there is general evidence that ferrite-containing austenitic stainless steel weld metals are less prone to microfissuring than fully austenitic welds, no definitive data have been developed documenting this behavior.

It is generally conceded that the fissuring phenomenon in austenitic stainless steels, whether it may be a fusion zone or a heat-affected zone (HAZ) occurrence, is related to a hot cracking (fissuring) mechanism. In

this regard a review of the literature surrounding the development of the various hot cracking theories is in order to provide a basis for future discussions.

Theories of Hot Cracking

The basis for the development of the first of several proposed theories of hot cracking of weld metal (fusion-zone-hot cracking) was established in Russia by Bochvar (2) in 1947. Closely related studies were published in the United States by Pumphrey and Jennings (3) and Pumphrey and Lyons (4) in 1948. These investigations coupled with the extensive subsequent work in the early 1950's by Medovar (5, 6, 7) led to the establishment of the Shrinkage Brittleness Theory.

The Shrinkage Brittleness Theory considers and recognizes the following:

1. That hot-cracks are initiated above the solidus temperature of the lowest melting constituent.

2. That within a certain critical temperature range during solidification a semirigid network of solid and liquid exists which is subject to rupture if sufficient strain is induced, thus forming hot-cracks.

3. That strains are inherent in the solidification process, induced either by thermal contraction or mechanical restraint.

4. That the amount and constitution of the liquid present during the transit of the critical temperature range is extremely important.

5. In addition, the theory recognizes the effect of the nonequilibrium solidification conditions inherent in welding.

Concurrent with the development of the Shrinkage-Brittleness Theory, a similar theory was advanced by Pellini (8) to explain the hot tearing of castings and was subsequently applied to weld metal hot-cracking by Apblett and Pellini (9). This theory, known as the Strain Theory, postulates the existence of thin liquid films at some stage during the solidification process and that cracking occurs during the thin film stage if sufficient strain is induced. This theory recognizes the effect of both the constitution of the material and the nonequilibrium solidification conditions on the nature of the thin films. However, the authors refute the argument of the Shrinkage-Brittleness Theory, that hot-cracking can occur during the mushy stage of solidification by stating that the induced strains are uniformly distributed during this period.

More recently, Borland (10) developed a Generalized Theory of Super-Solidus Cracking in Welds which modifies and extends both the Shrinkage-Brittleness and Strain Theories. The primary difference between Borland's theory and the Strain Theory of Pellini is that hot-cracking is most likely to occur when the thin liquid films are <u>almost continuous</u> thus providing narrow solid bridges between the solid portions of the weld. These narrow bridges must absorb the greatest proportion of the strains induced, or fracture thus forming hot-cracks. Furthermore, Borland elaborated on the mechanisms which control the distribution of the liquid films and the extent of the critical solidification range. Borland subsequently expanded and justified his theory (11), introducing in more detail the effects of alloy constitution (11), the partitioning of alloying elements during solidification (12) and solidification mechanics (13).

The three theories just described have become known as the liquation theories of hot-cracking for the reason that all postulate the existence of a liquid phase as a requisite for hot-cracking. However, another theory advanced by Movchan (14, 15, 16) and others (17, 18) postulates that hot-cracking may occur in the solid state. This theory is currently known as the Polygonization Theory, and suggests that at temperatures just below the actual solidus temperature dislocations and vacancies move under the influence of induced strains and form polygonized boundaries. The intersection of these boundaries with regions of high segregate concentrations are postulated to be the initiation site for hot-cracks, which upon propagation may intersect the liquid weld pool. The cracks which intersect the weld pool may partially fill with liquid metal and thus reduce the extent of cracking observed.

The theories of weld metal hot-cracking have not been without criticism (10, 19, 20, 21) while the theory of Borland, being very general, has received but little criticism. The critics of the existing theories along with others (16, 22, 23, 24, 25) have proposed both modifications to and extensions of these theories. These authors emphasize that the following considerations must also be reconciled with the existing theories:

1. The influence of the solidification substructure,
2. The rate of change of the strains induced during welding,
3. The relative deformability of the weld and heat-affected-zone,
4. The constitution of the material as inferred by the appropriate equilibrium diagram,

5. The effects of nonequilibrium solidification.

Thus the exact nature of hot-cracking in the weld fusion zone is still open to considerable debate.

The question of heat-affected-zone (HAZ) hot-cracking has received considerable attention since the early 1950's. Many of the theories of HAZ hot-cracking were initially derived from the liquation theories of weld metal cracking and to this date the existence of liquid films is deemed essential in the formation of HAZ hot-cracks by most investigators (8, 9, 10, 11, 12, 13, 14, 15, 23, 26, 38). However, there are a few investigators who continue to advance solid state cracking mechanisms (14, 18, 26). These authors also recognize that both liquation and solid state mechanisms may be operable at the same time and within the same temperature range.

The mechanism of formation of liquid films in the HAZ during welding has been related to:

1. Liquation of grain boundaries,
2. Low melting segregates,
3. Absorption of solute from the weld puddle,
4. Constitutional liquation of inclusions and second phase constituents.

The solid state mechanisms postulate that polygonized boundaries, solute segregation at grain boundaries and solute segregation at solidification subboundaries produce strain intolerant microstructural regions and thus sites for hot-crack initiation. All theories necessarily involve a strain induced during welding whether of thermal or mechanical origin or a combination of both.

At risk of oversimplification, it can be stated that the formation of a crack in a weldment requires:

1. That the material comprising the weldment exhibits a phase or a combination of phases which possess a limited capacity to tolerate strain within some critical range of temperature;

2. That the strain imposed upon the weldment by the combined action of thermal and restraint stresses within this critical range of temperature exceed the strain tolerance of the composite microstructure.

Any attack on the problem of hot-cracking (fissuring), regardless of the alloy type, must address itself to these two main features before it can become of any consequence.

Although the majority of austenitic stainless steels are considered readily weldable having considerable tolerance for variability in the welding parameters, the fully austenitic weld metals are known to be susceptible to fissuring in the weld metal of single run welds and in the HAZ of the preceding weld beads in multipass welds. The liquation theories as outlined above are believed to be relevant to the mechanism of formation of fissures in both cases.

The Question of Ferrite

In 1938 Scherer, Riedrich and Hougardy (39) first recognized that the presence of delta ferrite in the room temperature microstructure indicated a reduced fissuring tendency for austenitic stainless steel weld metals. They recommended that the weld metal should contain from 5 to 35 percent ferrite in the microstructure. Since then it has generally been accepted that the amount of ferrite required to prevent fissuring

is less than that indicated by Scherer et al. and is in the order of 5 to 10 percent. However, there is no quantitative data in the open literature to support either contention, and only speculative theories have been advanced to relate the ferrite content to the fissuring phenomenon.

The question of ferrite, its origin and its effects have been the subject of numerous discussions. The doubt which still exists as to whether the term "delta" or "alpha" should be applied to the ferrite present in the room temperature microstructure will not be resolved herein, but some generalizations are in order before proceeding with the discussion on the influence of ferrite on fissuring so that the reader will appreciate the uncertainty under which the investigators must labor.

In pure iron δ-ferrite is bcc and isomorphic with α-ferrite and is paramagnetic in its stable temperature range. α-ferrite is paramagnetic from 1670°F to 1414°F and ferromagnetic below 1414°F. In Fe-Cr-Ni alloys a γ loop forms such that the α and δ phase fields merge beyond about 13 percent Cr and thus there can be no real distinction between the α and δ denotations applied to ferrite. With nickel additions to Fe-Cr alloys, the γ phase has greater stability at lower temperatures. In the vicinity of the compositions representative of austenitic stainless steels (20 percent Cr, 10 percent Ni, 70 percent Fe), both the α and γ phases may coexist at room temperature depending on the thermal history of the alloy. A vertical section through the Fe-Cr-Ni diagram at 70 percent Fe is shown in Figure 1. This diagram is from the original work of Pugh and Nisbet (40) and has been used by numerous other investigators to explain the microstructures present in austenitic stainless steel weld

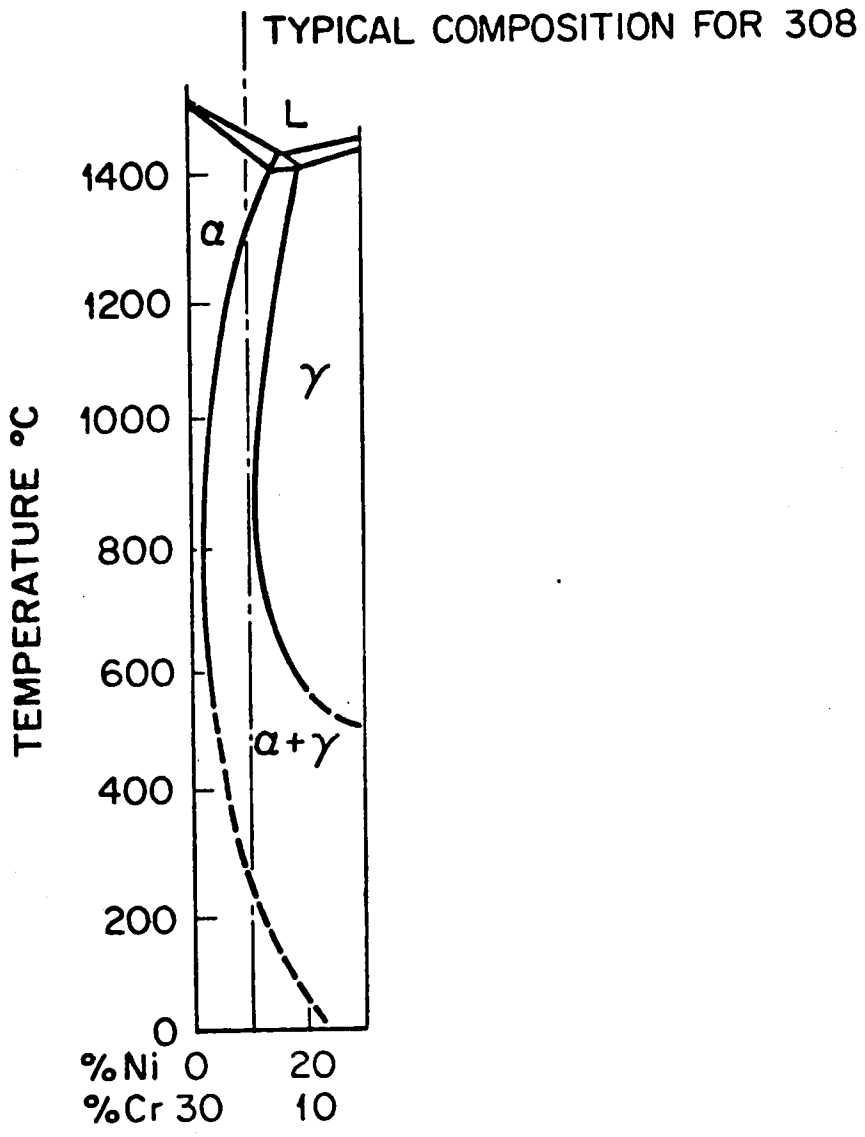

Figure 1. Vertical section of Fe-Cr-Ni system at 70 percent Fe.

metals. The vertical line shown represents a composition typical of 308 weld metal (10 percent Ni, 20 percent Cr, 70 percent Fe). Note that in addition to the $\alpha + L$, $\gamma + L$, $\alpha + \gamma$, α and γ phase fields, there exists a three-phase region, $\alpha + \gamma + L$, in the immediate vicinity of the austenitic alloys of interest. The exact nature of the three-phase reaction has never been fully explained and doubt exists as to the type of reaction occurring. Sections of this sort cannot be used to predict quantitative relationships between $\alpha + \gamma + L$ defining the composition or relative amounts of the phases present at any given temperature. However, this type of representation permits qualitative assessment of the transformational characteristics of the alloys in question.

Many others, including Masumoto (41) whose concepts will be discussed later, have made use of this diagram to justify their theories on the fissuring sensitivities of austenitic stainless steel weld metals. For alloys to the left of the three-phase reaction area, the primary solidifying phase is α, and subsequent transformation results in the formation of γ from the α by a solid-state, isomorphous reaction. The relative amounts of α and γ in the room temperature microstructure will be dependent on cooling rate as well as composition. Alloys to the right of the three-phase reaction field solidify initially to γ and subsequently transform to α upon cooling with similar restrictions for the phases present in the room temperature microstructure as was indicated for the alloys to the left of this reaction area.

Segregation naturally occurs during solidification for alloys both to the right and left of the three-phase region with the liquid composition being altered with decreasing temperature toward the

compositions of the three-phase field. The precise amount of segregation cannot be deduced from the section shown but no doubt exists as to the tendency of the liquid composition to reach the three-phase field region. If this occurs, then $\alpha + \gamma$ will form simultaneously from the liquid, a fact which every author to date has decided to overlook or assess with no significance accorded it. This fact alone may be the key to the fissuring behavior of the various austenitic stainless steels and may be the reason why composition control is so important.

The ferrite (in the room temperature microstructure) per se may not be related to the true mechanism of fissure formation but may only reflect the compositional effects directly responsible for fissure formation. Nonetheless, the presence of ferrite provides pragmatic means of assessing the capacity of a given weld metal to resist fissure formation. The term "ferrite" will be used throughout the majority of these discussions, and no differentiation will be made as to its origin, i.e., whether ferrite results from solidification or solid state transformation; but the origin may be an important key to the resolution of the entire problem.

Other alloying elements beside chromium and nickel have an effect on the amount of ferrite formed within the weld metal. Chromium, molybdenum, titanium, silicon, and columbium increase ferrite content and thus are termed "ferrite formers." On the other hand, nickel, carbon, nitrogen and manganese tend to decrease ferrite content and increase austenite content and are thus termed "austenite stabilizers."

Beside chemical composition and thermal effects, there are procedural factors which affect the resulting ferrite content. Increased

arc length allows enhanced nitrogen pickup in the weld metal. Since nitrogen is an austenite former, this results in a decrease in ferrite. Also dilution of the weld metal with the base metal will affect the ferrite level depending on the ferrite potential of the base metal. Thus for multipass welds deposited in a groove, the final beads will be relatively undiluted by the base metal and ferrite levels may vary across the fusion zone.

Gunia and Ratz (42) point out that ferrite levels vary appreciably on a microstructural scale. They report, for example, that a weld having an average of 2.8 percent may actually vary in ferrite content from 0.3 percent to 8.1 percent. Ferrite variations occur within the cross-section of a bead, along its length, and from bead to bead. The variation results from: (1) changes in chemistry within the bead due to the segregation of alloying elements upon solidification, (2) weld pool perturbations giving rise to intermittent solidification, and (3) variations in nitrogen pickup as welding progresses.

Goodwin, Cole, and Slaughter (43) report that the ferrite is, in all cases, located at the solidification substructure boundaries and in the areas which in a single phase alloy are the last to solidify. DeLong (44) states that because of the fast freezing of the weld metal, its ferrite structure is very fine, with the ferrite generally occurring in a lacy, interlocked dendritic structure. Furthermore, as the ferrite content increases, it becomes a continuous network at levels somewhere in the range of 4 to 7 volume percent. All of these characteristics have a bearing on the problem of measurement by magnetic means.

In 1967 Hull (45) summarized five theories that had been previously presented to explain the beneficial effect of ferrite in reducing fissuring tendency and then postulated his own theory.

The first and most common theory is based on the assumption that delta ferrite has a greater solubility than austenite for certain alloying elements, such as columbium and silicon, and trace elements, such as phosphorous and sulphur, which are believed to increase fissuring. Ferrite thereby reduces the extent of liquid film formation by decreasing the tendency of these harmful elements to segregate at the grain boundaries during solidification. If this occurs, fissuring will be decreased. This theory has been supported by Borland and Younger (12) and Marshall (46).

The second theory on the effect of ferrite is based on an increase in the total amount of grain boundary and interphase area with the generation of two phases, austenite and ferrite. This increased boundary area supposedly acts as a sink to decrease the concentration of impurities at the austenite-austenite boundaries and thus reduces fissuring. Curran and Rankin (47), Medovar (7), and Rollason and Bystram (48) have supported this theory.

A third theory on the effect of ferrite was proposed by Guessier and Castro (49) and by Kauhausen (50). It is based on the assumption that in a two-phase alloy the austenite grain size would be reduced. The small austenite grain size would increase the amount of grain boundary that could act as a sink for impurities and would thus reduce fissuring tendency.

The fourth theory, proposed by Noren and Hellerstrom (51), is based on the fact that ferrite reduces the solidification range of the weld metal, and thus there is a reduction in segregation of fissure-forming elements to the grain boundaries. However, Thielsch (51) and Hull (45) point out that there is little support for this theory since there is only a gradual change in solidification range as a function of composition whereas there is an abrupt reduction in fissuring with only a small amount of ferrite. Furthermore, it can be readily shown that a reduced solidification range does not necessarily mean a reduction in segregation tendency.

The fifth theory on the effect of ferrite is that fissuring is reduced because the bcc ferrite has a smaller coefficient of thermal expansion than the fcc austenite and thus shrinkage stresses are decreased (52). Hull (45) indicates that this theory lacks substance because the presence of the small percentage of ferrite required to prevent fissuring would have only a minor effect on the total thermal expansion coefficient.

Hull (45) proposed another theory to explain the role of ferrite in preventing fissuring. He postulates that the beneficial effect of ferrite results from the fact that the austenite:ferrite boundaries have a lower interfacial energy than the austenite:austenite boundaries. The austenite:austenite boundaries are wet by the last traces of liquid whereas the austenite:ferrite boundaries are not wet. Thus the austenite:ferrite boundaries can sustain the small but increasing stresses imposed by the contraction of the alloy as it freezes under restraint until all

the liquid has solidified and the austenite:austenite boundaries can bear their share of the load.

More recently Masumoto et al. (41) proposed that the determination of weld metal fissuring should be based on composition alone and not on ferrite content. Using the Fe-Cr-Ni phase diagram and weld metal of different compositions (of nickel and chromium with fixed amounts of iron), these investigators claim that fissuring depends on whether austenite or delta ferrite is the primary phase solidifying from the liquid. The alloys whose compositions nucleate austenite as the primary phase have a high sensitivity to fissuring. However, for the weld metals that nucleate delta ferrite as the primary phase, the sensitivity to fissuring is low even with high sulphur content (0.15 percent). Masumoto believes that when the delta ferrite nucleates as the primary phase, it is able to dissolve larger amounts of sulphur and other fissure-forming elements thus preventing the segregation of these elements to the grain boundaries where they are most influential in causing fissuring. It should be pointed out that Masumoto used a relatively simple slice of a three component phase diagram whereas the weld metal compositions he investigated had at least four major alloying elements and a host of minor or tramp elements. In all cases his sulphur content was considerably higher than any commercial filler metals and thus it would be anticipated that higher ferrite contents would be necessary to avoid fissuring in the more highly alloyed weld metals (310 type) that formed a part of his investigation. His results on sulphur-bearing base metal with Gas Metal-Arc (GMA) deposited wire are exactly what would be

predicted from present knowledge. His argument that the solidification mode is the controlling factor is weak in that he does not state how the solidification mode was determined and how it was deduced that the $\alpha + \gamma + L$ reaction is a eutectic.

While it is generally accepted that delta ferrite in welds is beneficial in preventing fissures, there are conditions under which it has an adverse effect. In some corrosive media it can cause severe local attack to occur and in high temperature service it accelerates transformation to the embrittling sigma phase. Sheddon and Pumphrey (53) recognized the need for ferrite control and placed an upper limit of 10 percent on delta ferrite to minimize sigma phase embrittlement.

Measurement of Ferrite

In 1949 Schaeffler (54) published his now well-known diagram which predicts ferrite level from the chemical composition of the austenitic stainless steel weld metal. This composition diagram was significantly revised in 1956 by DeLong, Ostrum, and Szumachowski (55) by including the effect of nitrogen and by modifying the slope of the lines so that the more highly alloyed types (309, 316, 317, and related analyses) show higher calculated ferrite levels. DeLong et al. made their determinations magnetically with an instrument known as a Magne Gage and claim an accuracy of ± 2 volume percent ferrite (Schaeffler claimed an accuracy of ± 4 volume percent ferrite). Long and DeLong (56) further revised this new diagram in 1973 to include the Welding Research Council Ferrite Number Scale.

Although the Schaeffler and DeLong diagrams have been valuable in predicting the ferrite content from deposited chemistry, the direct measurement of ferrite has proven to be more difficult. This is because of the morphology and distribution of ferrite in the austenitic matrix and its variation with location within the weld metal.

Stalmasek (57) in his summary report of work done by the IIW Commission 2, has stated that in addition to the Schaeffler and Delong diagrams over 22 methods or instruments have been devised to determine ferrite content in welds, castings, and wrought stainless steels. These methods have shown to produce a wide variation in results in the measurement of ferrite content in selected test samples. Through round robin testing programs in the United States and Europe conducted by the Welding Research Council and by the International Institute of Welding, it was established that the prime cause of the wide variations in ferrite determination was that there were no accepted common procedures or standards for calibration. Thus, one of the main obstacles in developing the ferrite-fissuring relationship has been the lack of a standardized means of measuring ferrite and reporting ferrite in the weld metals.

This obstacle essentially has been eliminated through the efforts of the Stainless Steel Advisory Subcommittee of the High Alloys Committee of the Welding Research Council. This subcommittee has been involved in a continuing study of the relationship between chemical composition, ferrite level, and fissuring tendencies of austenitic stainless steel weld metals. The work completed by the Stainless Steel Advisory Subcommittee has resulted in a standardization of the

measurement of ferrite through the establishment of correlations and the calibration of instruments with National Bureau of Standards (NBS) thickness standards (58). The standardization has resulted in a scale of Ferrite Numbers which is related to the ferrite content of austenitic stainless steel weld metals. This, in turn, has led to the incorporation in the American Welding Society (AWS) standards of specific procedures: "AWS A4.2-74, Standard Procedures for Calibrating Magnetic Instruments to Measure the Delta Ferrite Content of Austenitic Stainless Steel Weld Metal" (59).

Thus, specific and firmly established techniques are available for both the prediction and measurement of ferrite level. As a direct consequence of these efforts it was not possible to undertake the task of determining the fissuring tendency of austenitic stainless steel weld metal and relate this tendency to Ferrite Number.

Object

The object of this study is:

1. To devise a method for determining the ferrite-fissuring relationship in austenitic stainless steel weld metals. The weld metals selected for study are: 308, 308L, 316, 316L, 309, 318, 347 and 16-8-2.

2. To clearly define the test variables with the aim of providing a standardized test scheme applicable to the study of fissuring for a broad range of stainless steels.

3. To study the nature and morphology of fissures in austenitic stainless steel weld metals.

Organization

The results of the study fall quite naturally into three distinct areas both chronologically and topically, and thus the discussions that follow are divided accordingly. The data are arranged in this manner so that the reader will more easily appreciate the more salient features of the work.

CHAPTER II

THE FERRITE-FISSURING RELATIONSHIP IN AUSTENITIC STAINLESS STEEL WELD METALS

In November 1972 the Stainless Steel Advisory Subcommittee in concert with the Discontinuities Subcommittee of the Welding Research Council and twelve industrial laboratories (see Appendix A) undertook the task of determining the fissuring tendency of austenitic stainless steel weld metal in an effort to relate this tendency to Ferrite Number. As this study progressed, the Welding Research Council instituted a program at the Welding Laboratory of The University of Tennessee to provide a more thorough examination of the data obtained and to extend the effort toward understanding the ferrite-fissuring relationship.

Filler Metals Tested

The austenitic stainless steel weld metals selected for evaluation in the study of the ferrite-fissuring relationship were chosen because of their utility in the fabrication of nuclear and nonnuclear components for power plants and reactor vessels. The weld metals were deposited by the Shielded Metal-Arc (SMA) process with 1/8" diameter AC-DC (-16 coating) electrodes of the following types: 308, 308L, 316, 316L, 309, 318, 347, and 16-8-2.

Except for 16-8-2, the electrodes for each filler metal type were prepared in four lots. Each lot was designed to deposit weld metal of a different ferrite level. The four ferrite levels selected correspond to

approximately zero, two, four, and six Ferrite Numbers and were designated the A, B, C, and D levels, respectively. The 308, 308L, and 347 electrodes were fabricated from one heat of core wire while fabrication of 316, 316L, and 318 electrodes utilized a different heat of core wire. The 309 electrodes were fabricated from a third core wire heat. The 16-8-2 electrodes were selected from two commercial lots and thus no ferrite range was available. The chemical analyses of the core wires and the chemical analyses and Ferrite Numbers of the as-deposited weld metal pads made in accordance with MIL-E-0022200/2B (60) are presented in Appendix B. By employing commercially utilized coating compounding techniques, the ferrite level could be varied without the necessity of resorting to weld procedure variations. Thus, since the electrode fabrication method and the deposition technique correspond closely with commercial practice, a firm basis is provided for comparing the fissuring tendency of the respective filler metals.

The fissuring test utilized in this investigation is known as the "Fissure Bend Test." In this initial phase of testing a total of one hundred and eighty weld pads made from the eight selected austenitic stainless steel weld metals were produced and tested by the Fissure Bend Test method. The standard procedure for conducting the Fissure Bend Test and an evaluation of the important test variables are discussed in detail in Chapter IV.

The Ferrite-Fissuring Relationship

When the specimens produced by the Fissure Bend Test were examined in the as-ground, unbent condition, fissures were found in the 318 and

347 weld metals at the A and B ferrite levels. No verified fissures were found in 308, 308L, 316, 316L, 309 or 16-8-2 weld metals at any ferrite level in the as-ground, unbent condition. Subsequent to bending, fissures were found in all weld metals at the A ferrite level, and also fissures were found in 308L, 316, 316L, 309, 318 and 347 at the B ferrite level. No fissuring was detected at the C or D levels in any of the weld metals tested.

The extent of fissuring revealed by the bent specimens prepared by the industrial laboratories is presented in Figures 2 through 9. In these figures the verified fissure count in the center four inches of each specimen is shown as a function of Ferrite Number. The Ferrite Numbers used are those determined from the as-ground, unbent specimens because the bending operation tends to increase the Ferrite Number.

In the construction of curves shown in Figures 2 through 9, all data points were given equal weight even though the specimens for each weld metal type were prepared and tested by three different laboratories. The curves represent the best visual fit of the data. The legend in each figure identifies the data attributed to the specimens prepared by each of the laboratories. To facilitate a comparison of the fissuring behavior of the different weld metal types, the curves generated for Figures 2 through 8 are redrawn in a summary fashion in Figure 9.

Figure 2 shows the verified fissure count as a function of ferrite level for 308 weld metal. At very low ferrite levels, fissures were detected in the 308 weld metal. However, the fissuring tendency was eliminated at a ferrite level of approximately 2 Ferrite Number (FN).

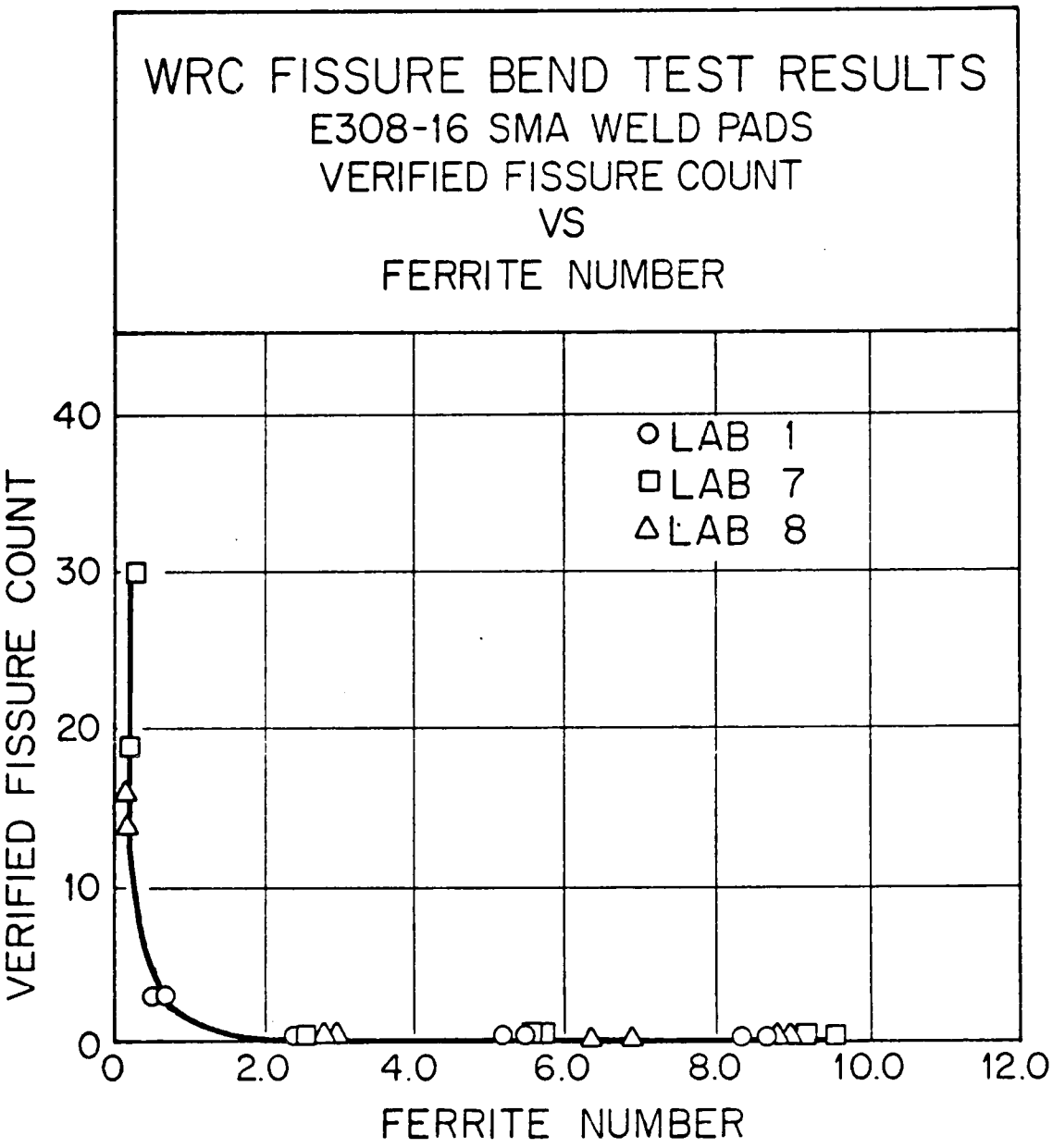

Figure 2. The ferrite-fissuring relationship for 308 weld metal.

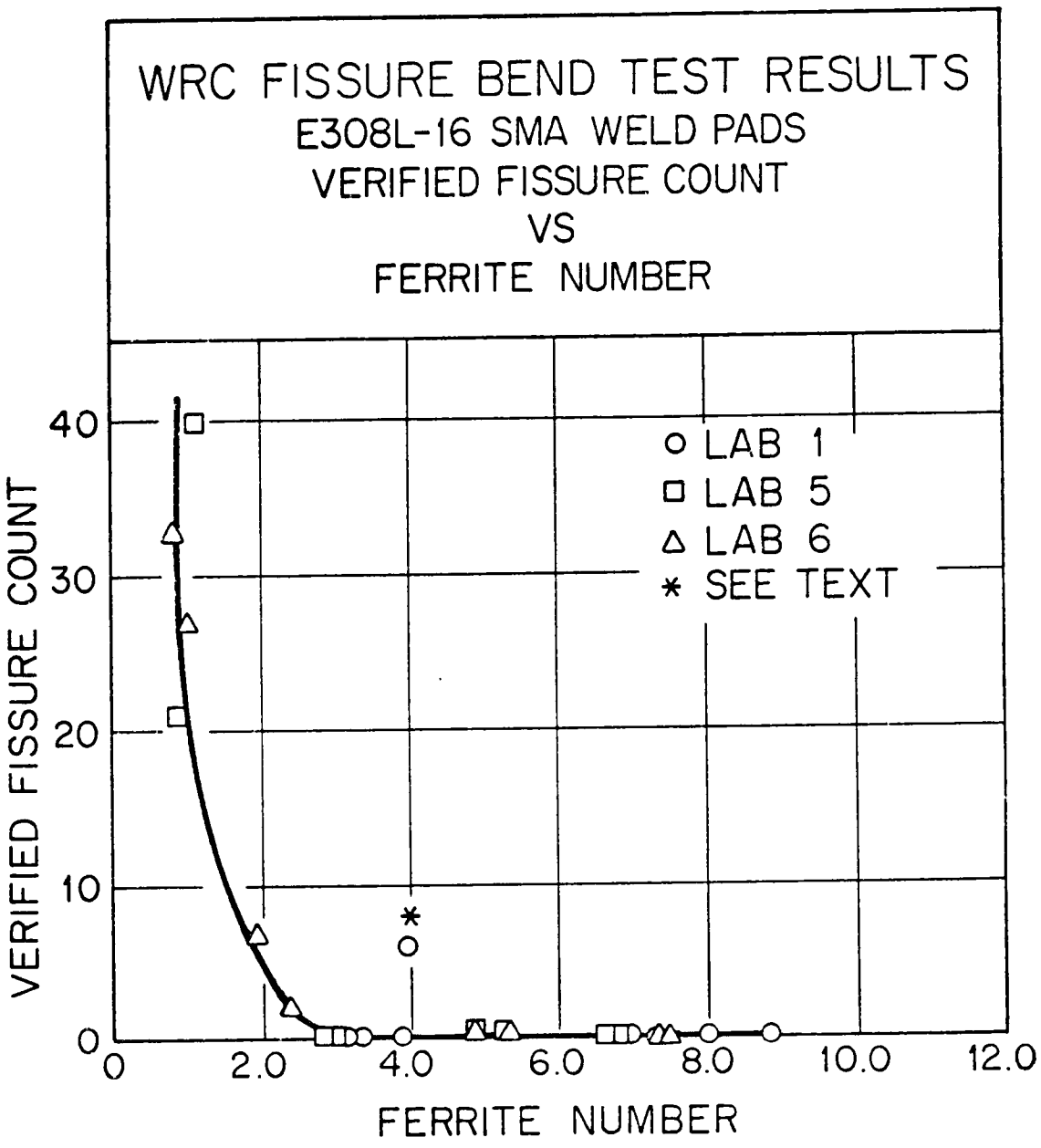

Figure 3. The ferrite-fissuring relationship for 308L weld metal.

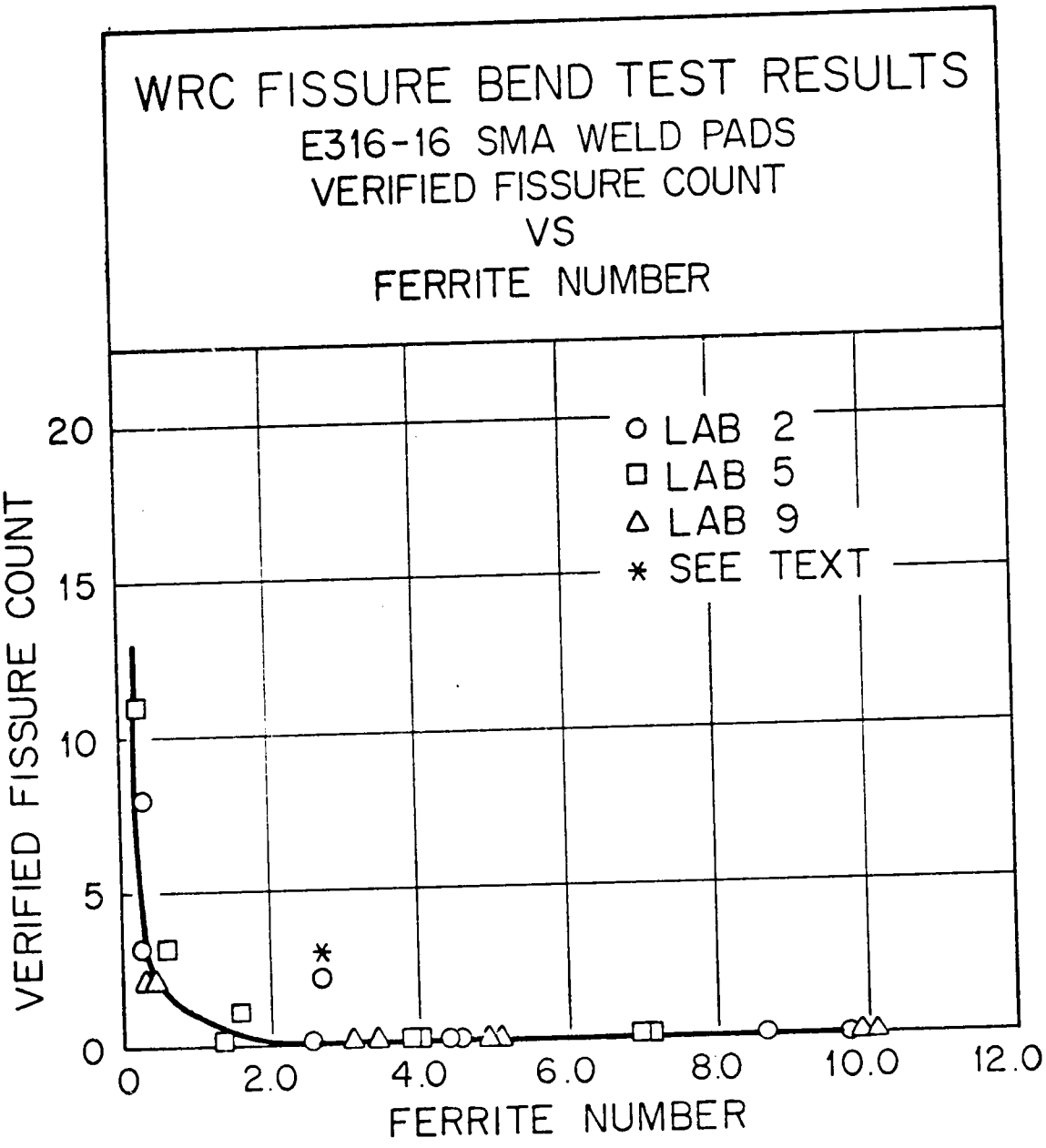

Figure 4. The ferrite-fissuring relationship for 316 weld metal.

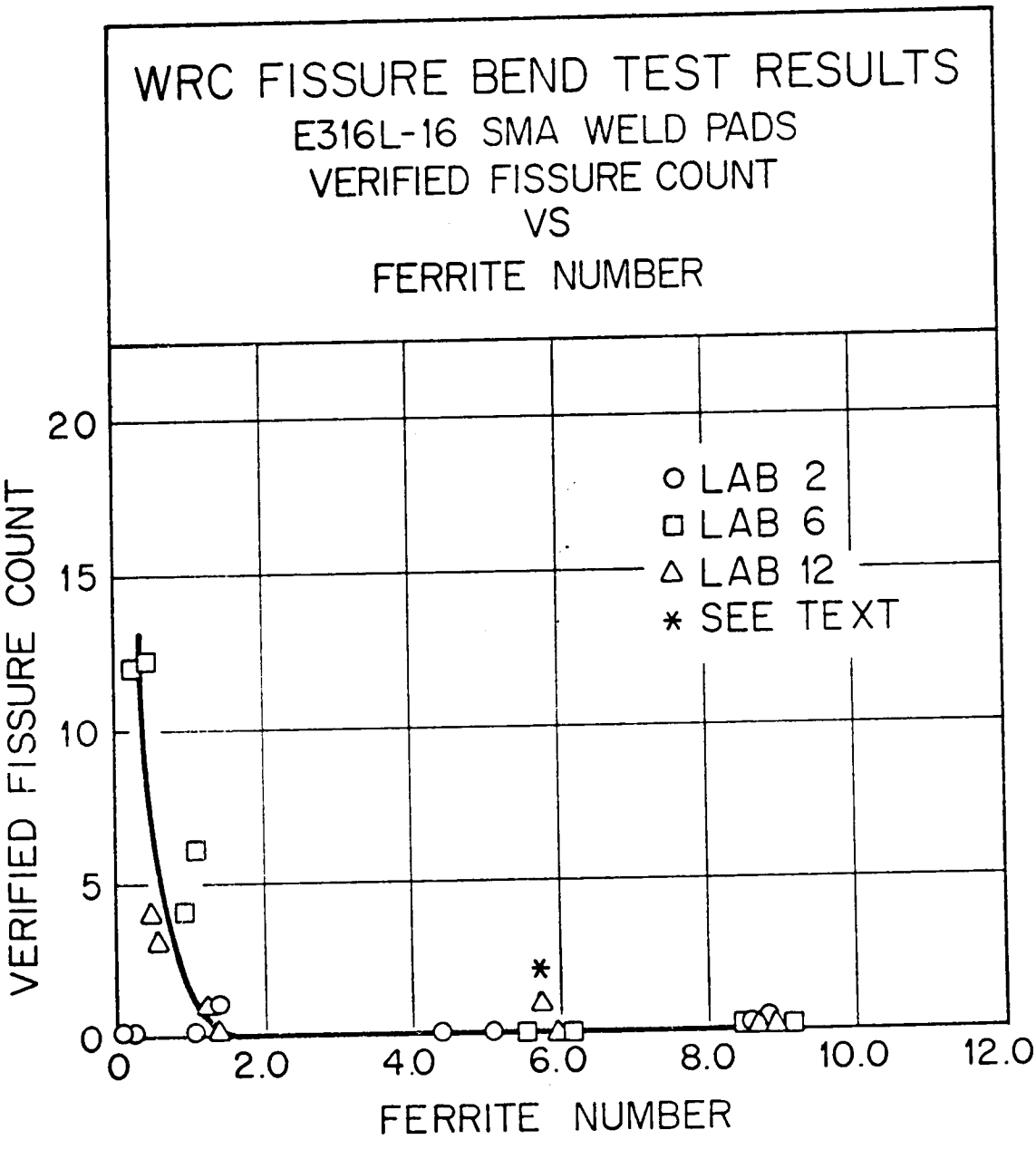

Figure 5. The ferrite-fissuring relationship for 316L weld metal.

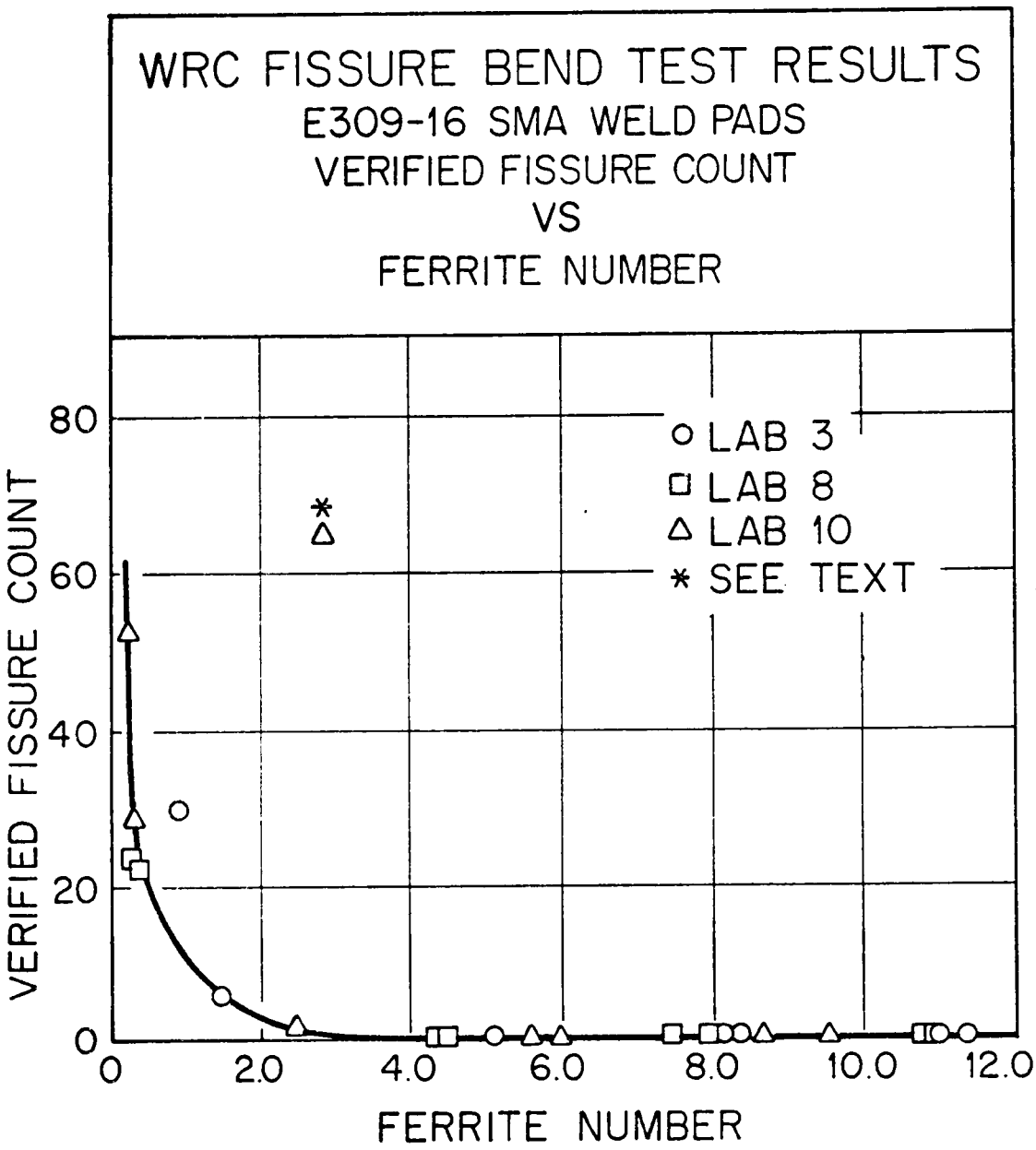

Figure 6. The ferrite-fissuring relationship for 309 weld metal.

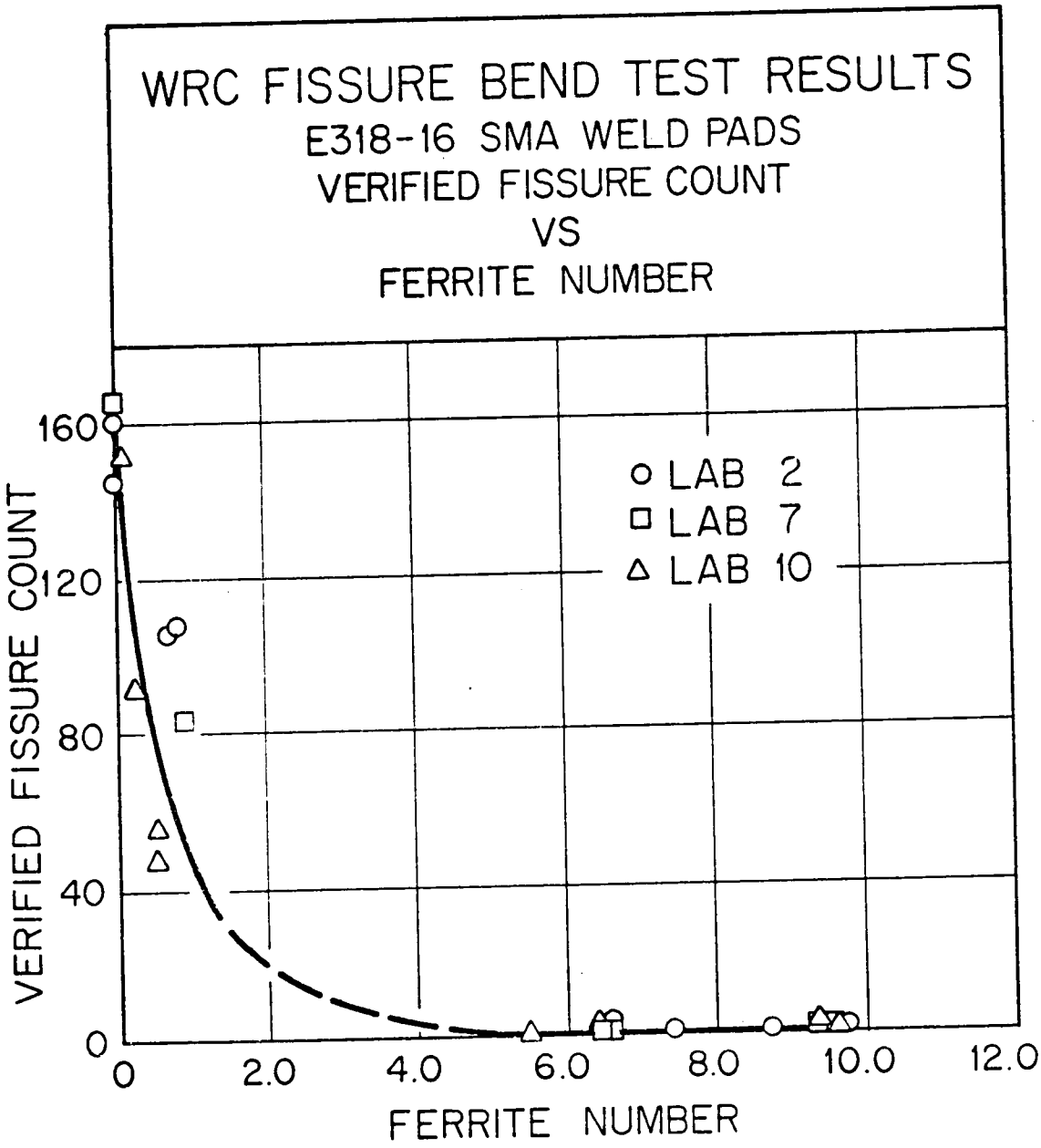

Figure 7. The ferrite-fissuring relationship for 318 weld metal.

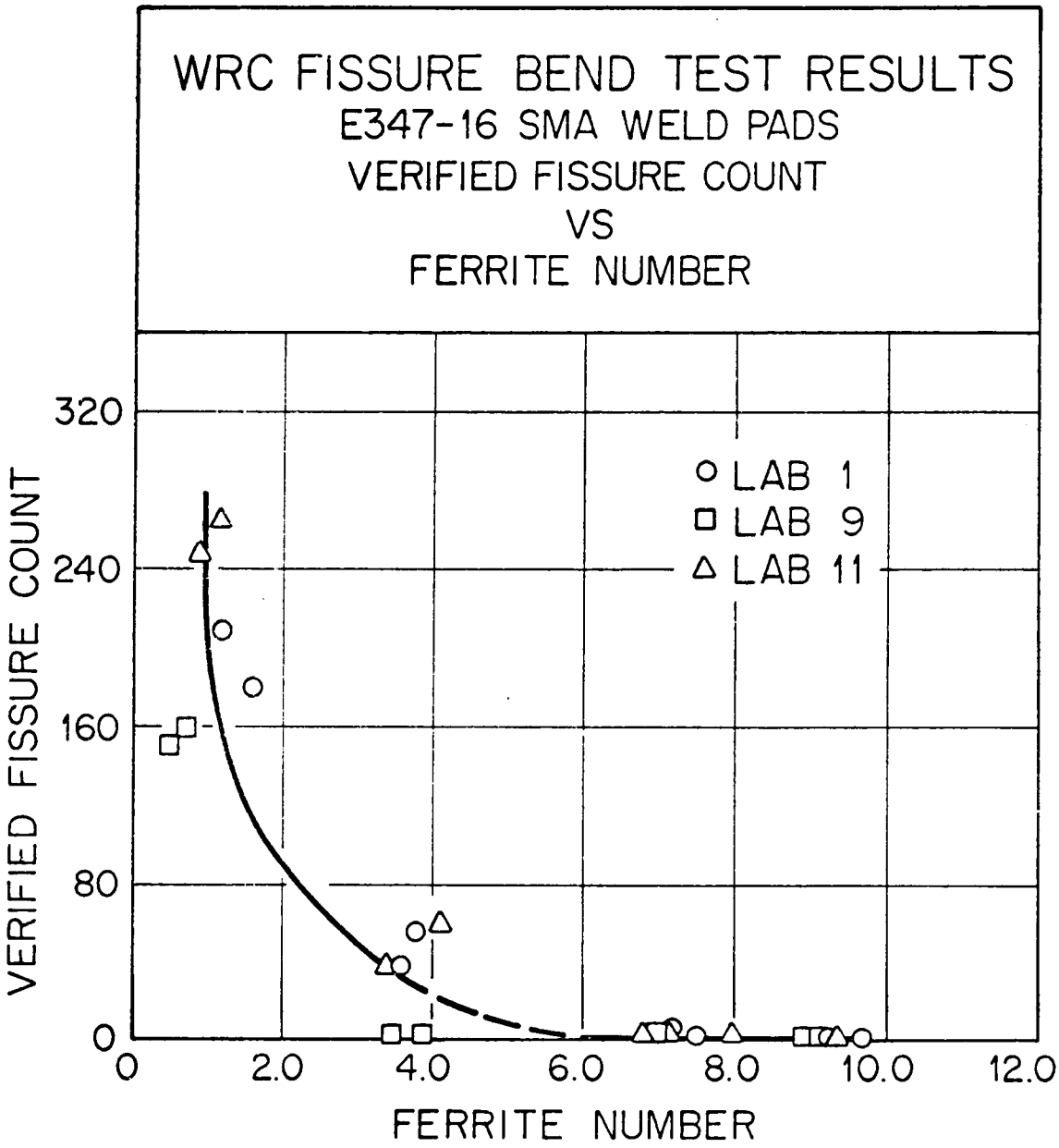

Figure 8. The ferrite-fissuring relationship for 347 weld metal.

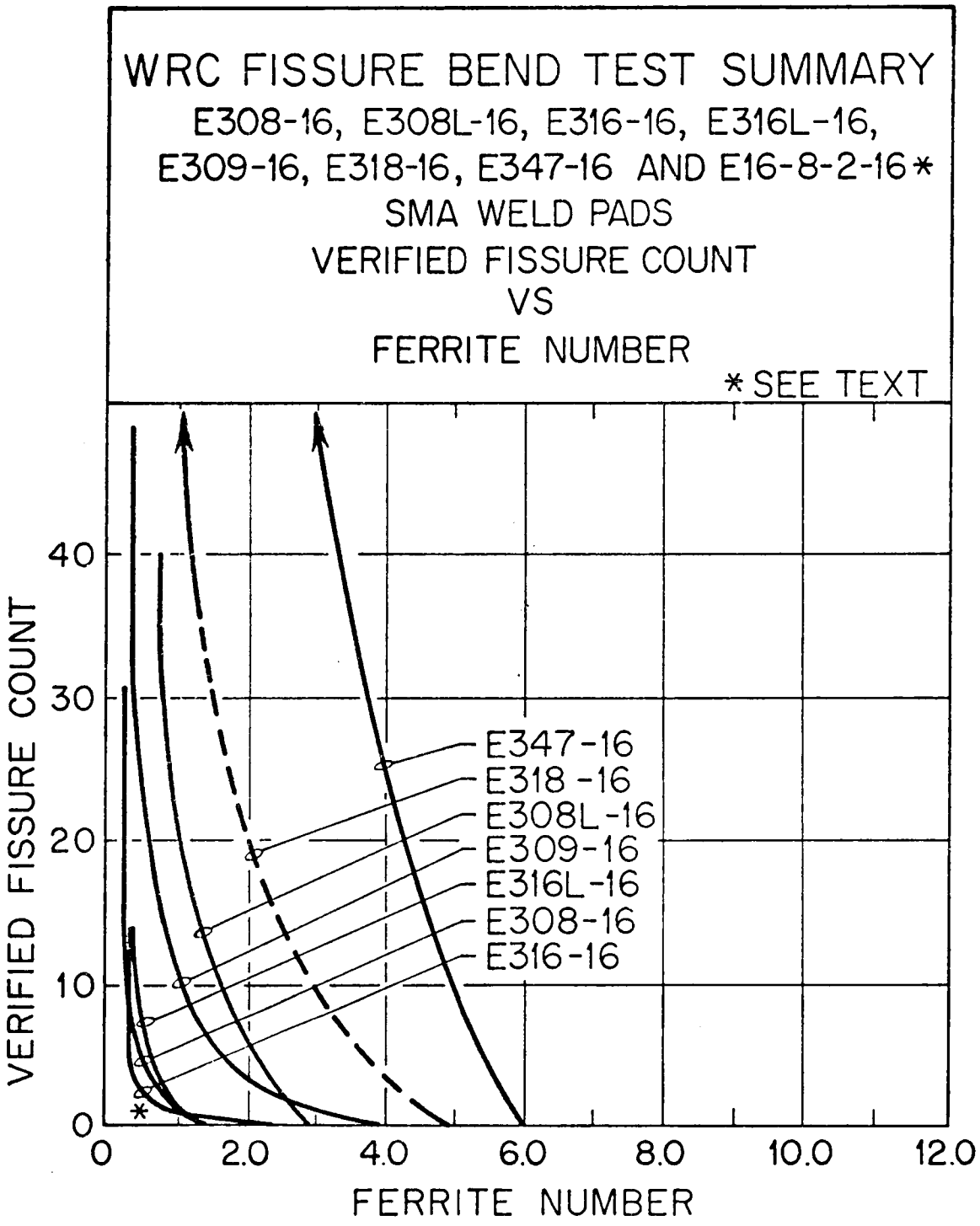

Figure 9. The ferrite-fissuring relationship summary.

The 308L weld metal exhibited a greater fissuring tendency than the 308 weld metal at comparable ferrite levels. As shown in Figure 3, a ferrite level of approximately 3 FN was required to eliminate fissuring in 308L weld metal. In one specimen with a Ferrite Number of approximately four, six fissures were found (see asterisk in Figure 3). These fissures were approximately 0.010 inch in length and were all located within 0.2 inch of each other along an interpass boundary. While the ferrite level in this general area was recorded to be 4 FN, metallographic evaluation on a polished and etched sample taken to include these fissures revealed that the area immediately adjacent to the fissures was essentially devoid of ferrite. A metallographic and scanning electron microscopy (SEM) documentation of these fissures will be presented in Chapter III.

Figure 4 shows the verified fissure count as a function of ferrite level for the 316 weld metal. As shown in the figure, the fissuring tendency is evident only at low ferrite levels and is completely eliminated at approximately 2 1/2 FN. In one specimen of the 316 weld metal at the B ferrite level (2 1/2 FN), two penetrant indications were found (see asterisk in Figure 4) the nature of which could not be unequivocally verified by optical microscopy. These indications were evaluated by light microscopy and the results will be presented in Chapter III. Edmonds (61) has determined the ferrite content of a 316 weld containing fissures as a function of fissure location. His data showed that only when the ferrite level decreased below approximately 3 FN did any fissures appear. These data are comparable to the 2 1/2 FN determined in this investigation.

The verified fissure count as a function of ferrite level for 316L weld metal is shown in Figure 5, page 25. Fissures were detected in these pads at very low ferrite levels, but the fissuring tendency was quickly reduced as the ferrite level increased. At a Ferrite Number of approximately 1 1/2, the fissuring tendency in the 316L weld metal was completely eliminated. There was one indication at the C ferrite level (see asterisk in Figure 5) in the 316L weld metal the nature of which could not be determined by dye penetrant testing or optical microscopy. Metallographic examination and scanning electron microscopy has revealed that the indication originated from a crack in an inclusion in the weld metal and that it was not related to fissuring of the weld metal in any manner. SEM documentation of this indication will be presented in Chapter III.

The fissuring tendency versus Ferrite Number for 309 weld metal is shown in Figure 6, page 26. The 309 weld metal exhibited a significant inclination toward fissuring at low ferrite levels. Fissuring tendency was completely eliminated at a Ferrite Number of approximately four. One specimen of the B level (see asterisk in Figure 6) exhibited an unusual behavior. Upon bending, a great number of cracks appeared across the surface of this specimen. However, these cracks occurred in a very random fashion across the pad surface and not along interpass boundaries as was the case for the remainder of the specimens of this lot. These cracks were investigated in the scanning electron microscope and the results will be presented in Chapter III.

Figure 7, page 27, shows the fissuring tendency as a function of ferrite level for 318 weld metal. The 318 weld metal exhibited a

pronounced sensitivity toward fissuring, being exceeded only by 347 weld metal. For the 318 weld metal the fissuring tendency was completely eliminated at a Ferrite Number of five. However, as shown in the figure, there is an absence of data between 1 FN and 5 FN since the A and B levels exhibited zero to one Ferrite Numbers and the C level showed Ferrite Numbers of five or greater. Thus the Ferrite Number necessary for elimination of fissures may be considerably less than 5 FN.

The 347 weld metal exhibited the greatest fissuring tendency of all weld metals tested. Figure 8, page 28, shows the fissuring tendency as a function of ferrite level for the 347 weld metal. Over 240 fissures were found in each of two specimens of approximately 1 FN. Fissuring tendency was reduced as the ferrite increased, but a ferrite level of approximately 6 FN was required to completely eliminate fissuring in the 347 specimens.

The 16-8-2 weld metal was the least prone to fissuring of all the weld metals tested. In fact, in only two of the twelve 16-8-2 specimens were any fissures found, and a total of only four fissures were detected in all. Thus no graphical presentation of the ferrite-fissuring relationship for 16-8-2 was attempted. The ferrite level of the 16-8-2 was from 0 to 2 FN because the electrodes were taken from two commercial lots not especially produced for utilization in this study. The data indicate that a ferrite level of 2 FN is sufficient for elimination of fissuring in 16-8-2 weld metal.

It may be advantageous and convenient to express the results in terms of a ferrite level which completely eliminates fissures. This criterion may be determined from the summary curves in Figure 9, page 29,

by noting the Ferrite Numbers at which the curves intersect the abscissa. Table I presents the results of such an assessment.

The data produced in this initial phase of testing were reproducible and are characteristic of the fissuring tendency of austenitic stainless steels in accordance with the currently accepted concepts. Thus it was now considered possible to utilize the Fissure Bend Test in continued studies to more clearly document the nature and morphology of fissures in austenitic stainless steel weld metals and to extend the effort of understanding the factors responsible for the fissuring tendency.

TABLE I

FERRITE NUMBERS NEEDED FOR FISSURE ELIMINATION

Weld Metal Type	Ferrite Numbers Needed for Fissure Elimination
16-8-2	0-2
316L	1 1/2
308	2
316	2 1/2
308L	3
309	4
318*	5
347	6

*Ferrite level required may be less than 5 FN. See text.

CHAPTER III

THE NATURE AND MORPHOLOGY OF FISSURES IN AUSTENITIC STAINLESS STEEL WELD METALS

Introduction

In Chapter I, Introduction and Historical Review, the currently recognized hot cracking (fissuring) theories were discussed, and it was stated that the fissuring phenomenon in austenitic stainless steel is related to a hot cracking mechanism. In Chapter II the ferrite-fissuring relationship was developed for eight austenitic stainless steel weld metals through utilization of the Fissure Bend Test method. It was also concluded that by the employment of the Fissure Bend Test, the nature and morphology of fissures could be studied. Before this is documented, a review of the literature concerning fissuring in austenitic stainless steel weld metals is in order.

Fissuring in Austenitic Stainless Steel Weld Metals

It is recognized that austenitic stainless steel weld metals are susceptible to fissuring in the fusion zone of single-run weld beads (41, 62-64), in the base metal HAZ (62, 65-72), and in the HAZs of weld metal produced by subsequent beads in multipass welds (48, 65, 66, 73-83). The fissuring in single-run welds is normally combated by reduction of weld metal restraint and by composition control to assure residual ferrite in the room temperature microstructure. The base metal HAZ phenomenon has been largely associated with the stabilized grades of

stainless such as 347 and in recent years has become a relatively minor problem due to improved residual elemental control in the melting and processing of the wrought materials.

Microfissuring in multipass welds in austenitic stainless steels has become of greater importance in recent years due to the increased utilization of heavy section stainless weldments. There is almost universal agreement among investigators that the fissuring in multipass welds is restricted to the weld metal HAZs produced by the multiple weld passes needed to complete a heavy section weldment (74, 77-79, 81-83). It has also been established that composition control of the deposited weld metal, resulting in a modest amount of ferrite in the room temperature microstructure, will essentially eliminate the microfissuring tendency. This level of ferrite was more firmly established for eight austenitic stainless steel weld metals (see Chapter II).

In some studies (81-83) utilizing actual production weldments of 316 stainless steel, the investigators did not find any instance of base metal HAZ cracking, nor did they find any microfissures in the last or cover passes in the weld metal. All of the fissures found were within the bulk of the weld metal (buried) in the HAZ of subsequently deposited beads. Literally hundreds of microfissures were observed and fissure densities of up to 70 fissures/in^2 were recorded on polished and etched weld sections. The observations of the fissuring tendency in the weld metals studied in the initial testing phase confirm those reported for the production weld metals. Haddrill and Baker (74) and Honeycombe and Gooch (77-79) utilized 310 and 316 weld metals in their work, and found as others had before (73), that fully austenitic weld metals are prone to

microfissuring. They confirm the observations in the multirun welds (using pad specimens) that the fissuring is relegated to the underlying HAZs and virtually never occurs in passes not subjected to subsequent thermal cycles. Unfortunately, the fissuring of austenitic stainless steel weld metals in multipass heavy section weldments has not been studied extensively to date and much work remains to be done.

Most investigators (74, 76, 77, 81-83) writing on the specific nature of the fissures, their location in the microstructure and the mechanism of formation of the fissures agree that:

1. Fissures invariably occur along grain boundaries regardless of whether they are located in the base metal HAZ, weld metal HAZ or in weld beads minimally affected by subsequent weld passes.

2. The fissures are most prone to form in the weld metal HAZs produced by subsequent weld passes.

3. The fissures form at elevated temperatures (above 1600°F) and may result from more than one basic (hot cracking) mechanism.

4. Fissuring tendency decreases when the weld metal contains ferrite (room temperature microstructure); and when fissures do occur in ferrite-containing weld metals, they form in "ferrite-free" areas.

The cause of fissure formation in stainless steels has been studied by several investigators (10, 12, 41, 62, 64, 66, 67, 70, 72-77, 79, 80, 84-87) in recent years. Three basic concepts have been presented to explain the mechanism of hot cracking in stainless steels:

1. Solidification-Segregation (Super Solidus) Cracking. This mode of cracking occurs during the actual deposition of individual weld beads

and is related to solute redistribution upon solidification. As indicated above, this mode does not appear to be significant in austenitic stainless steel weld metals because it is not often observed with commercially utilized filler metals.

2. HAZ Liquation Cracking. This phenomenon is the basis for most hot cracking theories applied to austenitic stainless steel weld metals. It requires that liquation of low melting segregates, partitioned to grain boundaries, occurs in a given temperature range (usually near the bulk solidus temperature) in concert with a strain of sufficient magnitude to rupture the liquid films.

3. Ductility-Dip Cracking. This type of cracking results from a loss in ductility occurring over a given temperature range below the bulk solidus (from 1650°F-1830°F for 310 according to Haddrill and Baker (74), around 1560°F and again around 2010°F for 347 according to Truman and Kirkby (84)). This loss in ductility is sufficient to produce cracking under the influence of welding-induced strains.

Haddrill and Baker (74), Shackleton (72), and Honeycombe and Gooch (77) report that both HAZ liquation and ductility-dip cracking may be operative in the weld metal at the same time. However, Honeycombe and Gooch believe that HAZ liquation is the dominant mechanism while Haddrill and Baker maintain that ductility-dip cracking is more prevalent.

Regardless of the specifics of the mechanism, it can be simply stated that:

1. The material comprising a weldment exhibits a region (degraded microstructure) which possesses a limited capacity to tolerate strain within some critical range of temperature.

2. The strain imposed upon the weldment by the combined action of thermal and restraint conditions within this critical range of temperature exceeds the strain tolerance of the degraded microstructural region.

A degraded microstructural region in an austenitic stainless steel weld may be solidification segregation related but may not be influential in regard to fissuring until conditioned by the thermal cycles from succeeding passes. After the weld metal has been thermal cycled by subsequent passes, it may be more susceptible to fissuring. In addition, if the matrix is strengthened by a precipitation reaction which is enhanced by subsequent weld cycles, the fissuring tendency may be influenced in that the strains occurring during the subsequent thermal cycles may be forced to occur in and about the degraded microstructural region.

Alternately, it may be the accumulation of strains produced by subsequent thermal cycles which is responsible for cracking. When the strain accumulation is sufficient, rupture or fissuring occurs. It is, however, most likely a number of factors operating together which are ultimately responsible for the type of fissuring observed in austenitic stainless steel weld metals. It is to this end that the research presented in this chapter has addressed the issue of fissuring in austenitic stainless steel weld metals.

Fissure Morphology in Austenitic Stainless Steel Weld Metals

General. As a result of the testing program to develop the relationship between ferrite and fissuring in 308, 308L, 316, 316L, 309, 318, 347, and 16-8-2 austenitic stainless steel weld metals, numerous well-documented specimens were available for study. With the exception of 16-8-2, each weld metal was available at four ferrite levels (approximately 0 FN, 2 FN, 4 FN, and 6 FN) so that the influence of ferrite on fissure morphology and location could be assessed.

The aforementioned testing utilized the Fissure Bend Test method which employs a multirun, double-layer, weld pad deposited by the SMA process to evaluate fissuring in relatively undiluted weld metal. In this testing scheme the pad surfaces are prepared by milling, grinding or polishing, and then are bent in tension to a 120° included angle to expose fissures for detection by fluorescent penetrant inspection and binocular microscopy (for a more detailed description of the Fissure Bend Test see Chapter IV). From the well-documented welds produced during the testing phase, a number of metallographic and scanning electron microscopy (SEM) samples were removed from as-deposited bent and unbent weld pads to characterize the nature and morphology of the fissures present. The samples were chosen from weld specimens of low ferrite content (0-1 FN) where a high incidence of fissuring was observed and from specimens of higher ferrite content (2-3 FN) where fissuring tendency was significantly reduced. In addition, specimens exhibiting penetrant indications of unusual or unexpected nature were thoroughly examined and documented.

Fissure appearance and location. In any discussion concerning planar sections through a discontinuity-containing three-dimensional solid, some knowledge of the volumetric configuration of the discontinuity is necessary to gain a full appreciation for its appearance on a planar surface. For the case of fissures, they should be considered essentially disc-shaped with a circular aspect. Thus any cut through a fissure (except for that which lies in the plane of the fissure and would be quite rare) would be displayed as a "line" on a planar section regardless of the angle of cut. If the fissure has some thickness (separation), however, the more oblique cuts would yield more widely separated faces.

All fissures examined in this investigation, regardless of weld metal type, were located along weld metal grain boundaries in the HAZ of a subsequently deposited bead. For example, Figure 10, a light micrograph showing a fissure in a polished and etched, transverse, unbent section of a 316L weld pad (0.5 FN), illustrates that the fissure occurs entirely within the weld metal and is located along a grain boundary. In addition, it is to be noted that the fissure is proximate to an interpass boundary (see arrow) and is in the HAZ of the succeeding weld bead. Figure 11, a light micrograph of a fissure revealed in a polished and etched, transverse, bent section of 309 weld metal (0.4 FN), also shows the grain boundary mode of fissuring and the relationship of the fissure to the interpass boundary (see arrow). Note that the fissure in the bent pad shown in Figure 11 is about the same width as the fissure in the unbent pad shown in Figure 10. The bending of the weld per se does not appear to influence the width of a fissure as long as it is wholly



Figure 10. Light micrograph of a fissure along a grain boundary near an interpass boundary (see arrow) in a polished and etched sample of 316L austenitic stainless steel weld metal (0.5 FN), unbent, transverse section. 100X.

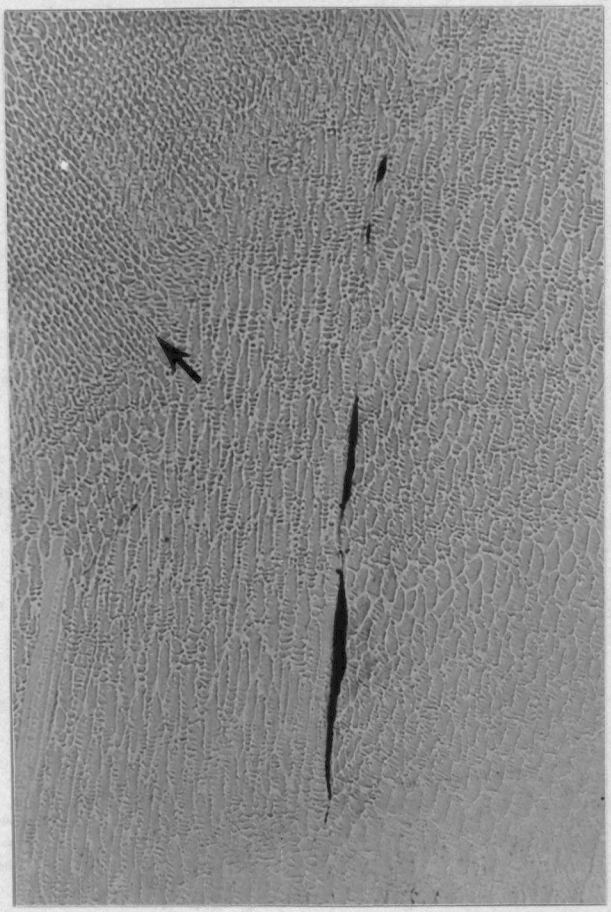

Figure 11. Light micrograph of a fissure along a grain boundary near an interpass boundary (see arrow) in a polished and etched sample of 309 austenitic stainless steel weld metal (0.4 FN), bent, transverse section. 100X.

contained within the weld metal remote from a free surface. Thus it appears that fissures may be present in as-deposited weld metal in much the same form as in the bent pads.

The scanning electron microscope (SEM) may be utilized to study polished and etched weld metal sections in much the same manner as the light microscope revealing essentially the same information. At times the depth-of-field of the SEM is an advantage in studying both the polished and etched sections and the bent pad surfaces. Figure 12 is an SEM micrograph showing a fissure in a polished and etched, transverse, unbent section of 308 weld metal of low ferrite content (0.3 FN). The fissure is located along a grain boundary and, similar to the other fissures discussed, is adjacent to an interpass boundary (see arrow). The fissure surfaces are in much more intimate contact in this instance than was the case for the 309 fissure and the 316L fissure shown previously. It should be noted that the fissures in unbent 308, 308L, 316, 316L, and 16-8-2 types were generally "tighter" than those observed in the 309, 318, and 347 weld metals.

Locations where two or more HAZs overlap in underlying beads occur throughout thick section, multipass weldments, and these locations are prime sites for fissure formation. Figure 13, a light micrograph obtained from a transverse, polished and etched, bent section of 309 weld metal (0.4 FN), shows a fissure in just such a location. In this figure portions of three weld beads are shown and the two sets of arrows delineate the interpass boundaries which separate them. The fissure occurs in the first bead deposited, and it is to be noted that the

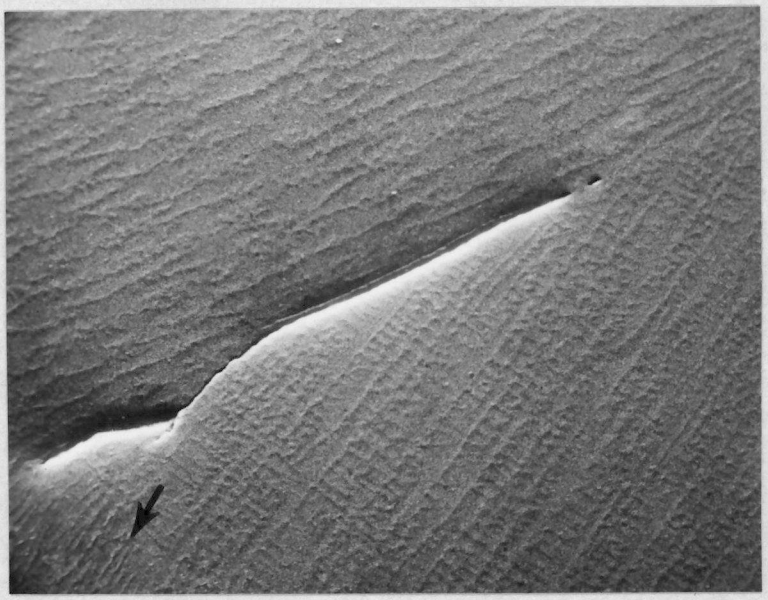

Figure 12. SEM micrograph of a fissure along a grain boundary near an interpass boundary (see arrow) in a polished and etched sample of 308 weld metal (0.3 FN), unbent, transverse section. 200X.

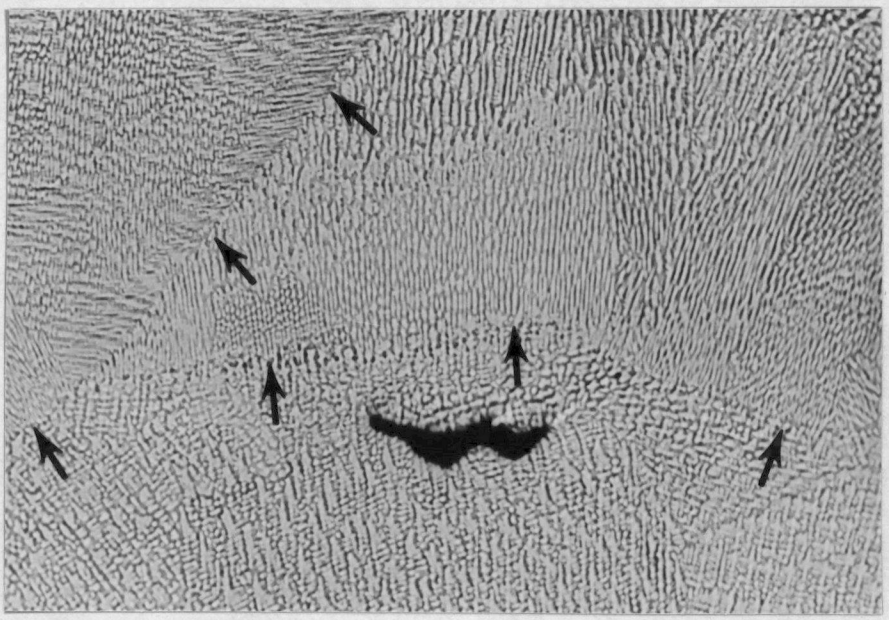

Figure 13. Light micrograph of a fissure near two interpass boundaries (see arrows) in a polished and etched sample of 309 weld metal (0.4 FN), bent, transverse section. 100X.

fissure is in the HAZ of the other two subsequently deposited beads. The fissure is also situated along a grain boundary as is the case for virtually all fissures. It will be shown later that weld metal at a location in a weld reheated to a high temperature by two or more subsequently deposited beads (and thus lies in the overlapping HAZs of those beads), experiences an increased susceptibility to fissuring.

Fissures are also observed on the weld pad surface of Fissure Bend Test specimens of low ferrite content. These fissures intersect the prepared surface, are opened by bend testing, and are subsequently revealed by penetrant and visual examination. Figure 14 is a light micrograph showing two fissures in a polished and etched, transverse section of a bent specimen of 309 weld metal (0.4 FN). The larger fissure in the upper right corner of the micrograph occurs along a grain boundary and is open to the surface of the weld pad. This fissure, and other fissures similarly opened to the pad surface, would be easily detected by penetrant testing and visual examination of the pad surface. Note that the fissure is also proximate to an interpass boundary (see arrows) and is thus located in the HAZ of a subsequently deposited bead. The small fissure in the lower left of the micrograph clearly occurs along a grain boundary and is also situated at the interpass boundary. Figure 15 shows this same fissure at a higher magnification. In only a few cases were fissures observed to be located precisely at or to span an interpass boundary.

The fissures discussed thus far all occurred in weld metal of low ferrite level (less than 1 FN in each case). Most austenitic weld metal types exhibit a general fissuring tendency at this low a ferrite level.



Figure 14. Light micrograph of two fissures (one open to surface) near an interpass boundary (see arrows) in a polished and etched sample of 309 weld metal (0.4 FN), bent, transverse section. 100X.

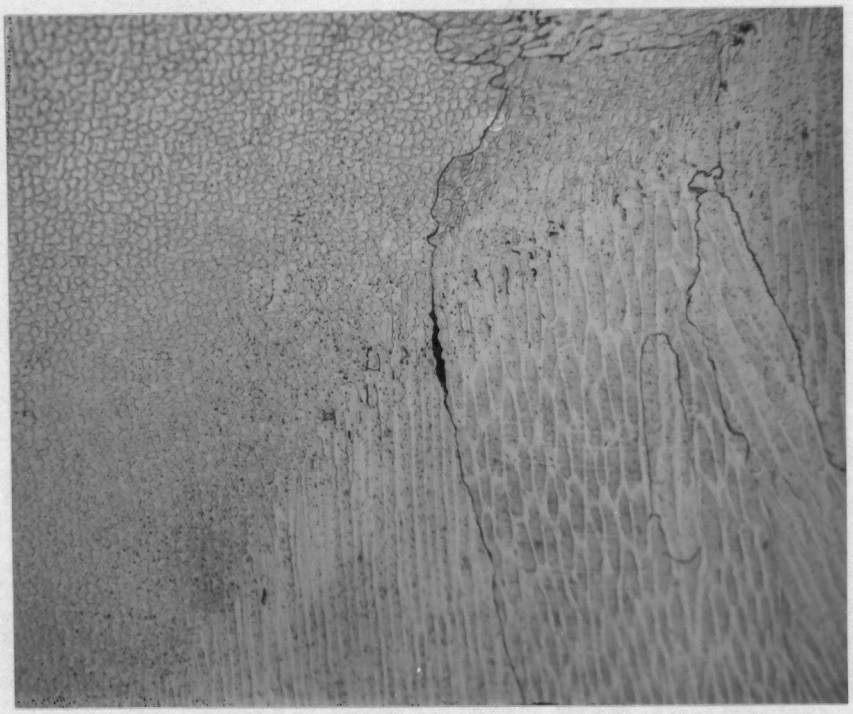

Figure 15. Light micrograph of smaller fissure in Figure 14 at 200X.

With increasing amounts of ferrite in the weld metal, the fissuring tendency quickly diminishes and is eventually eliminated at a ferrite level which may vary from 3 FN to 6 FN depending on the weld metal type. The nature and distribution of ferrite phase varies over this same range. At low ferrite levels the ferrite occurs as discrete particles located at the cellular dendritic substructure boundaries with a dominance for triple point intersections. As the nominal ferrite level is increased, the ferrite tends to progressively occupy more of the cell boundary area until at about 4 to 7 percent (44) the network becomes continuous throughout the cellular dendritic structure. A high nominal ferrite content does not, however, ensure uniform distribution throughout the weld metal. Gunia and Ratz (42), for example, report that a weld metal having an average of 2.8 percent ferrite may actually vary in ferrite content from 0.3 percent to 8.1 percent. This type of variation in ferrite level was observed and confirmed in many metallographic and SEM samples in the present study and also has been shown by others (44, 57, 82).

The result of ferrite variation within the microstructure is clearly illustrated by a consideration of data presented previously (see Figures 3 and 4, pages 23 and 24) and the micrographs shown in Figures 16, 17, and 18. Figure 16 is a light micrograph showing a fissure in a polished and etched metallographic specimen taken from a bent 316 weld pad (ave. 2.5 FN). This particular weld pad exhibited two penetrant indications which was considered unusual since the average ferrite level was higher than that determined to be necessary to prevent fissuring in 316 weld metal (see Figure 4). One of the indications was identified as a small area of lack of fusion between two weld beads which was not removed during

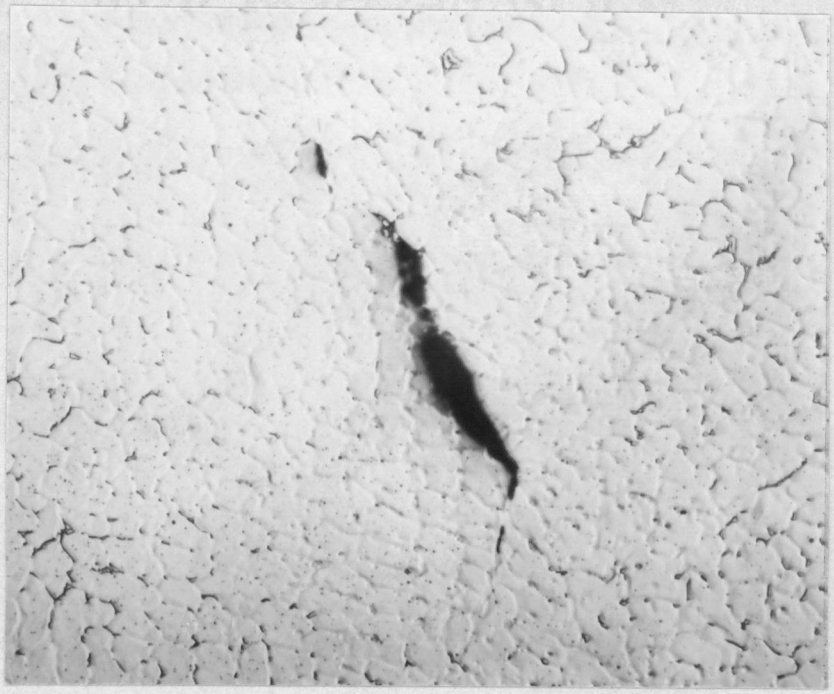

Figure 16. Light micrograph of a fissure in a ferrite-free area of 316 weld metal (ave. 2.5 FN), bent, longitudinal, top view section. 250X.



Figure 17. SEM micrograph of three fissures in a ferrite-free area near an interpass boundary (see arrows) in a polished and etched sample of 308L weld metal (4.0 FN), bent, longitudinal, top view section. 100X.



Figure 18. Light micrograph of a fissure in a ferrite-free area in a polished and etched sample of 308L weld metal (4.0 FN), bent, longitudinal, top view section. 150X.

pad surface preparation. The second indication proved to be the fissure shown in Figure 16. The ferrite in this figure is the dark constituent appearing predominantly along the cellular boundaries on the left and right sides of the micrograph. It is to be noted that the ferrite content in the immediate vicinity of the fissure is significantly lower than that in the surrounding areas.

The occurrence of fissures in ferrite-free areas was also observed in 308L weld metal. It had been previously determined that a ferrite level of approximately 3 FN in 308L weld metal is sufficient to prevent fissuring. However, in one bent weld specimen of 308L with ferrite level of approximately 4 FN, six closely grouped fissures were found (see Figure 3, page 23). These fissures were approximately 0.010 to 0.020 inches in length and were all located within 0.20 of an inch of each other near an interpass boundary. The ferrite level of this general area was recorded to be 4.0 FN when measured with a Magne Gage. Metallographic evaluation of a polished and etched sample taken to include these six fissures revealed that they were located in an essentially ferrite-free area. This occurrence is best illustrated by the SEM micrograph of the polished and etched surface taken to include three of the six fissures (Figure 17). In this figure the ferrite is the light constituent in the cellular boundaries and it occurs extensively in the region to the right of the interpass boundary (see arrows). It is observed that ferrite exists only along portions of the grain boundaries in the bead to the left of the interpass boundary, and the remainder of the substructure in this bead is essentially ferrite-free. Furthermore,

the fissures extend toward the interpass boundary but only up to the location where ferrite is present in the grain boundaries along which they occur.

To those unfamiliar with the interpretation of SEM micrographs taken from polished and etched surfaces, one of the six fissures discussed above is shown in the light micrograph in Figure 18. From this figure it is clear that the fissure is in an area devoid of ferrite, but high concentrations of ferrite exist in close proximity to the fissure.

The evidence presented is surely sufficient to illustrate that fissures can occur in nominally "high" ferrite-containing weld metals, but these fissures are confined to the randomly occurring ferrite-free regions.

Other discontinuities detected. During the course of the investigation to determine the ferrite-fissuring relationship in austenitic stainless steel weld metals, several penetrant indications were found that resulted from discontinuities other than fissures. These indications were originally considered to be fissures, but metallographic and scanning electron microscopy examination later revealed the true nature of the discontinuities.

One type of indication is illustrated in Figures 19A and 19B which are light micrographs of the surface of a polished and etched, bent sample of 308L weld metal (2.5 FN). These figures show, at 250X and 500X respectively, tears along cellular intersections where austenite and ferrite exist. The tears were caused by surface grinding during weld pad preparation and they were detectable by fluorescent penetrant testing.

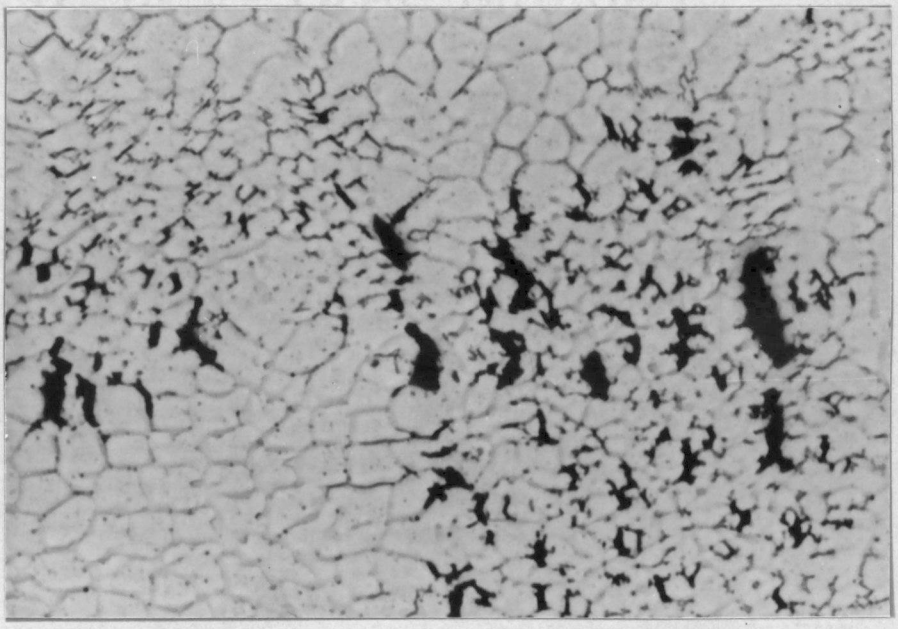

A. 250X

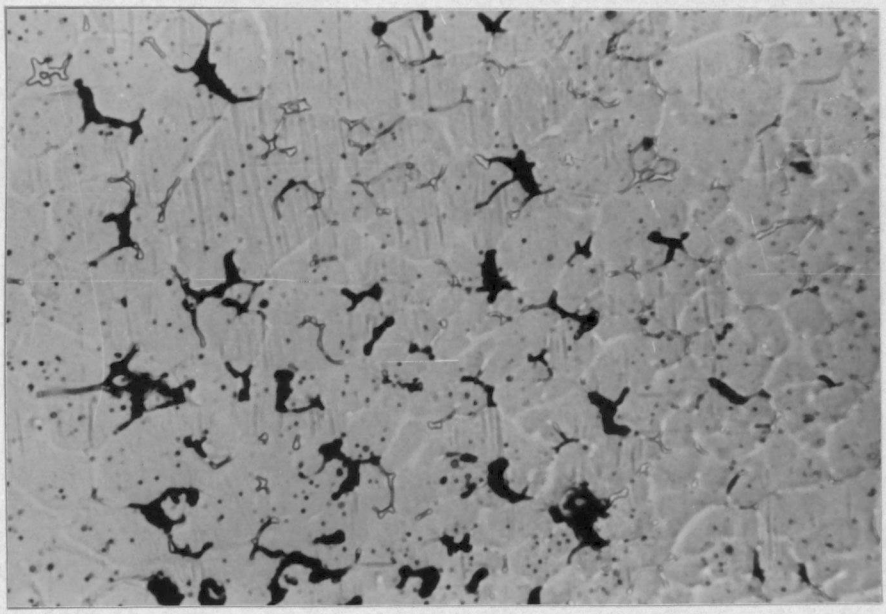

B. 500X

Figure 19. Light micrograph of grinding tears in a polished and etched sample of 308L weld metal (2.5 FN), bent, longitudinal, top view section.

Tears such as these occurred in areas of high ferrite content and they did not appear in areas almost wholly austenitic. The observation of these grinding tears in high ferrite areas is in contrast to the occurrence of fissures which generally appear in ferrite-free areas.

Another type of indication that was originally mistaken for fissuring was observed in a specimen of 309 weld metal (see Figure 6, page 26). The specimen had a ferrite level of 2.8 FN and was expected to exhibit a very low fissuring tendency. However, upon bend testing of the specimen, over 60 cracks appeared across the surface of the weld metal. All of the cracks in this specimen exhibited an unusual morphology in that they occurred both perpendicular to the grinding direction and almost perfectly perpendicular to the direction of the tensile strain generated during bend testing. Furthermore, they occurred in a very random fashion across the pad surface and were not located near the interpass boundaries as was the case for true fissures observed in other specimens.

Figure 20, an SEM micrograph of the bent surface of the pad, shows one of the cracks described. Note that the crack is generally shallow as were the other cracks observed in this pad. The grinding marks are clearly evident, running from top to bottom in this micrograph. They are perpendicular to the longitudinal axis of the crack and are aligned with the length of the weld pad specimen. The severity of the grinding marks is characteristic of good grinding practice and is not considered to be related to this crack formation mechanism.

The fracture surface of a crack typical of those found in this sample is shown in the SEM fractograph in Figure 21. The crack exhibits



Figure 20. SEM micrograph of a surface fissure in an as-ground 309 weld metal pad (2.8 FN), bent, longitudinal, top view section. 100X.

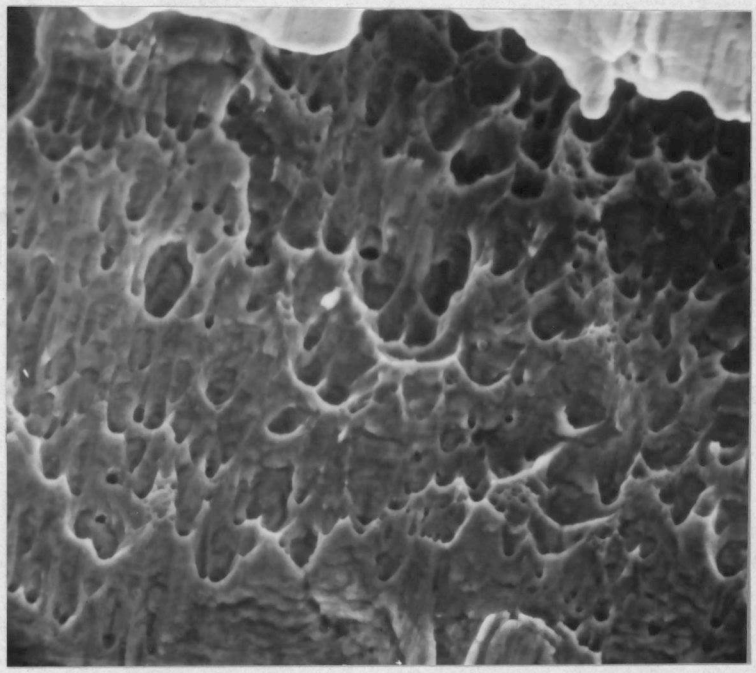

Figure 21. SEM micrograph of fissure surface (Figure 20) showing ductile fracture characteristics in a 309 weld metal pad (2.8 FN), bent, longitudinal, top view section. 2000X.

a dimpled surface characteristic of ductile rupture. The dimpled surface is not in keeping with the appearance of cracks or fissures resulting from one of the hot cracking phenomena to be discussed at length in a subsequent section. The precise cause for cracking in this one specimen (its companion specimen at identical ferrite level behaved in the expected manner) has not been determined.

Another penetrant indication originally identified as a fissure was a discontinuity found in a bent 316L weld pad at a ferrite level of 5.6 FN (see Figure 5, page 25). This discontinuity is shown in Figure 22. In Figure 22A, an SEM micrograph of the pad surface, the discontinuity outwardly appears to be a true fissure. However, because it had been determined that a ferrite level of 1.5 FN was sufficient to prevent fissuring in 316L weld metal, an explanation for the occurrence of this "fissure" at a ferrite level of 5.6 FN was in order. Thus a metallographic sample containing the "fissure" was removed from the pad and polished and etched in order to determine its true nature. Figure 22B, an SEM micrograph obtained from the polished and etched sample, clearly shows that the discontinuity is, in actuality, a crack in an inclusion within the weld metal. Note that the distribution of ferrite in the cell boundaries of the weld metal surrounding the inclusion is virtually continuous at this ferrite level of 5.6 FN. The crack extends across the inclusion but does not extend into the surrounding weld metal. Thus the discontinuity is not related to fissuring of the weld metal in any manner. Apparently, the crack formed as a result of differential contraction rates during solidification or because the inclusion was unable to deform with the surrounding material during bending. Due to the



A. Discontinuity on as-ground pad surface. 500X.

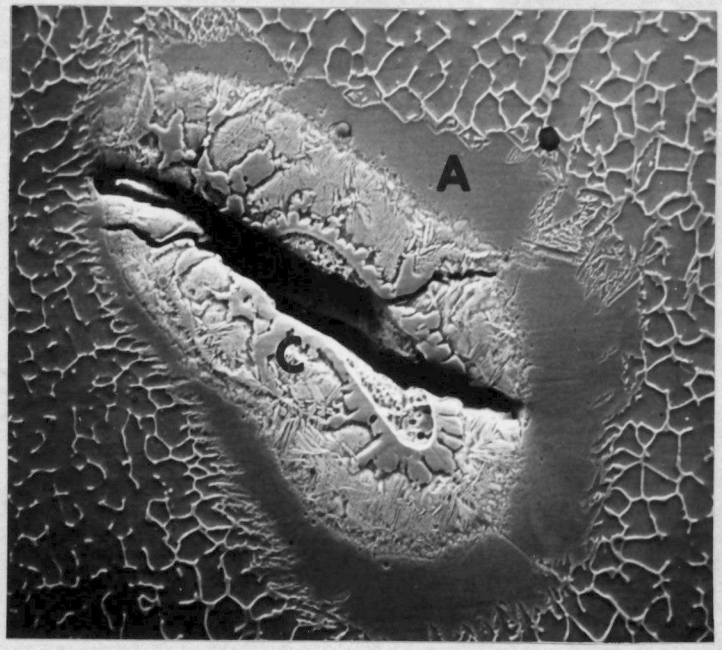

B. Discontinuity on polished and etched surface. 500X.

Figure 22. SEM micrograph of a discontinuity in a 316L weld metal pad (5.6 FN), bent, longitudinal, top view section.

unusual appearance of the inclusion, microanalysis was performed on various areas (see Figure 22B, areas A, B, and C) by utilizing the energy dispersive x-ray mode of the SEM. The elemental distribution was determined in the three regions shown. Iron, nickel and chromium were found in region A and the analysis of region B yielded iron, nickel, and chromium with a small indication of sulphur. The elements in the center region C were iron and sulphur only. Thus the inclusion was determined to be of a duplex nature with the crack occurring in the center core of FeS.

While the occurrence of the discontinuities discussed above has been observed only in isolated cases, the documentation of their true nature has proven beneficial because it has been shown that "fissure-like" indications at high ferrite level in austenitic stainless steel weld metals may be unrelated to the fissuring behavior of the weld metal per se. Thus it is not always equitable to disparage the soundness of the weld metal without sufficient investigation and documentation of the occurrence.

Fissure behavior during bend testing. The examination of unbent, surface prepared Fissure Bend Test pads (whether they be milled, ground, or metallographically polished and etched) rarely reveals any fissures for most austenitic weld metals. Weld metals 347 and 318 studied here are notable exceptions as these metals exhibited a significant number of fissures on surface ground, unbent pads of low ferrite level. To enhance fissure detection, the test specimen is bent so that the pad surface is subjected to a tensile strain. In general, for all weld metal types at

low ferrite content, the bending operation exposes fissures intersecting or proximate to the pad surface. The number of fissures detected is dependent on many factors including: the weld metal type, the bending strain, the method of surface preparation, the type of microscope utilized, and the magnification at which the pads are examined for fissures. However, since fissure detection was facilitated by bending, the question of whether the bending operation produced fissures, caused fissures to propagate or elongate, or merely opened the fissures laterally for detection had to be answered. Thus a testing program was initiated to determine: (1) whether the bending operation produced fissures; (2) the extent of bending strain necessary to expose fissures for detection; and (3) whether fissures extend in length during bending. To accomplish this task, several Fissure Bend Test pads of 308, 316 and 16-8-2 weld metal (all of low ferrite level) were deposited, ground and metallographically polished; and then the pads were examined for fissures. The surfaces were then etched and reexamined. The pads were next subjected to bending in incremental steps and were thoroughly examined after each bending operation. During each examination, particular attention was paid to the interpass boundary region where fissures were expected to be found. Examination of these test specimens at 100X to 200X revealed only two fissures in the unbent pads, one being in a 308 specimen and the other in a 316 specimen. It was somewhat surprising that so few fissures were found even though the pads were polished, etched and examined at 200X.

When each pad was bent to cause a small but perceptible degree of plastic flow ($\simeq$ 0.4 percent strain, $\simeq 1^{\circ}$ bend angle), they were carefully

and thoroughly examined and some fissures were found in the 308 and 316 weld metal. However, for the 16-8-2 weld metal pads about 2 percent plastic strain ($\simeq 4^{\circ}$ bend angle) was necessary to initially discover any fissures on the pad surface. Upon further study it became apparent that the orientation of a fissure with regard to the longitudinal strain applied was the primary condition determining the extent of fissure interface separation. The degree of plastic flow on a microscale as influenced by the orientation of the grains surrounding the fissure location also affects the extent of fissure interface separation. For each weld pad examined, the number of fissures was counted at different degrees of bending, and it was determined that more fissures were found as the bend angle increased or alternately as the extent of straining intensified. To document the phenomenon occurring as bending strain was increased, photomicrography at 200X was carefully and painstakingly performed to unequivocally document the change in fissure appearance. It is to be noted that it was extremely difficult to predetermine the location of fissures in unbent samples even when the microstructure was studied at 500X magnification.

Figures 23 through 26 are a series of light and SEM micrographs documenting the appearance of a fissure in 308 weld metal (0.4 FN) at increasing levels of bending strain. In Figure 23 the weld metal has been subjected to about 1 percent plastic strain. The cellular substructure is discernible and the slip bands are clearly confined to particular grains but cross the cell boundaries without alteration of direction. The surface contour is changing from the plane produced during polishing to an undulating surface as each grain flows in

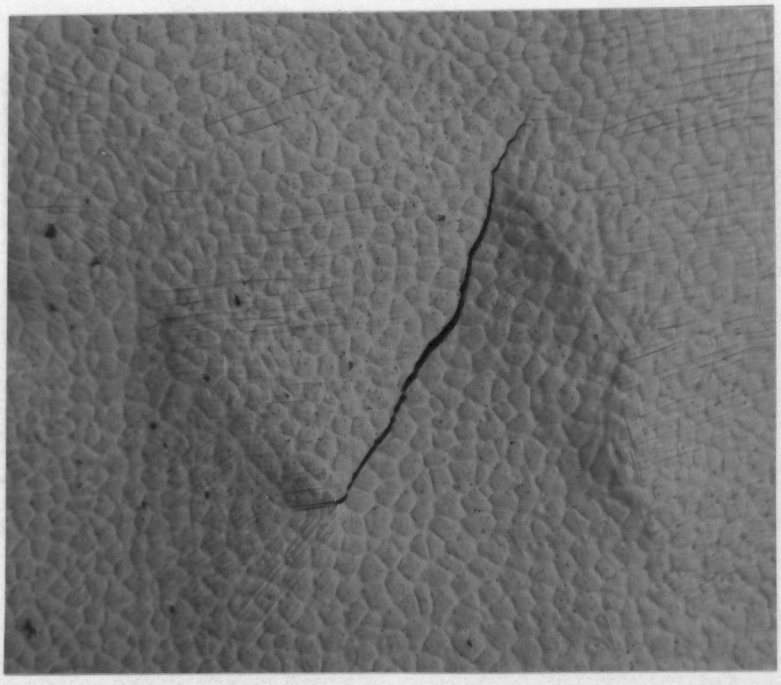

Figure 23. Light micrograph of a fissure in a polished and etched 308 weld metal pad (0.4 FN), 1 percent plastic strain, longitudinal, top view section. 200X.

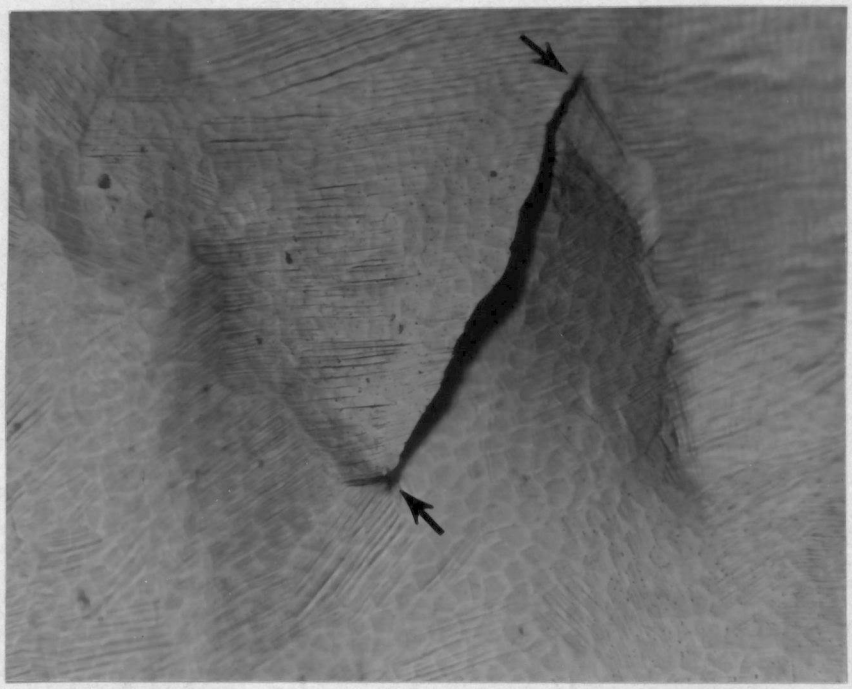

Figure 24. Light micrograph of the same fissure shown in Figure 23, 4 percent plastic strain. 200X.

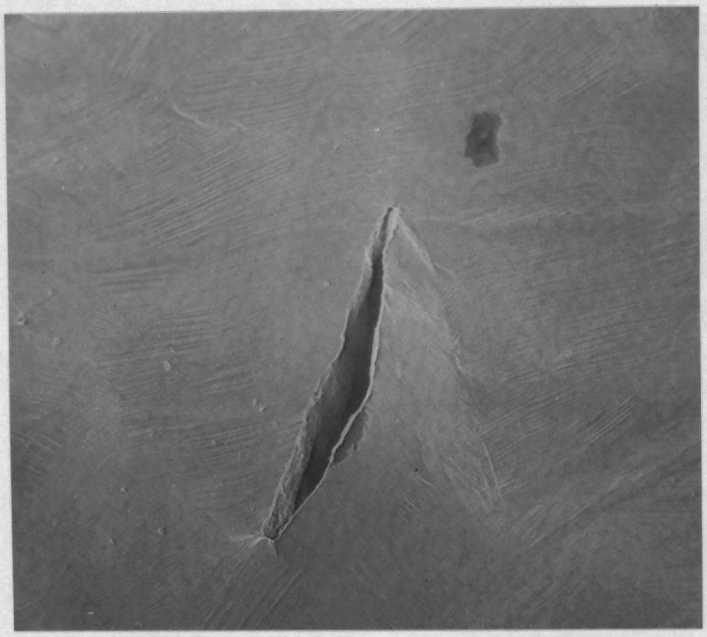

Figure 25. SEM micrograph of the same fissure shown in Figures 23 and 24, 20 percent plastic strain. 180X.

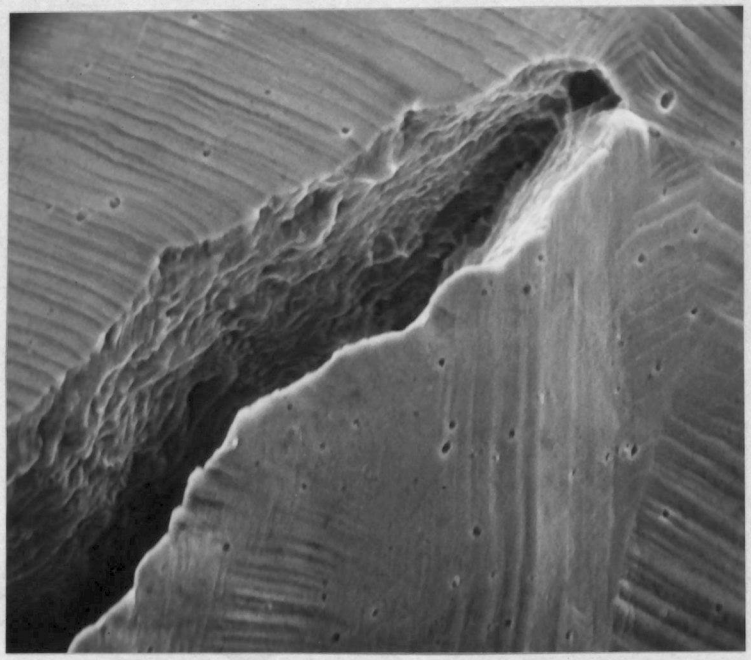

Figure 26. SEM micrograph of the tip of the fissure shown in Figure 25. 1800X.

response to its particular orientation and degree of strain. The fissure in the figure is about 0.011" in length and its ends are well defined. Because the slip band orientation is different on either side of the fissure, it is obvious that the fissure is located along a grain boundary. This becomes even more evident in Figure 24. Note that there is very little evidence of ferrite in the microstructure. Figure 24 shows the same fissure after the pad has been bent to produce 4 percent plastic strain (20° bend angle). The fissure width has increased but the length of the fissure is exactly the same as in Figure 23. The slip bands across the grains are becoming more extensive and the strain concentration at the ends of the fissure (see arrows) is evident. Because of the curvature of the weld pad surface and because of the differences in surface contour between the grains, several areas of the micrograph are slightly out of focus. The use of the scanning electron microscope eliminates the depth of field difficulty, and this is illustrated by the SEM micrograph in Figure 25 showing the same fissure after the weld pad has been bent 60° (120° included angle). The weld metal in the area of the fissure was subjected to about 20 percent plastic strain from the bending, and the severity of the surface deformation is evident. The amount of tilt and the slight difference in magnification of this micrograph from the previous two micrographs prevent a direct comparison of the size of the fissure. However, it is obvious that the fissure has not extended in length but has merely opened in width. Figure 26 is a SEM micrograph showing a portion of the tip of the fissure shown in Figure 25. The slip bands in the grains surrounding the fissure are easily seen.

The ends of the fissure appear blunted, and again it is plainly evident that the fissure did not propagate.

The effect of bending strain on the appearance of a fissure in 316 weld metal (0.4 FN) is similarly illustrated in Figure 27. Figure 27A is a light micrograph showing the fissure in the weld metal subjected to 0.4 percent bending strain. The fissure, 0.010" in length, is located along a grain boundary and its ends appear well defined. Only a small number of slip bands is evident on the weld metal surface. Figure 27B is a light micrograph showing the same fissure after the weld metal has been subjected to 1 percent plastic bending strain. The extent of strain at the ends of the fissure is evident from the slip bands concentration. By comparison of Figures 27A and 27B, it appears that the fissure increased slightly in length at one end (see small arrow in Figure 27B). However, this small portion of the fissure lies approximately parallel to the direction of bending (see large arrows), and thus the 0.4 percent plastic bending strain as shown in Figure 27A may have been insufficient to expose this segment of the fissure. Figure 27C is a light micrograph showing the fissure after the weld pad was subjected to 2 percent plastic strain. The concentration of strain at both ends of the fissure is severe, but it is obvious that the fissure has not propagated. The fissure has widened and it is to be noted that the direction of shift of the fissure walls is in the direction of the applied bending strain (see arrows, Figure 27C). Figure 27D is an SEM micrograph of the fissure, taken at a slightly reduced magnification and at a high degree of tilt, after the weld metal was subjected to about 20 percent

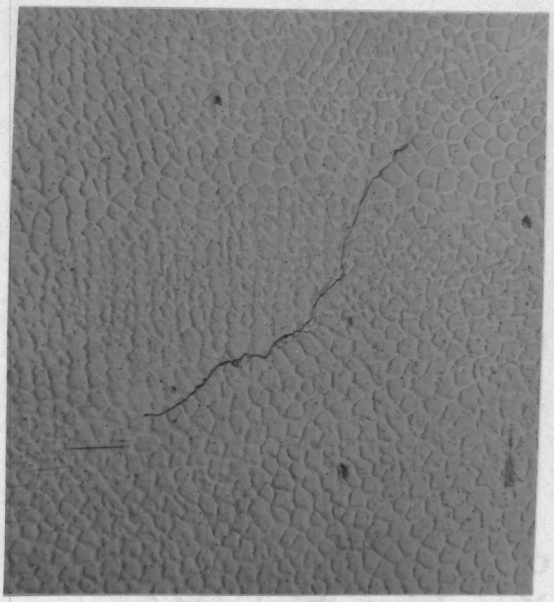

A. Light micrograph, 0.4 percent plastic strain. 200X.

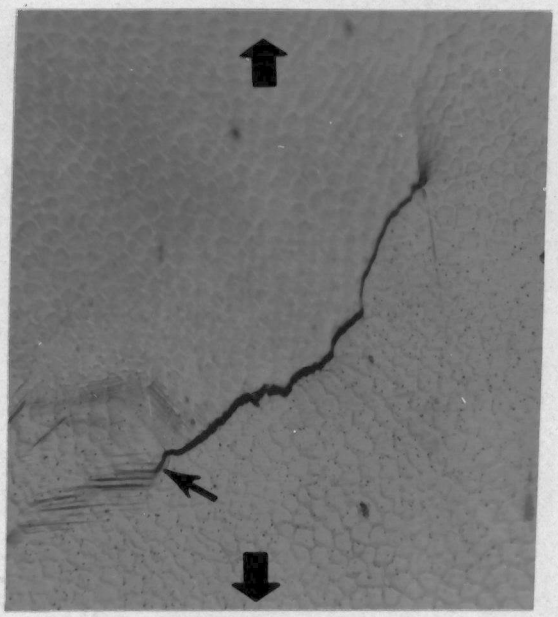

B. Light micrograph, 1 percent plastic strain. 200X.

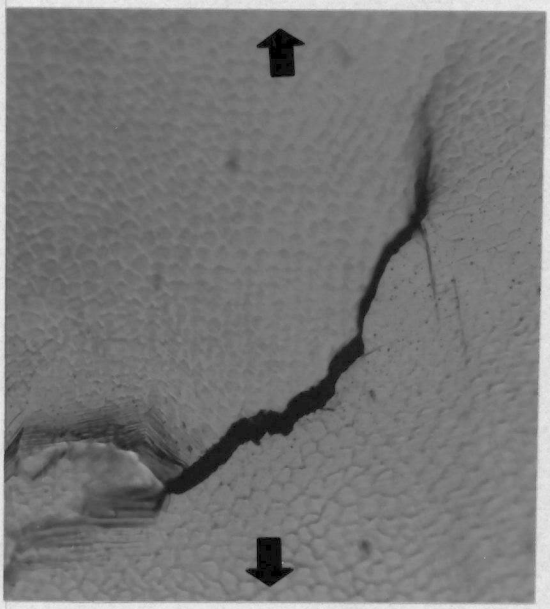

C. Light micrograph, 2 percent plastic strain. 200X.



D. SEM micrograph, 20 percent plastic strain. 180X.

Figure 27. Micrographs of a fissure in a polished and etched 316 weld metal pad (0.4 FN) as a function of bending strain, longitudinal, top view section.

plastic bending strain. The fissure has opened but clearly has not increased in length even with this extensive amount of bending strain.

During the investigation to determine the effect of bending strain on fissure appearance, it was decided to document two closely spaced fissures at increasing levels of bending strain to discern if they would interconnect. The fissure area selected is shown in Figure 28, a series of light micrographs illustrating two closely spaced fissures on a 316 weld pad (0.4 FN) surface. Figure 28A shows the area selected after the pad has been bent to produce approximately 0.4 percent plastic strain. In this figure there are two fissures, with one appearing in the top (totally contained within the micrograph) area and with one in the lower portion extending outside the confines of the photomicrograph. The fissure at the top of Figure 28A is 0.010" in length and is located about 0.008" from the other fissure. Figure 28B shows the two fissures after the weld metal pad has been subjected to about 1 percent plastic strain. Portions of the figure are slightly out of focus because of the curvature of the weld pad surface due to bending. It is to be noted that the fissures have not propagated or interconnected. The fissures are shown in Figure 28C after the weld metal was subjected to 4 percent bending strain. The fissures have not interconnected and show no indication of propagating. In fact, when the fissures were subjected to full bending (about 20 percent plastic strain), they did not interconnect or show any tendency to propagate.

The preceding three series of micrographs are typical of all weld metals tested with regard to the appearance of fissures and the manner in which they open with increasing amounts of bending strain. In only

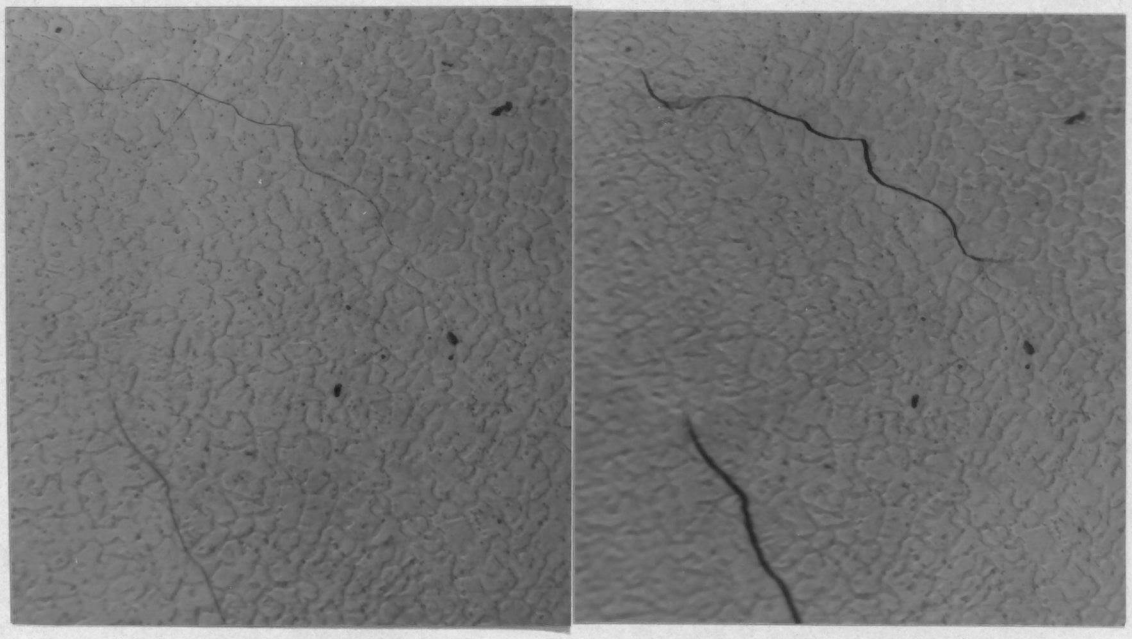

A. 0.4 percent plastic strain. 200X.

B. 1 percent plastic strain. 200X.

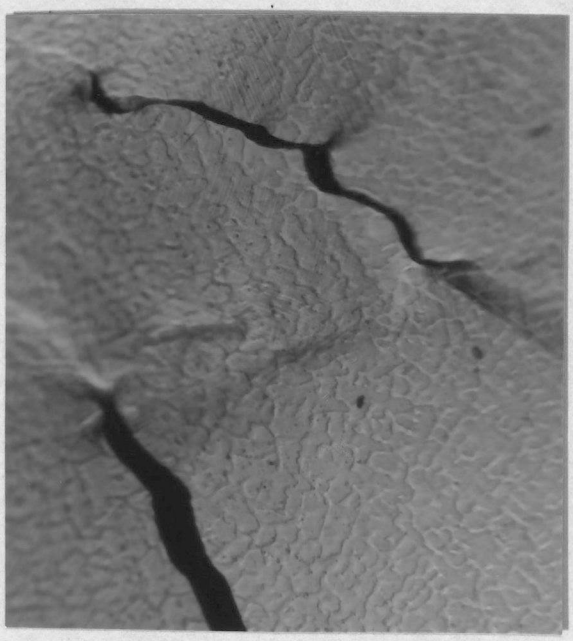

C. 4 percent plastic strain. 200X.

Figure 28. Light micrograph of two fissures in a polished and etched 316 weld metal pad (0.4 FN) as a function of bending strain, longitudinal, top view section.

two instances were fissures observed to propagate or interconnect during bending. This occurred only when two fissures were very closely aligned axially (and thus most likely situated along a mutually shared grain boundary). In both instances the amount of weld metal separating the fissures was small in comparison to the size of the fissures, and the fissures may very well have been interconnected before bending along the grain boundary in the weld metal beneath the plane of examination.

In order to determine if the orientation of the weld beads with regard to the direction of applied strain (longitudinal) in the Fissure Bend Test scheme would alter the location of the fissures or change the extent of fissuring, a study where the beads were deposited transverse to the longitudinal axis of the test specimen was undertaken. This transverse bead sequence yielded the same area for evaluation and about the same length of interpass boundary. There was no difference in location, size or distribution of fissures, and the number of fissures was of the same order as that found in the longitudinal weld beads.

Before leaving the subject of the influence of strain on fissuring, several salient points should be made. As indicated in the introduction, strain invariably plays a part in the fissuring mechanism. Naturally the strains experienced by actual weldments occur over a range of temperatures and are altered as each bead is deposited in a multipass weld. The level of strain experienced during welding has been the subject of continued research but is fraught with the necessity to deal with high temperatures and their attendant problems in the realm of measurement. However, several investigators have documented the extent

of surface strains both transverse and longitudinal to the weld bead. Williams et al. (88) report that the transverse strains are approximately twice as large as the longitudinal strains in austenitic stainless steel welds. For a single weld bead deposited in a groove in thick plate, surface strains of approximately 4 percent are obtained in the transverse direction. These authors also state that the strains beneath the surface are much higher but naturally defy direct measurement. Zhitnikov and Zemzin (89) report very similar results for austenitic stainless steel, confirming that the strains adjacent to a weld bead are 3 to 4 percent as a minimum. They further state that the strains between two closely spaced beads may be twice as high as those occurring along side a single weld bead. Shron (90) discussed the triaxiality of strain in thick weldments and relates the strain accumulation in any one zone to the properties of that zone.

The extent of strain through the thickness of a heavy section, multipass weld is not well known but Brooks and Spruiell (91) report that from dislocation densities present in 2 1/2" thick 308 weldments, the accumulated strain may be as high as 20 percent. One can easily visualize high strains in thick section weldments after once observing the extent of distortion evident if improper weld restraint is not utilized during welding. Suffice it to say that strains of 4 percent and greater always occur during welding of stainless steels and that the subsurface strains are much higher and may reach 20 percent.

Consider now the pad type specimens utilized for bend testing. These "deposited on the surface" beads would naturally be less severely strained

than those beads deposited in a groove in a heavy section weldment. In fact these test pads should represent the minimum restraint. The additional strain applied during bend testing may be equated to the additional strains occurring in thick section weldments (where fissures are observed). However, it should be recognized that all the additional strain in bend testing is applied at room temperature whereas in a weldment the strains accumulate over a range of temperatures (any testing scheme suffers from some deficiencies). Nevertheless, the fissures observed in the bend specimens occur at the precise location and have the same appearance as those occurring in thick section weldments (81-83). An almost unbelievable one-to-one correlation exists. These observations strongly suggest that the same phenomena are occurring during pad production as occur in the heavy section weldments, save for a lesser total amount of strain accumulating in the pad. Thus, it appears that the fissures are present but tightly closed until the strain is applied during bend testing. Then and only then do they open sufficiently for detection.

If fissures in austenitic stainless steels are to be assessed as important in regard to mechanical properties, the "openness" of the fissures will not be an influential parameter. The size, shape, location and notch acuity are the truly important aspects. Thus whether a fissure is "tight" or "open" should not be important, and an incipient (unopened) fissure will be as important (<u>if important at all</u>) as one which is open and observable. In light of the influence of a fissure on the mechanical properties of austenitic stainless steel, it should be noted again that

the fissures did not propagate during bend testing and, in fact, the ends of the fissures actually become blunted during deformation

Fissure surface morphology and energy dispersive analysis. To gain insight into the mechanism of fissure formation in austenitic stainless steels, the surfaces of the fissures in many weld metal types were examined utilizing the scanning electron microscope. In addition, energy dispersive x-ray analysis was performed on the fissure surface in an attempt to document segregation of certain elemental species. This examination technique and an indication of the useful information which can be obtained has been described by Lundin (76, 87) and Honeycombe and Gooch (77, 78, 92).

Honeycombe and Gooch (77) claim to have documented three different fracture morphologies for 310 and 316: (1) a morphology which exhibited generally smooth features, (2) a morphology which showed dendritic films, (3) a morphology which showed a relatively featureless surface with many small particles on the surface. Lundin (76, 87) has observed morphology one in nickel, 310 stainless, X-750, TZM, molybdenum and Inconel 600, and he has observed morphology three in Inconel 600. Honeycombe and Gooch report that form one predominates and that forms two and three were less prevalent. This is in line with the observations of Lundin and the studies in this case for all the weld metals investigated.

In both morphologies one and two a liquid film plays a role in the cracking mechanism. In morphology one a single film generally covers the entire surface while in morphology two the film may result from two different liquated phases. In all of the observations in this study, only one film type was noted.

The three SEM fractographs shown in Figures 29A and 29B and Figure 30 characterize the observations in this instance. Figures 29A and 29B show the predominant morphology at approximately 1000X and 2000X respectively. The pad surface can be seen in the upper and lower portions of Figure 29A with the fissure surface extending across the central portion. The central portion only is shown in Figure 29B. Note that the surface has a smooth appearance with a number of small holes and also protuberances extending upward from the surface. All of these features suggest, as has been shown by others (76, 77, 87), that a liquid film existed in this region at the time separation of the material occurred causing a fissure. The general shape of the cellular dendrites can be discerned (extending upwards in these micrographs). The protuberances extending upward from the surface result from the liquid metal necks that developed during separation with the liquid film present. The necked regions subsequently ruptured as the fissures opened. The features present on the surface defy explanation except for a liquid film hypothesis. Thus the fissures exposed during fissure bend testing originated at an elevated temperature and were not created during bending.

The fissure surface shown in Figure 30 at 4500X is typical of only a small number of fissures, and it appears to be slightly different from those surfaces typified by Figures 29A and 29B. Although it has relatively smooth features characteristic of the prior presence of liquid film, its features are somewhat finer. It is not considered to be associated with distinctly different mechanisms of fissure formation.

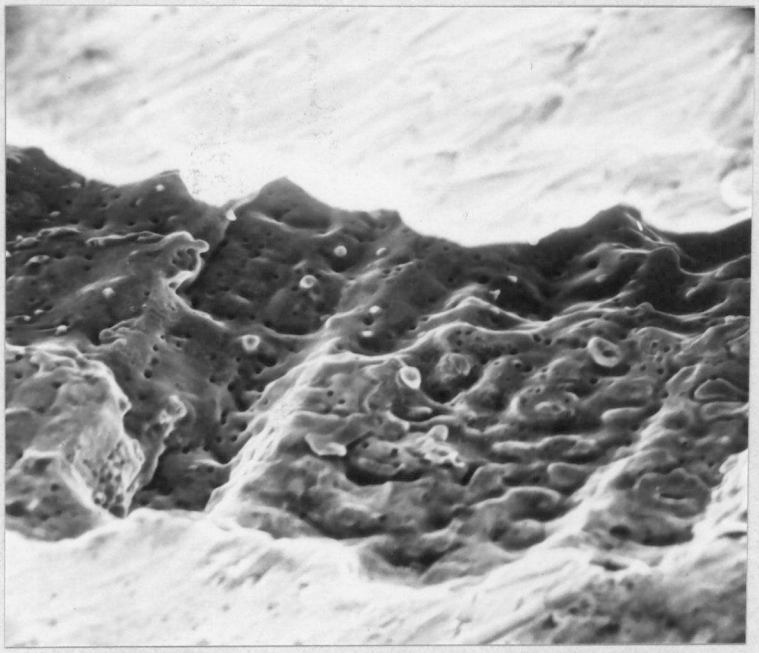

A. 1000X.

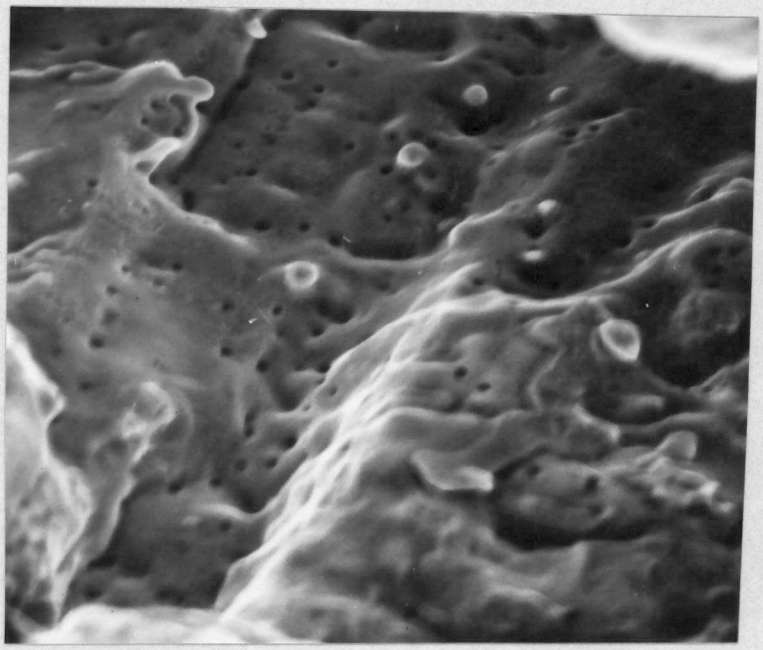

B. 2000X.

Figure 29. SEM micrograph showing the predominant type of fissure surface morphology.

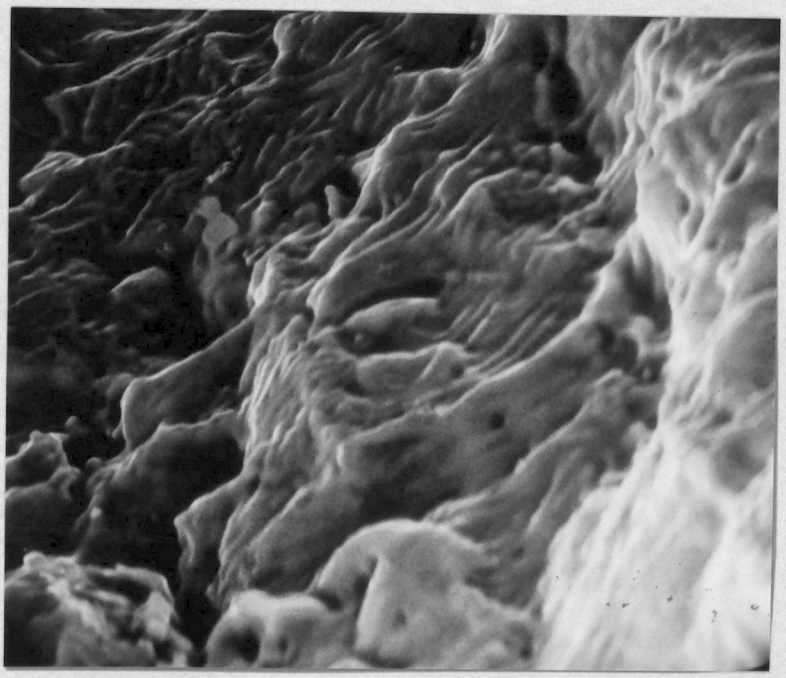

Figure 30. SEM micrograph of secondary fissure surface morphology. 4500X.

The fissure surfaces were analyzed using the energy dispersive x-ray mode of operation in the scanning electron microscope. As was anticipated and attested to by Honeycombe and Gooch (77), only the major alloying elements, iron, nickel, and chromium, and where appropriate molybdenum and columbium, were revealed. The SEM does not have the capability of detecting, even qualitatively, small amounts of trace elements on fracture surfaces, and it fluoresces the material to a considerable depth thus precluding elemental characterization of the remnants of the liquid film alone. Auger electron spectroscopy is perhaps an alternative approach to the problem although it is difficult to apply.

In summation, it is clear that a liquid film plays a dominant role in the fissure formation observed in all of the stainless steel weld metals studied. However, the elemental species responsible for or associated with these films has not been revealed.

Fissure sizes. The size of fissures present in austenitic stainless steel weld metal is of prime importance in that the fracture mechanics approach to weldment failure is in some instances able to predict crack propagation under service conditions. This has in essence been recognized by code writing bodies, in particular the AEC in their Regulatory Guide 1.31 (1) of June 1973 as modified by a position statement in April 1974.

For the 308, 308L, 316, 316L, 309, and 16-8-2 weld metal pads tested in the initial phase of this study, the fissures found very rarely exceeded 1/16 inch in length (only one fissure out of 460 exceeded 1/16"). The majority of the fissures were less than 1/32 inch in length.

The 318 and 347 weld metals exhibited larger fissures at the A ferrite level than did the other weld metals tested. Approximately 5 percent of all fissures in the 318 weld metal (A ferrite level) and almost 10 percent of all fissures in the 347 weld metal (A ferrite level) were 1/16 inch in length or longer. In general, when comparing the average fissure size between the A and B levels in the initial phase of study, the fissures were smaller for the B ferrite level than for the A ferrite level. This applies to all the weld metals tested in which fissures were detected at both A and B ferrite levels.

Arata et al. (64) have published some recent data on the crack sizes of autogenous bead-on-plate austenitic stainless steel welds. Their information was obtained by utilization of the Varestraint technique (93, 94) which applies an arbitrary level of strain on the solidifying weld bead. Their data agree with that found in this study in that the fully austenitic stainless steel welds exhibit more extensive fissuring and increased fissure size as compared to austenitic stainless steels with delta ferrite present in the weld microstructure. For ferrite-containing welds, their data show that both the maximum crack size and the total extent of cracking decrease as ferrite level increases. Unfortunately, their study did not include a range of ferrite for any of the stainless steels investigated as the ferrite level was obtained from the ferrite potential of the autogenously melted wrought plate. However, it is of note that the maximum crack size reported (for 316L--0 percent ferrite) was 0.049 inches. As the ferrite level increased to approximately 2 percent (for 316), the maximum crack size decreased to

approximately 0.024 inches, a size comparable to those measured in the present study.

During the investigation of the important variables of the Fissure Bend Test (see Chapter IV), three methods of pad preparation were utilized and evaluated with regard to the detection of fissures in 308, 316 and 16-8-2 weld metals. This evaluation yielded information as to the number of fissures detected, size of fissures, and size distribution of fissures in these weld metals. The fissure size-preparation data are shown in Figures 31 through 36. These figures will be useful in gaining an appreciation for the size distribution of the fissures and for illustrating how the "apparent" average fissure size varies with the ultimate resolution possible from the preparation and measurement techniques.

Figures 31, 32, and 33 present the data for the 308 weld metal, and Figures 34, 35, and 36 show the data for the 316 weld metal. In each of these figures the percentage of the total number of fissures observed within each 0.0025" size increment is shown. (Note that the total number of fissures observed varies for each surface preparation technique.) Three different surface preparation techniques were evaluated: (1) "Milled"--milling the surface and finishing with a 0.002" milling cut, (2) "Surface ground"--milling the pad surface followed by grinding with eight passes of 0.001" and finishing with four passes of 0.0005", (3) "Metallographically polished"--milling followed by grinding with eight passes of 0.001" and four passes of 0.0005" and finished by metallographically polishing the surface.

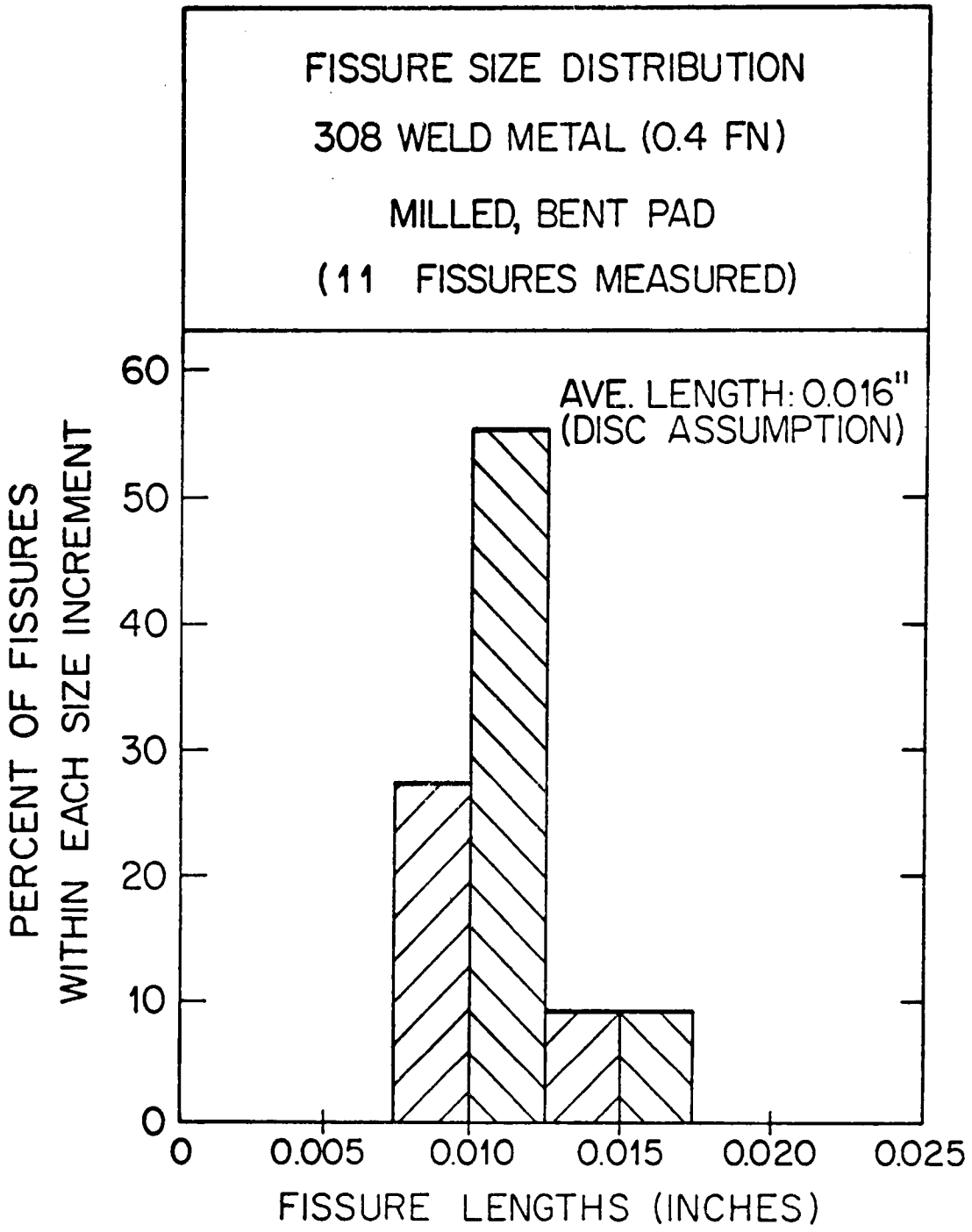

Figure 31. Fissure size distribution for 308 weld metal, milled surface.

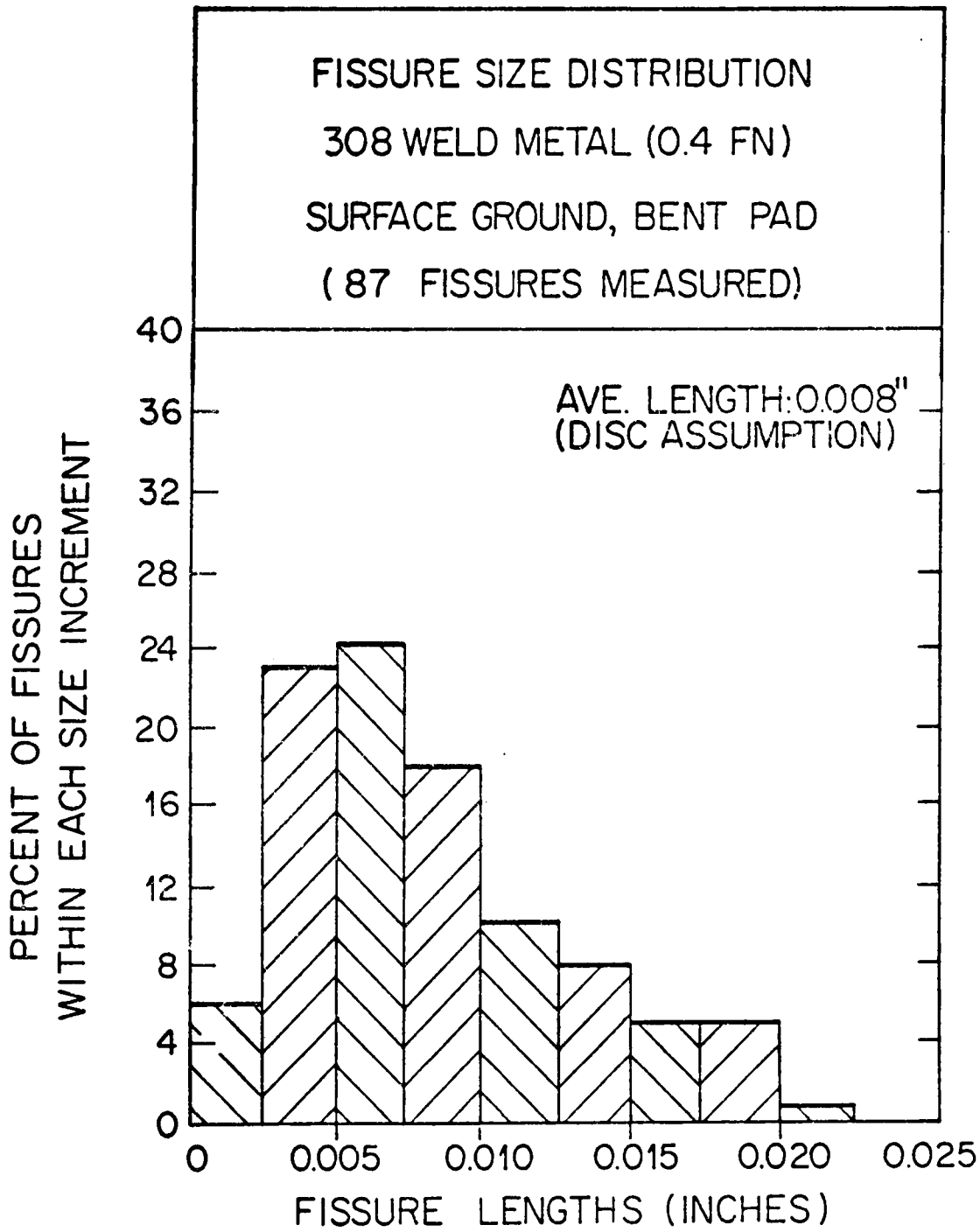

Figure 32. Fissure size distribution for 308 weld metal, ground surface.

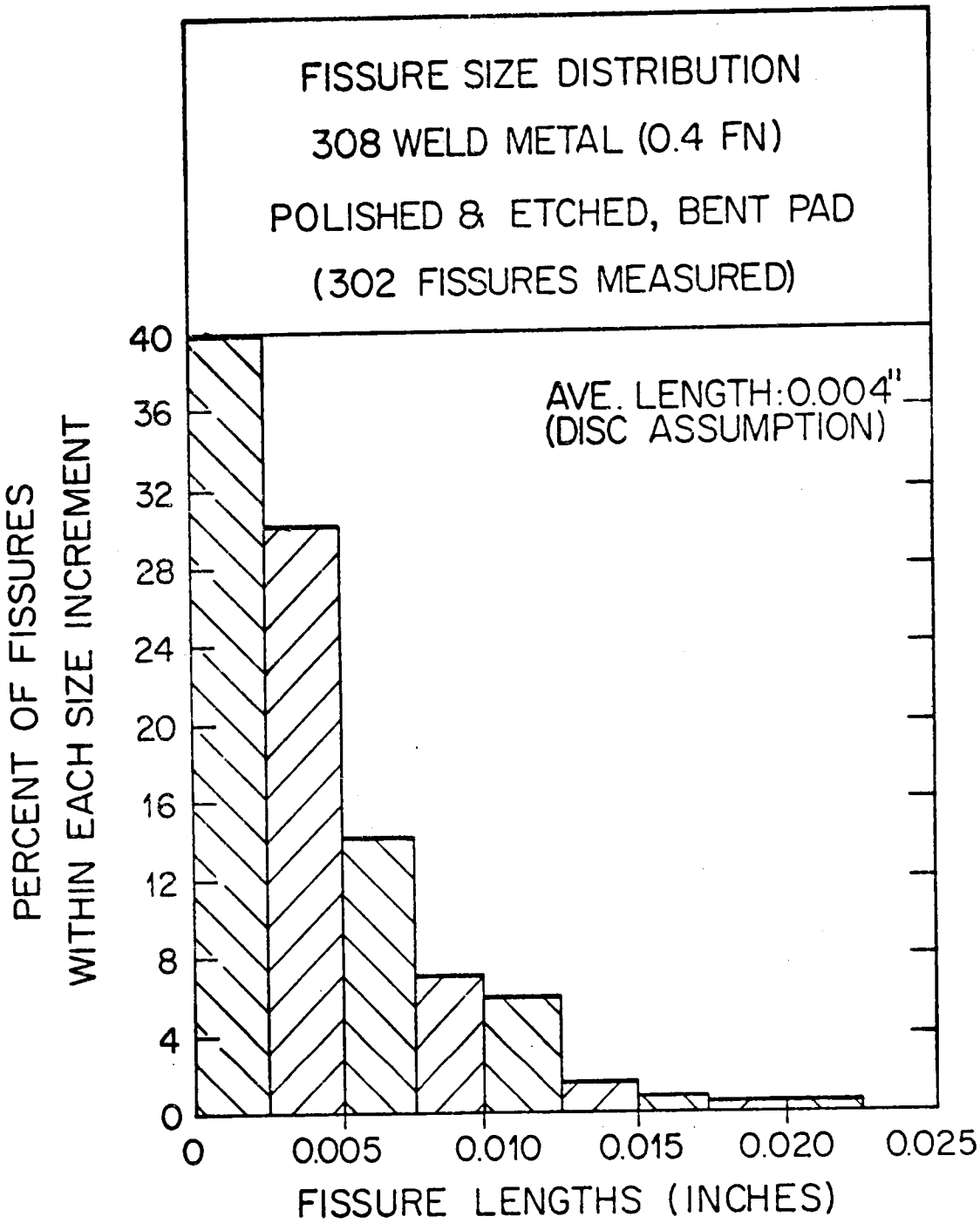

Figure 33. Fissure size distribution for 308 weld metal, polished and etched surface.

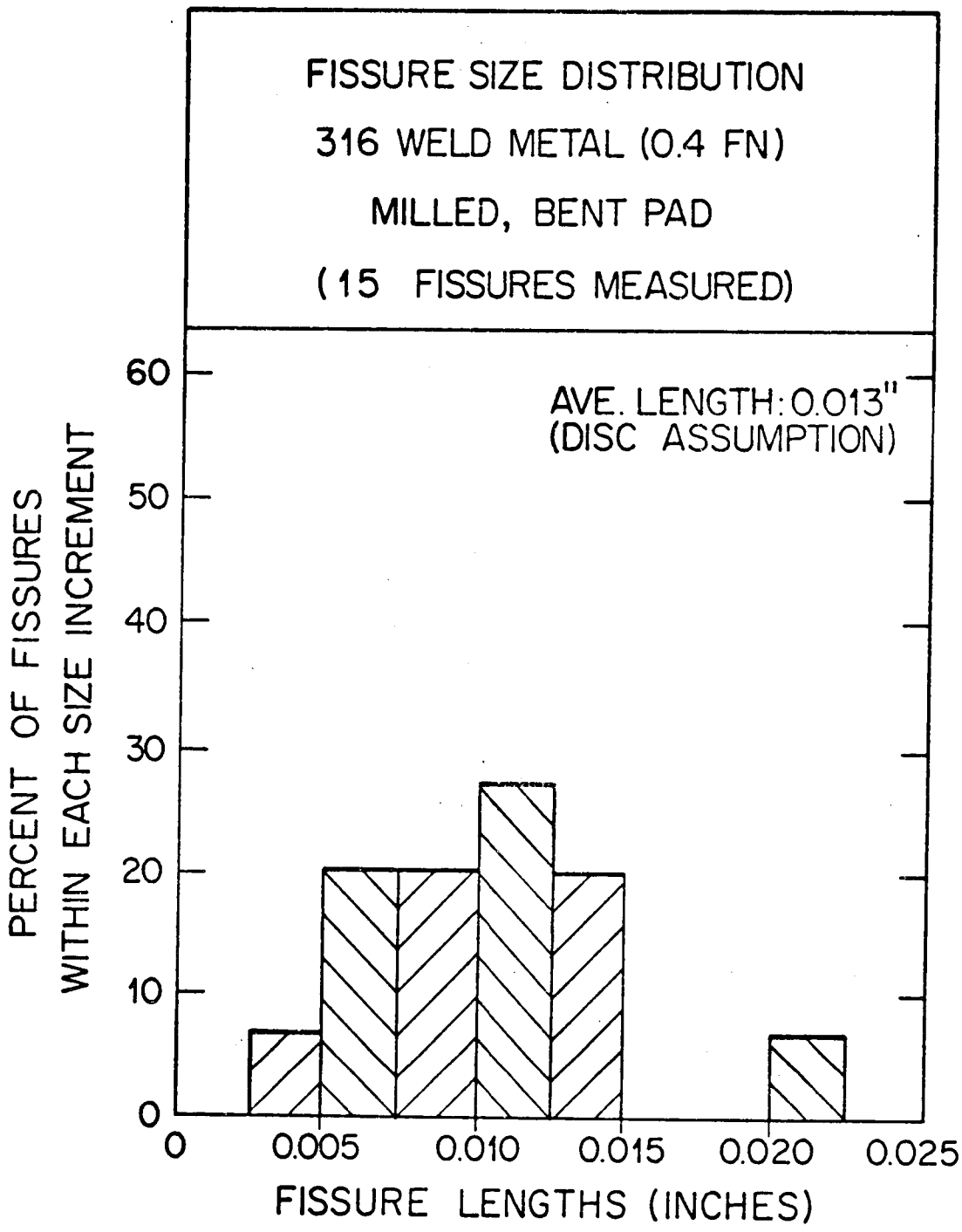

Figure 34. Fissure size distribution for 316 weld metal, milled surface.

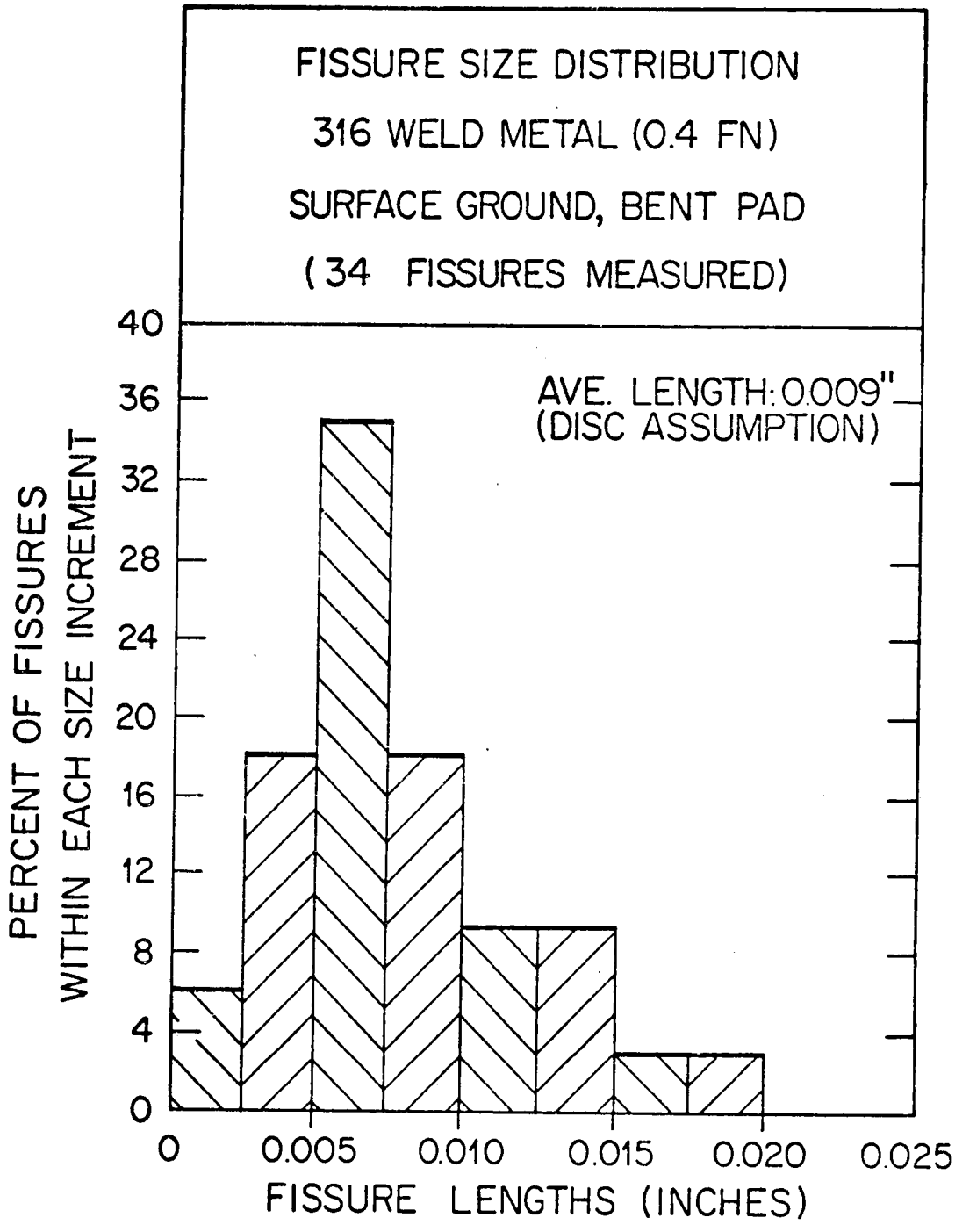

Figure 35. Fissure size distribution for 316 weld metal, ground surface.

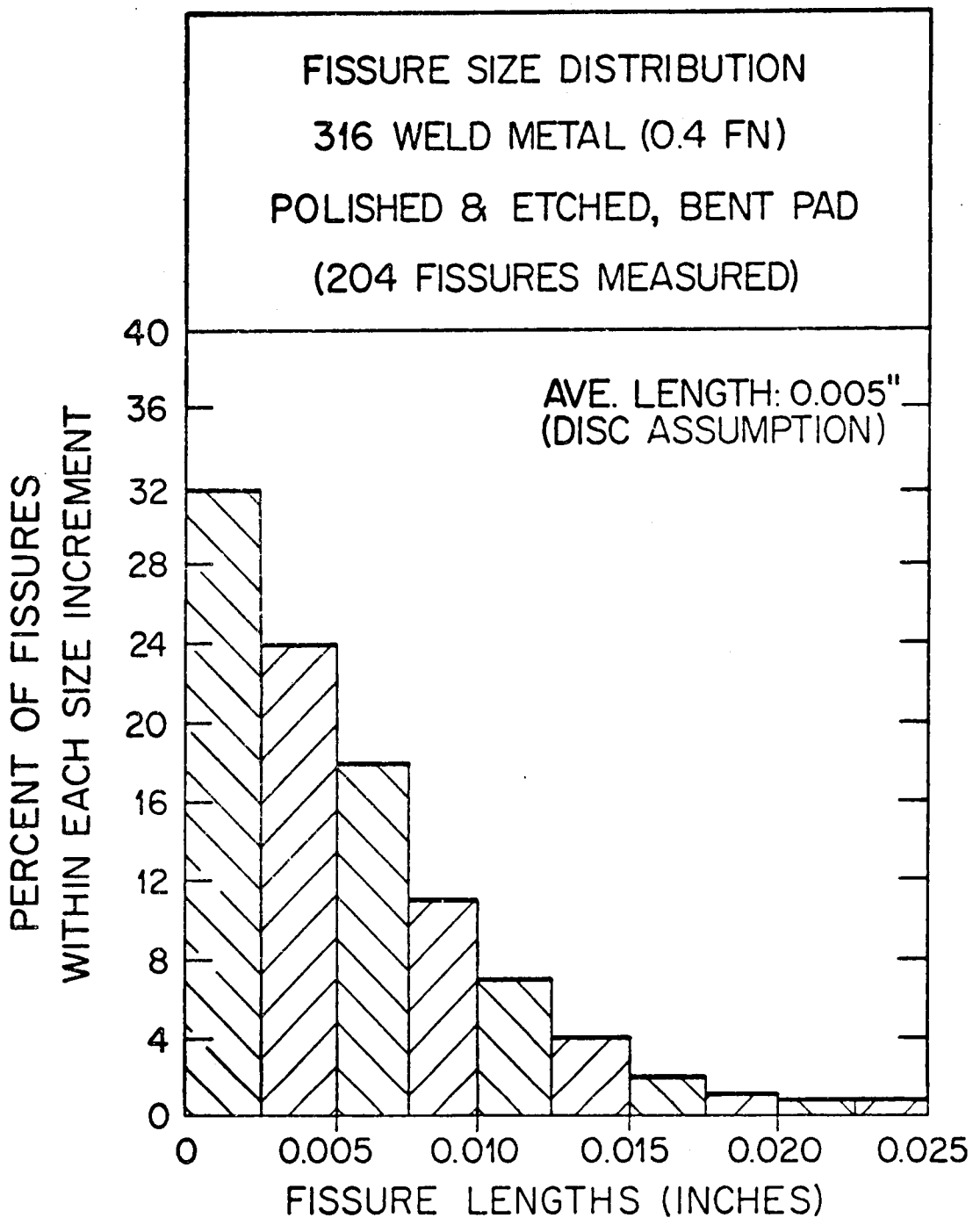

Figure 36. Fissure size distribution for 316 weld metal, polished and etched surface.

The fissure size distribution for the 11 fissures in two bent pads of 308 weld metal (0.4 FN), surface prepared by the "milling" technique and examined at 40-50X, is shown in Figure 31. Note that most of the fissures detected were approximately 0.010" to 0.012" in length and that no fissure smaller than about 0.008" in length was detected. It is apparent that if fissures smaller than 0.008" are present, then the surface roughness from milling prevented their detection. Also because of the high degree of surface roughness, examination of these pads at a magnification higher than 40-50X was not possible optically nor practical in the SEM. Fissures are considered to be present in the weld metal in approximately the shape of a disc, and thus the extent of a fissure exposed by surface preparation can vary from the full diameter of the disc to a very short segment of it. When a disc assumption is utilized, then the average length of the fissures in the weld metal can be calculated from lengths of the fissures measured on the pad surface (95). The average length of the fissures in the 308 weld metal detected on the milled surface (Figure 31) was calculated to be 0.016".

Figure 32 shows the fissure size distribution for the 87 fissures detected in two bent pads of 308 weld metal (0.4 FN) finished by the "surface ground" technique and examined at 40-50X. Clearly the surface ground pad preparation technique reveals significantly more fissures (87) than does milling (11). Moreover, because the grinding technique causes less surface distortion, fissures smaller (as small as 0.002" in length) than those observed on the milled pads could be detected. It should be noted that the majority of the additional fissures detected are in the

smaller size range (less than 0.010" in length). Utilizing the data from the ground pads, the average fissure length is calculated to be 0.008" (cf milled).

Figure 33 presents the fissure size distribution for two bent pads of 308 weld metal (0.4 FN) surface finished by metallographic polishing and etching and examined at 100-200X. Three hundred and two fissures were detected in the two pads and it is to be noted that the majority of them were less than 0.005" in length. The calculated average length of the 302 fissures found in the metallographically polished and etched 308 weld pads was 0.004". Quite obviously the smooth and well-defined nature of metallographically polished and etched pads, in conjunction with the high magnification at which they could be examined, permitted the detection of a large number of very small fissures. The number of larger fissures (greater than 0.010" in length) found in the metallographically polished pads compares favorably with the number (which are greater than 0.010") found in the surface ground pads. In general, the larger fissures on the weld pad surface can be detected by any of the three methods of surface preparation while most of the smaller fissures can be found only on metallographically polished pad surfaces.

The size distributions of fissures measured in the 316 weld metal pads finished by three different surface preparation methods are shown in Figures 34, 35, 36, pages 87, 88, 89, respectively. It is to be noted that for both weld metal types (308 and 316), a similarity is evident in the size distribution when comparing corresponding surface preparation techniques. Figure 31, page 84, resembles Figure 34; Figure 32, page 85, resembles Figure 35; and Figure 33, page 86, resembles Figure 36. The

fissure size distribution for the 15 fissures found at 40-50X in 316 weld metal (0.4 FN) on two milled, bent pads is shown in Figure 34, page 87. Similar to the 308 weld metal, there were few fissures detected in the small size range (the smallest fissure was 0.004" in length). The average length, again using disc assumption, was calculated to be 0.013". Figure 35, page 88, shows the fissure size distribution for the 34 fissures found in two bent pads of 316 weld metal (0.4 FN) finished by surface grinding and examined at 40-50X. Again fissures occurred over a range of sizes, but only five fissures less than 0.0025" in length were found. The average fissure length was calculated to be 0.009". Figure 36, page 89, shows the size distribution for the fissures in two bent pads of 316 weld metal (0.4 FN) metallographically polished and etched and examined at 100-200X. Two hundred and four fissures were found and the average fissure length was 0.005". The data compares remarkably well with that shown in Figure 33, page 86, in that a very large number of small fissures (less than about 0.005") could be found on the metallographically polished pads examined at 100-200X.

Weld metal 16-8-2 was also evaluated using metallographically polished and etched pads. However, only three fissures were detected and thus the data were not amenable to either graphic presentation or the calculation of an average fissure size. The fissures found in the 16-8-2 material were from 0.0015" to 0.0020" in length and fall in the smallest size range of the 308 and 316 weld metals. Figure 37, an SEM micrograph at approximately 800X, shows one of the three 16-8-2 fissures as it appears in the polished and etched bent pad surface. Note what

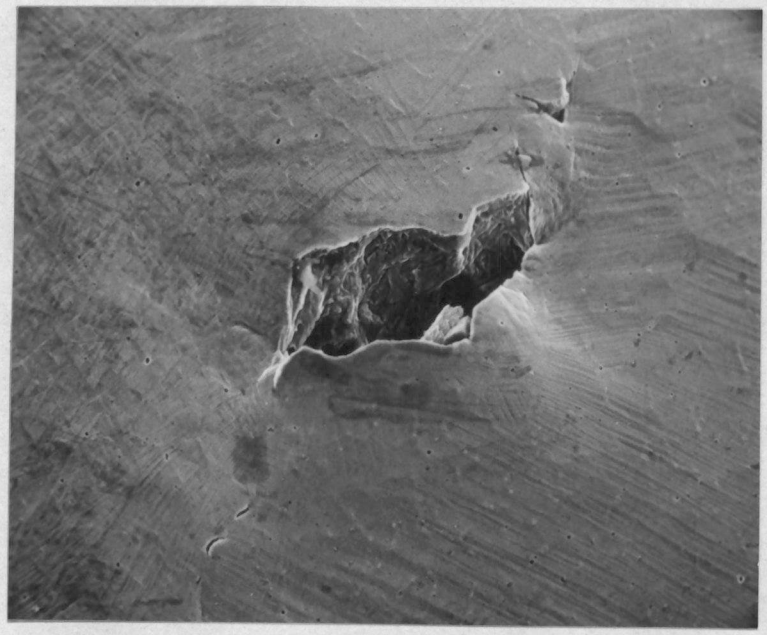

Figure 37. SEM micrograph of a fissure in a polished and etched 16-8-2 weld metal pad (1.5 FN), bent, longitudinal, top view section. 800X.

appear to be additional, extremely small (0.0001") fissures at either end of the fissure.

By referring to Table II, the above presentation may be summarized by noting that the apparent fissure size decreases as the surface preparation technique improves and the observation magnification and the resolution increases. The true average fissure size (disc assumption) is considered to be that determined from the polished pad data since it includes a statistically significant number and accounts for even the small fissures present. This yields an average fissure size of approximately 0.004"-0.005" for 308 and 316 weld metal. When comparing the average size for 316 weld metal with those obtained from production fabricated heavy section 316 weldments, a significant difference is noted. The average size reported for actual weldments is approximately 0.014" (81). (The ferrite levels for the tests reported here and the production weldments were about the same, $\simeq$ 0.5 FN.) The larger sizes in heavy section production weldments may be due to the fact that the strains accumulate at higher temperatures than in the room temperature bent pads and the degree of restraint may even impose higher total strains.

The Influence of Thermal Cycling on Fissure Occurrence

In previous discussion it was emphasized that fissures occur only in the weld metal HAZs of subsequent weld passes. This was invariably true for the Fissure Bend Test pad studies and those fissures studied by others (81, 82, 83) in production weldments.

TABLE II

AVERAGE NUMBER OF FISSURES AND AVERAGE FISSURE SIZE (BASED ON DISC ASSUMPTION) FOR 308 AND 316 WELD METAL AS A FUNCTION OF PAD SURFACE PREPARATION TECHNIQUE (MEASURED ON BENT SAMPLE)

Surface Preparation	308 (0.4 FN)		316 (0.4 FN)	
	Ave. No.	Ave. Size	Ave. No.	Ave. Size
Milled	6	0.016"	8	0.013"
Surface Ground	44	0.008"	17	0.009"
Metallographically Polished	151	0.004"	102	0.005"

In this study two different sequences of bead deposition were utilized and are shown in Figure 38. In the original testing of fissure pad bend testing scheme, the top layer weld beads were deposited in sequence from one side of the pad to the other. This bead sequence is shown in Figure 38A where beads 7-12 constitute the top layer and were deposited from left to right in the order shown. Thus bead 7 receives the high temperature thermal cycle effects from bead 8, and bead 8 is subjected to the same thermal cycles by bead 9, and so on with bead 12 being the only deposited upper layer bead not to be subsequently thermal cycled. Fissures were never found in bead 12 but only in the HAZ regions of beads 7-11, thus underscoring the weld metal HAZ fissuring phenomenon.

In follow-on investigations evaluating the Fissure Bend Test variables, an altered weld pad bead sequence was fortuitously utilized for the 316, 308 and 16-8-2 pads to be evaluated with metallographic preparation of the pad surface. This altered bead sequence is shown in Figure 38B. Notice that bead 1, in the lower layer and bead 2, which forms a portion of the upper layer, were deposited before any other beads. Bead 3 caused bead 2 to experience a high temperature excursion and later bead 8 subjected bead 2 to a high temperature thermal history. Thus, bead 2 in the upper layer and in the final plane of examination was subjected twice to high temperature HAZ excursions. This was the only bead so influenced in the upper layer with the remainder experiencing only one high temperature HAZ excursion as described above.

For the specimens with the altered bead sequence, it became apparent that the majority of the fissures found were occurring in bead 2 (in the

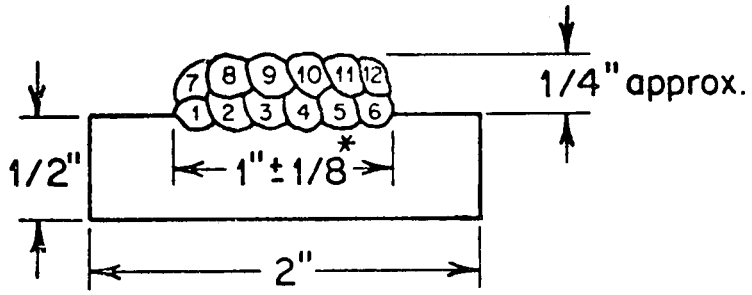

A. Recommended bead sequence.

*Weld pad must be within these limits to minimize variation in total pad surface area and variation in pad height.

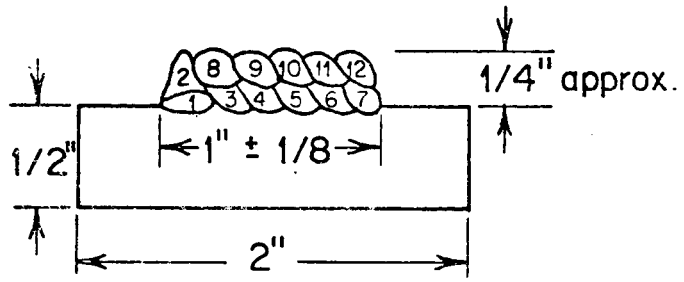

B. Alternate bead sequence resulting in two high peak temperature HAZ thermal cycles in bead 2.

Figure 38. Weld pad cross-section showing bead sequence.

double HAZ produced by beads 3 and 8). The fissure count for the low ferrite pads (0.4 FN for 308 and 316, and 1.5 FN for 16-8-2) was treated so as to recognize this occurrence by computing the areal fissure density and the density along each interpass boundary (a linear density) for the single and double HAZ instances. The areal density in the double HAZ region revealed approximately 95-120 fissures per square inch, whereas for the single HAZ region the density was only 8-17 fissures per square inch. The linear density (along the interpass boundary) was 19-24 fissures per inch of interpass for the double HAZ occurrence while it was 2-4 fissures per inch of interpass for the single HAZ. These data encompass both 308 and 316 weld metal with no clear distinction between the two. The 16-8-2 fissured an insignificant amount with only three fissures being found on two pads (8 sq. in., 40 inches of interpass). However, it is to be noted that the three fissures found were in the double HAZ region.

From this treatment it was clear that the double HAZ occurrence is a significant factor in the fissuring tendency of 308, 316, and 16-8-2 weld metals at low ferrite levels. When the ferrite level for 316 was increased to 3.2 FN, fissures again occurred but only in the double HAZ region. For this pad there was a linear density of 3 fissures per inch of interpass (compared to approximately 20 fissures per inch at 0.4 FN) in the double HAZ region. However, for a 308 pad at a nominal ferrite level of 2.5 FN, no fissures were found even in the interpass region of the bead subjected to the double HAZ thermal cycle. Additional testing has supported the fact that 316 weld metal at ferrite levels of

3.0 FN to 3.2 FN displays a low fissuring tendency in double HAZ regions but that 308 weld metal at ferrite levels of 2.5 FN to 3.1 FN is insensitive to this occurrence. Thus double HAZ overlapping will be influential in the determination of the minimum ferrite level to prevent fissuring.

To more clearly define the effect double HAZ thermal cycling has on fissuring tendency, a series of experiments was conducted utilizing a Gas Tungsten-Arc (GTA) remelt of surface ground SMA deposited pads. Both 316 and 308 (0.6 FN) were utilized in the study. The GTA process was selected to remelt the SMA pads because it produces a smooth flat bead with a well-defined fusion line and is a quiescent process with minimal weld pool perturbation. Thus it is easy to document the location of any fissure with regard to the weld fusion line. The entire SMA pad surface was remelted by a series of overlapping GTA beads. Where double and triple HAZ experiences were desired, a given bead was refused two or three times thus producing double or triple HAZs experiences in the preceding bead. Care was exercised to control preheat and interpass temperatures in all cases to precisely maintain fusion line location. The energy input was varied from 6-60 KJ per inch for individual weld pad studies incorporating energy input as a variable. It is to be noted that the Ferrite Number was altered by the energy input variations. At low energy input, the Ferrite Number was 0.5 FN and with 60 KJ per inch the Ferrite Number was 1.4 FN (for a complete treatment of the Ferrite Number changes with energy input and travel speed, see Appendix C).

Regardless of the energy input for the GTA remelt studies, no fissures were found upon bend testing along interpass boundaries which

were subjected to only a single HAZ experience. Only when a weld bead underwent double or triple HAZ experiences did any fissures appear upon bend testing, thus confirming the results of the directly deposited SMA weld bead studies.

Measurements of fissure locations from both the GTA and SMA pads were utilized to determine the exact region of the HAZ in which fissures occurred. These measurements for SMA beads showed that fissures were found in a region from the fusion line to approximately 0.050" from the fusion line. The fissures never crossed the interpass boundary and rarely extended to the interpass boundary. The majority of the fissures were found in a band 0.010" to 0.030" from the fusion line.

With the precise fissure location in the HAZ thus defined, it was now possible to determine the cracking temperature range by measuring the thermal distribution in the HAZ. This was accomplished for both the SMA and GTA weld beads utilizing the thermocouple implantation technique (96). The welding conditions exactly duplicated the SMA (16 KJ per inch) conditions. From these thermal measurements it was determined that a point 0.050" from the fusion line reached a peak temperature of approximately 1630°F, a point 0.030" reached a peak of 1950°F and a point 0.010" from the fusion line reached 2400°F. Thus the overall HAZ temperature range in which the fissures were found extended from the bulk solidus ≈ 2630°F to 1630°F while the majority of the fissures fell in a range experiencing peak temperatures of 2400°F-1950°F.

The hot cracking temperature range for austenitic stainless steels was determined by Honeycombe and Gooch (77), Shackleton (72), and Senda et al. (63), using the Varestraint-thermocouple technique developed by Savage

and Lundin (93, 94). Shorshorov and Sokolov (97) utilized an implanted thermocouple technique and Haddrill and Baker (74) utilized a hot ductility apparatus for their determinations of the cracking range.

Those investigators utilizing the Varestraint technique record the hot cracking temperature range as extending from the bulk solidus to about 2300°F for a variety of austenitic stainless steel weld metals (GTA remelted). These data should be treated with caution especially at the high end of the range because Lundin (98), utilizing high speed motion pictures showing Varestraint crack formation, has found that cracking initiates a short distance behind the instantaneous position of the solid-liquid interface and the cracks often propagate to the solid-liquid interface. (Cracks which propagate to the solid-liquid interface will always be coated with a liquid film.) Haddrill and Baker (74) report a cracking temperature range of from 1650°F to 1830°F and Shorshorov and Sokolov (97) report a range of 1740°F to the bulk solidus.

The overall temperature range determined in this study (1630°F-2630°F) fits well with those of others. However, this study has shown that the majority of the fissures form at a temperature significantly below the bulk solidus in a range of 1950°F-2400°F.

By combining the information or observations as to the bead sequence in multipass welds and the data on the location of fissures and the temperature range over which they are most prone to occur, one can better analyze the nature of fissuring in austenitic stainless steels. In regard to the Fissure Bend Test specimens in which the double HAZ cycling occurs, the influence of bead sequence can be clearly discerned by reference to

Figure 39. The photomacrograph in Figure 39A was obtained from a transverse section of an unbent 316 (0.4 FN) weld pad in which bead 2 experienced a double HAZ cycle from beads 3 and 8 (see Figure 38B page 97, and associated discussion). The passes are numbered on the macrograph and the interpass boundaries can be clearly seen. The sketch in Figure 39B (at the same scale as the macrograph) shows the weld bead fusion lines and the 1630°F peak temperature isotherms produced during the deposition of beads 3 and 8. Note that the cross-hatched region represents that area over which double HAZ (greater than 1630°F) thermal cycling has occurred. In this particular case a fissure exists in the center of the double HAZ region (it is difficult to see, however, at the magnification of the macrograph).

When the weld pad plane of examination passes through the double HAZ region, fissures may be found on the pad surface. However when the weld pad plane of examination does not pass through the double HAZ region, the chance of finding fissures along the interpass exposed on the weld pad plane of examination is reduced. Figure 40 shows an incidence of just such a case. This transverse section from a 308 (0.4 FN) weld pad is similar to the one shown in Figure 39, and the peak temperature isotherms of 1630°F are illustrated as obtained from beads 3 and 8. Due to the location and shape of beads 3 and 8 at this sectioning point and the weld pad plane of examination depth, the double HAZ region does not extend to the examination surface. The cross-hatched region lies entirely below the plane of examination, and thus the chance of finding a fissure along the interpass boundary between beads 2 and 8 at this section location in the examination plane is minimized.

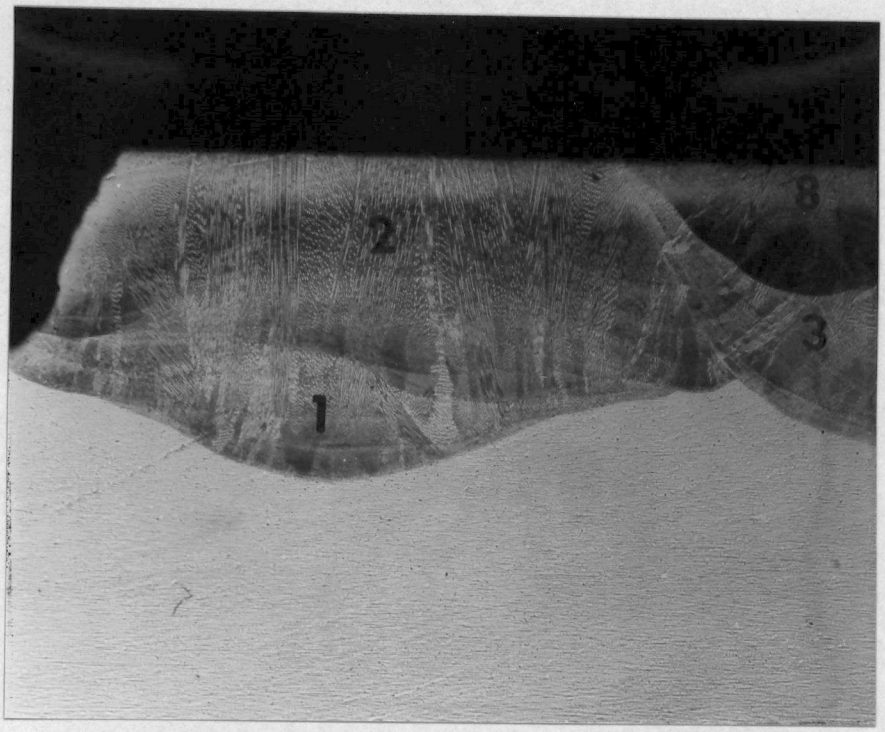

A. Light macrograph. 12X.

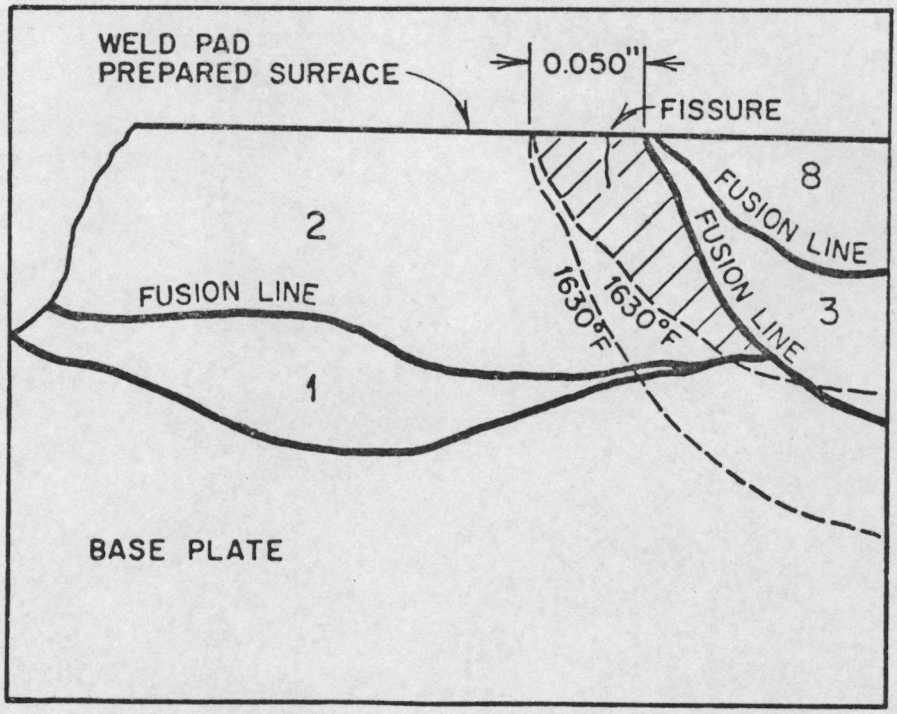

B. Sketch. 12X.

Figure 39. Portion of weld pad cross-section showing overlapping HAZ and its intersection with the prepared pad surface.

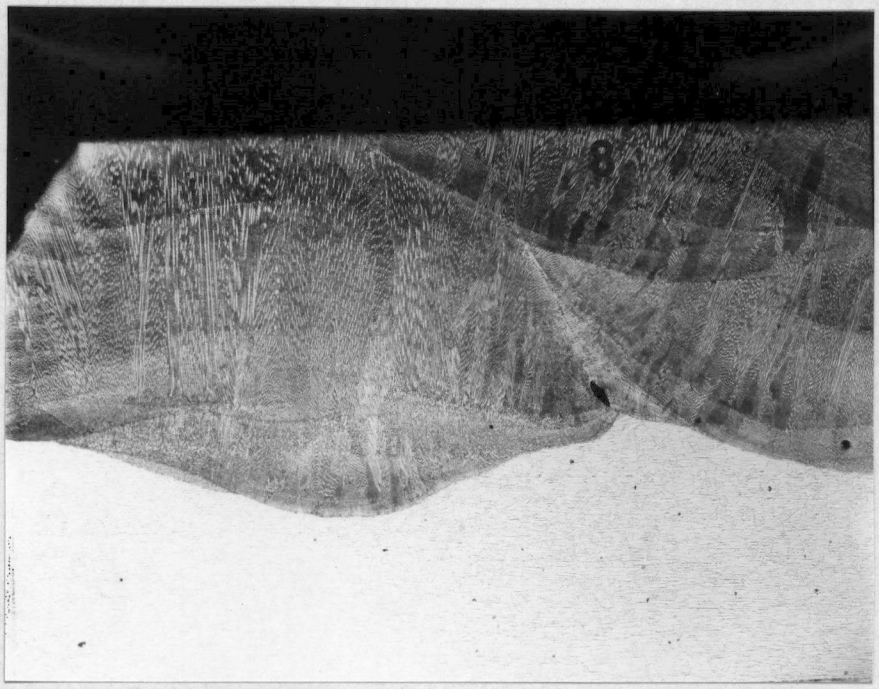

A. Light macrograph. 12X.

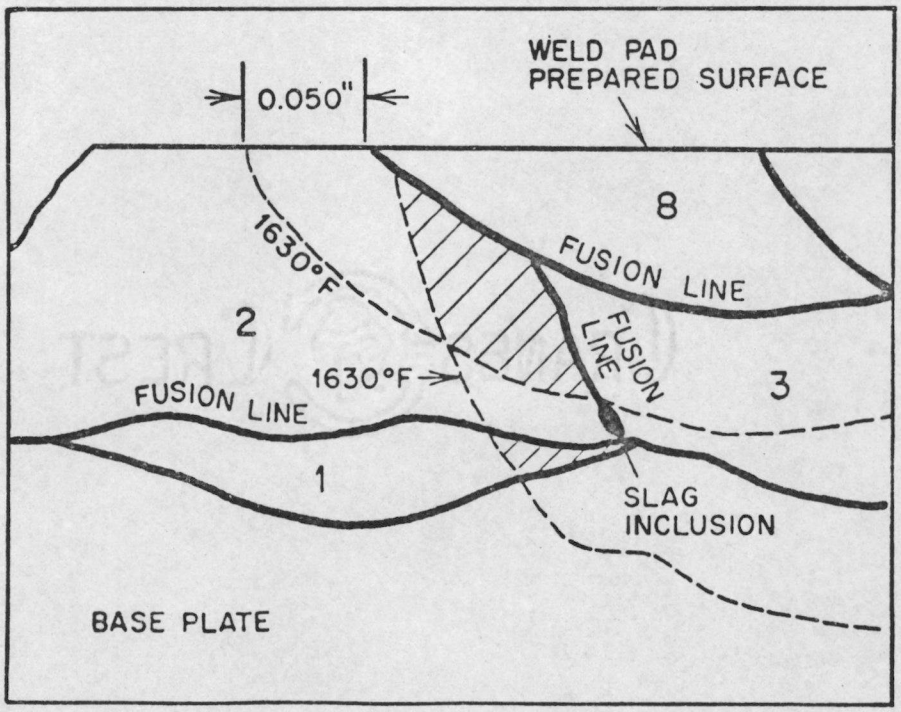

B. Sketch. 12X.

Figure 40. Portion of weld pad cross-section showing overlapping HAZ which does not intersect prepared pad surface.

It should be noted that the cross-hatched region (double HAZ) is contained near the triple junction of beads 2, 3, and 8. When configurations such as this occur, it has been observed that fissures tend to predominate there rather than at other locations. These observations were made by others (81, 82, 83) in the examination of production fabricated multipass welds.

Factors Contributing to the Multiple HAZ Thermal Cycle Phenomenon

The effect of multiple weld metal HAZ thermal cycles on the fissuring propensity of austenitic stainless steel weld metal is unmistakable in light of the foregoing discussions. This phenomenon appears to be the most influential element in the gamut of fissuring influences in austenitic stainless steels.

Since the occurrence of a single weld metal HAZ experience does not produce myriads of fissures upon the application of strain, it is clear that the strain tolerance of the grain boundary microstructural regions is significantly reduced by multiple thermal cycling. This degradation of grain boundary ductility can be due to:

1. Enhanced segregation due to continued partitioning of harmful trace elements to the grain boundaries followed by liquation and rupture under strain.

2. Additional strengthening of the matrix by thermally-induced precipitate reaction as is the case for some ductility-dip incidences. The increased strength of the matrix may cause strain accumulation in the degraded grain boundary microstructural region thus leading to rupture.

3. Strain-induced precipitation leading to a strengthened matrix and the subsequent accumulation of strain in the degraded microstructural region.

4. The simple accumulation of thermal and restraint strains over a range of temperatures produced by continued thermal cycling causing the strain tolerance of the grain boundary microstructural region to be exceeded.

Each of the above elements of the phenomenon may be operational at the same time. However it is also clear that liquation plays a role in the majority of fissuring occurrences and must, therefore, be a part of the mechanism. Thus it appears that enhanced partitioning or segregation during thermal cycling can play a decisive role.

The results of the testing discussed in this chapter, along with the results obtained in the initial testing phase as presented in Chapter II, provide the basis for the investigation and evaluation of the variables of the Fissure Bend Test. Thus the presentation of the procedure for conducting the Fissure Bend Test and the evaluation of the variables of the test will be the topic of the next chapter.

CHAPTER IV

THE FISSURE BEND TEST

Introduction

Over thirty different direct* welding tests have been developed to investigate various types of cracking in austenitic stainless steels and other alloys (99). Most of these tests were devised to evaluate one particular type of cracking problem such as base metal cracking, cold cracking, or hot cracking. Among other things, a welding test should be (1) economical, (2) simple to conduct and evaluate, (3) reproducible, and above all, (4) capable of showing a direct correlation with fabrication and service conditions. All the hot cracking tests, with the possible exception of the Varestraint Test (93, 94) do not fulfill one or more of these criteria. However, the Varestraint Test requires special automated apparatus and finds its greatest versatility and reproducibility when utilizing the Gas Tungsten-Arc (GTA) process to measure the hot cracking susceptibility of autogenously melted wrought plate or previously deposited weld metal. It is more difficult to apply to directly deposited SMA, Submerged-Arc (SA) and other filler metal-added processes.

Since austenitic stainless steels and other alloys that are susceptible to hot cracking or fissuring are often deposited by the SMA process as multipass welds, there was a need for developing a test to

*Those which involve making an actual weld.

determine fissuring tendencies in multipass weldments in an economical and reproducible manner. Such a test has been developed and has become known as the Fissure Bend Test. The Fissure Bend Test has the favorable features desired in a weldability test in that it is economical, easy to conduct, reproducible, and capable of evaluating fissuring in multipass weldments very similar to those used in current fabrication procedures.

The Fissure Bend Test evolved from the electrode research programs of both the Teledyne McKay Corporation (100) and the A. O. Smith Corporation (101). In the initial testing phase of this study, the Fissure Bend Test was successfully utilized to establish the relationship between Ferrite Number and fissuring sensitivity of eight different austenitic stainless steel weld metals. However, it is not often that the variables of a new test are thoroughly investigated or the procedures firmly established early in the development of the test. The consequence is that individual laboratories often establish their own variations of the test so that results obtained by different laboratories are not comparable. Thus it is the intention of this chapter to set forth the procedure for conducting the Fissure Bend Test and to explain in detail the important test variables. This will be accomplished in two parts. The first part presents the detailed procedure for conducting the Fissure Bend Test. It is anticipated that this section can be used directly by other investigators to prepare specimens and conduct the test. It is also believed that by strict adherence to this procedure results obtained by different investigators will be directly comparable. The second part presents the details and explanation of the variables for conducting the

test, and it should be sufficient for understanding the influence each variable has on the test results.

Procedure for the Conduct of the Fissure Bend Test

General. The Fissure Bent Test employs a multirun, double-layer, weld pad to permit the evaluation of fissuring on relatively undiluted weld metal. The weld pad is deposited by the Shielded Metal-Arc process on a rigidly clamped base plate as twelve 8" long stringer beads, six beads to each layer. The pad is then ground to produce a smooth surface for examination. The Ferrite Number of the deposit is determined on the ground surface. Examination of the pad for fissuring is conducted both before bending and after bending. An example of a ground, bent pad is shown in Figure 41. For each weld pad tested the relationship between the Ferrite Number and the number of fissures observed on the bent pad is developed. Data obtained in this manner permit the ranking of weld metals as to their fissuring tendency and the influence of ferrite on the fissuring behavior.

Test plate preparation and fixturing. Cut the 304 or 304L base plates to specimen size: 1/2" thick, 2" wide, 9" long. Remove the scale on the base plates by grinding or grit blasting. Restrain the plates by clamping each end to a heavy backup to prevent excessive bowing. The clamping fixture shown in Figure 42 can accommodate three test plates and is recommended for use. To facilitate the subsequent grinding of the specimens while still retained in this fixture, the base plates are

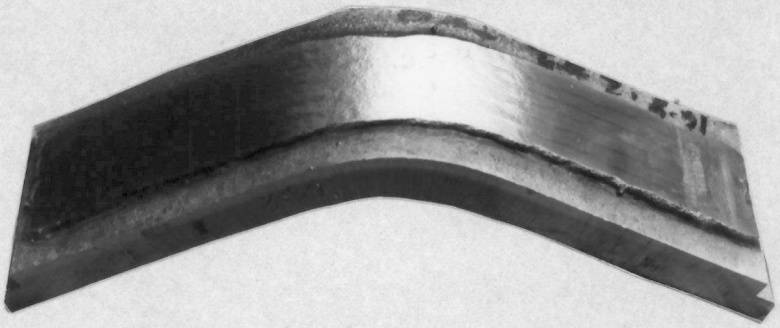

Figure 41. Photomacrograph of Fissure Bend Test specimen (120° included angle).

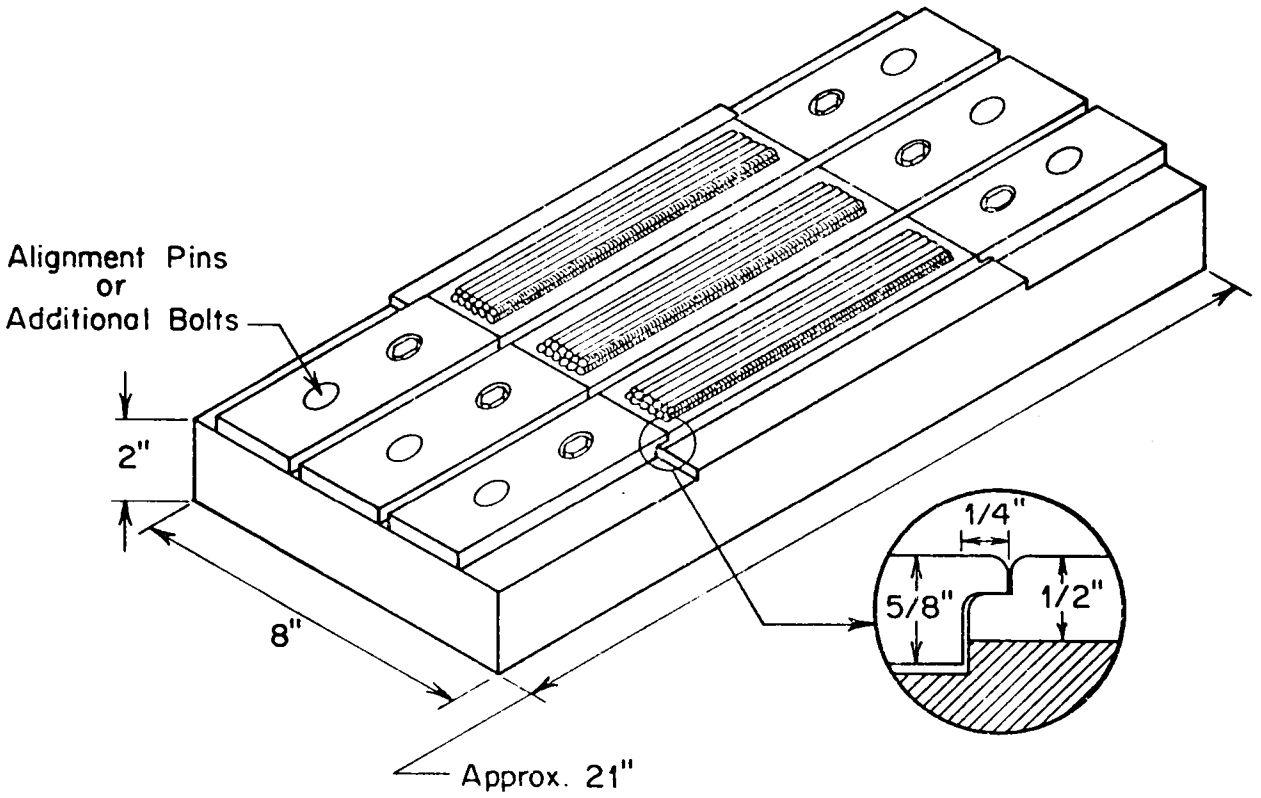

Clamps - 6 required - 5/8" x 2" x 6" Heat treated to prevent deformation
Bolts - 6 required - Allen head cap screw, 1/2" - 13
Backup plate - Carbon steel 2" thick (min.)

Figure 42. Recommended clamping fixture.

notched on the ends. Thus the clamps will not project above the height of the ground weld pad surface.

Since the weld pad restraint technique does not appear to influence the test results, alternate methods of restraint may be used. The base plates may be fillet welded either on the ends or all-around to a heavy backup thus eliminating the need for the clamps. This, however, hinders the specimen removal for subsequent testing.

Welding. The welding conditions recommended below are suitable for use with 1/8" coated electrodes. To help maintain proper position and alignment of the first bead, scribe or punch a guideline onto the base plate. Direct the arc into the prior bead to minimize dilution from the base plate. Beads should be about 8" long and bead overlap should be such as to produce as flat a deposit as possible. The resulting pad should be approximately 1/4" x 1" x 8" with its configuration as shown in Figure 43. A cross-section of the pad is shown in Figure 38A, page 97. The bead sequence indicated should be followed unless double thermal cycling of beads in the top layer is desired.

The welding conditions given may have to be varied slightly depending on the electrode and power source, but they are to be regarded as aims (coating redness is often a better criteria than amperage; a red stub about 2 1/2" long should result after completing the 8" long bead). It is recommended that the welder produce a practice pad in order to make the adjustments necessary so that pad configuration falls within the prescribed dimensions.

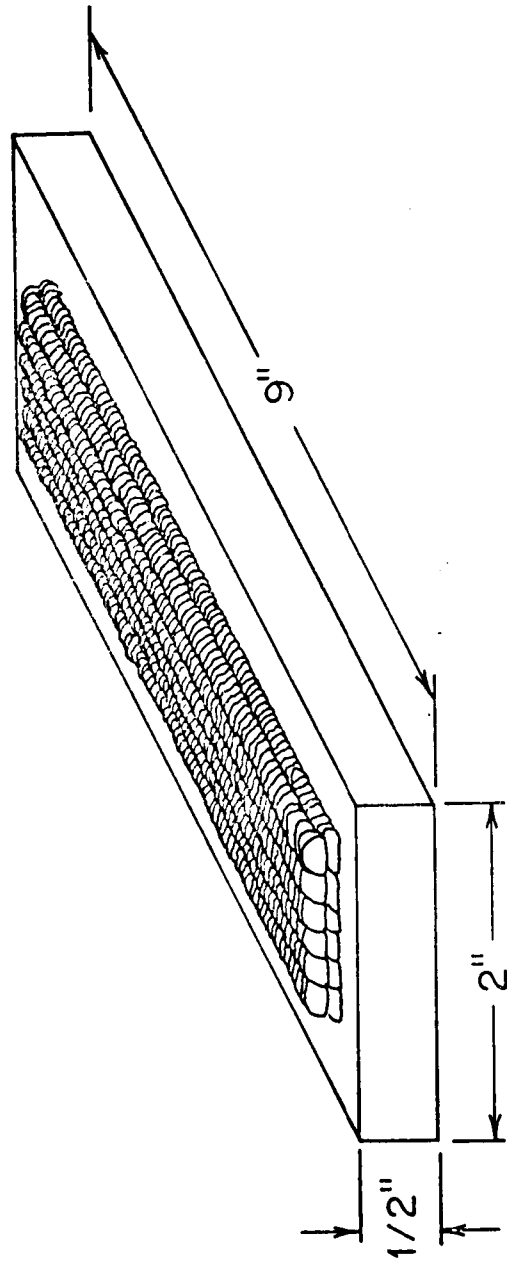

Figure 43. Fissure Bend Test weld pad configuration.

Recommended Conditions, 1/8" AC-DC Electrode

Current ---------- 96 amp DCRP

Voltage ---------- use good "close arc" stainless practice

Travel Speed ---------- aim 8 ipm

Interpass Temperature ------ 200°F

Heat Input ---------- ≈ 16-17 kj./in

It is recognized that it may be desired to evaluate other sizes and types of electrodes and welding techniques. For welding conditions other than those given here it may be difficult to maintain the pad size recommended and/or keep six beads in each layer. To facilitate comparison of data when such variations are unavoidable, see discussions on pages 120 and 121 for recommended procedural techniques.

(NOTE: It is often advisable to determine the Ferrite Number on the as-welded pad surface. If this is desired, make the determination as outlined on page 115.)

Surface preparation. With the pads still in the clamping fixture (or fillet welded to a backup) mill the surface using a 0.010" depth of cut on each pass until the surface in the center 4 inches is clear of almost all irregularities. Then grind the pad surfaces on a surface grinder using a wheel recommended for stainless steel. (Do not use a cup-type grinder that leaves arc-shaped grinding scratches.) A twelve pass sequence is recommended with the first eight passes each removing 0.001" and the final four passes each removing 0.0005". Use flood cooling

during grinding. The grinding operation should remove most of the irregularities left on the pad surface. A few small irregularities can be tolerated without affecting the results.

After grinding, release the specimens from the clamping fixture (or cut the fillet welds joining the base plates to a heavy backup), and using a suitable solvent remove all traces of the cutting fluids.

Ferrite Number determination. Measure the Ferrite Number in the center 4 inches of the ground pad at a series of locations using a Magne Gage calibrated to AWS A4.2-74 (59). It is recommended that a 15 intersection grid layout as shown in Figure 44 be used to insure a sufficient number of determinations for computation of a statistically significant average value. The average value of the Ferrite Number is used in the development of the ferrite-fissuring relationship.

Fissure evaluation. Fissure evaluation is performed in the center 4 inches of each specimen. This evaluation is a two-step process: (1) fluorescent penetrant testing to detect surface indications, (2) binocular microscopic examination of these indications.

Apply a light coating of the fluorescent penetrant onto the weld pad surface. Allow a penetration time of 10-15 minutes to permit the penetrant to soak into all fissures and other surface discontinuities. Remove the penetrant by rinsing the weld pad for 30 seconds with a warm water spray wash. Dry each specimen under a warm air dryer on in a recirculating oven. Drying time should be just long enough to remove moisture from the pad surface. Allow a developing time of 10 minutes

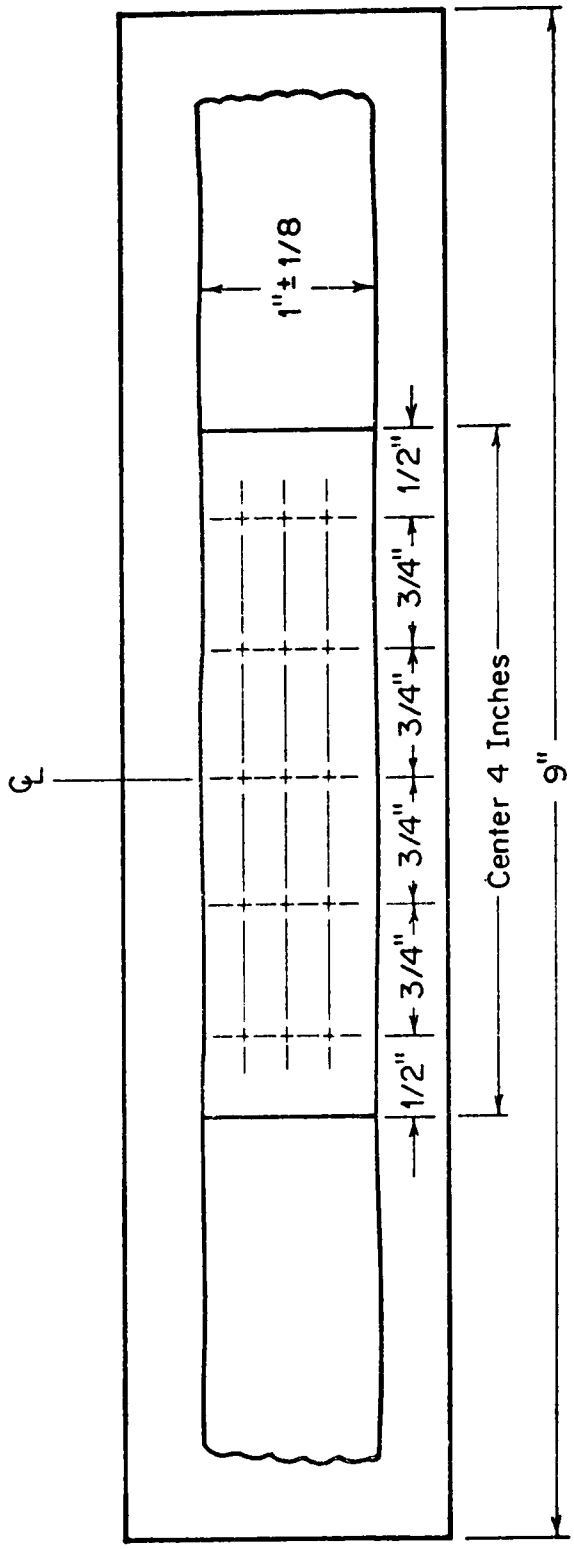

Figure 44. Recommended grid spacing for Ferrite Number determination.

to permit the penetrant to exude from fissures and other surface discontinuities and then inspect the pad under a standard black light in a dark area. The indications of discontinuities will fluoresce with a brilliant yellow-green light in the darkness. Count and circle with water-soluble ink all linear indications in the center 4 inches of the pad. These indications generally denote fissures. Inspect each of these linear indications by optical microscopy at 40-50X; then count and measure the length of those indications verified as fissures. Bend the specimen to an included angle of 120° in a fixture similar to the one shown in Figure 45. Repeat the entire fissure evaluation process on the bent specimen and record the number and size of the fissures on the bent pad as was done on the unbent pad.

The ferrite-fissuring relationship. The relationship between Ferrite Number and fissuring sensitivity is best expressed in graphical form such as shown in Figure 46. In this figure each data point represents the number of verified fissures found on a singular weld pad in the bent condition as a function of the Ferrite Number of the ground, unbent pad. Testing a number of weld pads of differing Ferrite Numbers produces a series of data points thereby illustrating the ferrite-fissuring relationship. An important aspect of this relationship is the minimum Ferrite Number needed to eliminate fissuring (3 FN in Figure 46). To compare the ferrite-fissuring behavior for more than one type of weld metal under investigation, the data can be presented as was previously shown in Figure 9, page 29.

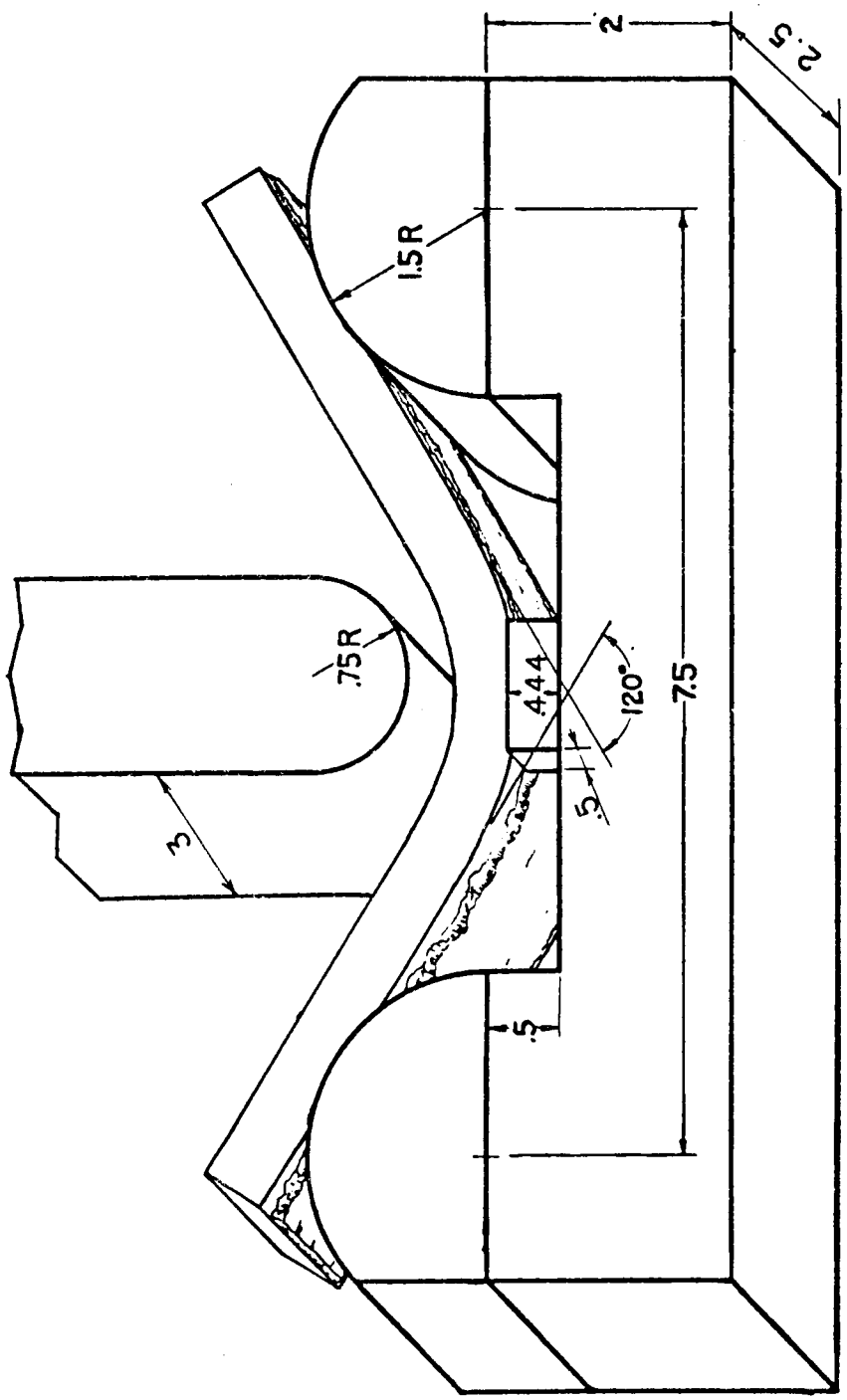

Figure 45. Fissure Bend Test fixture.

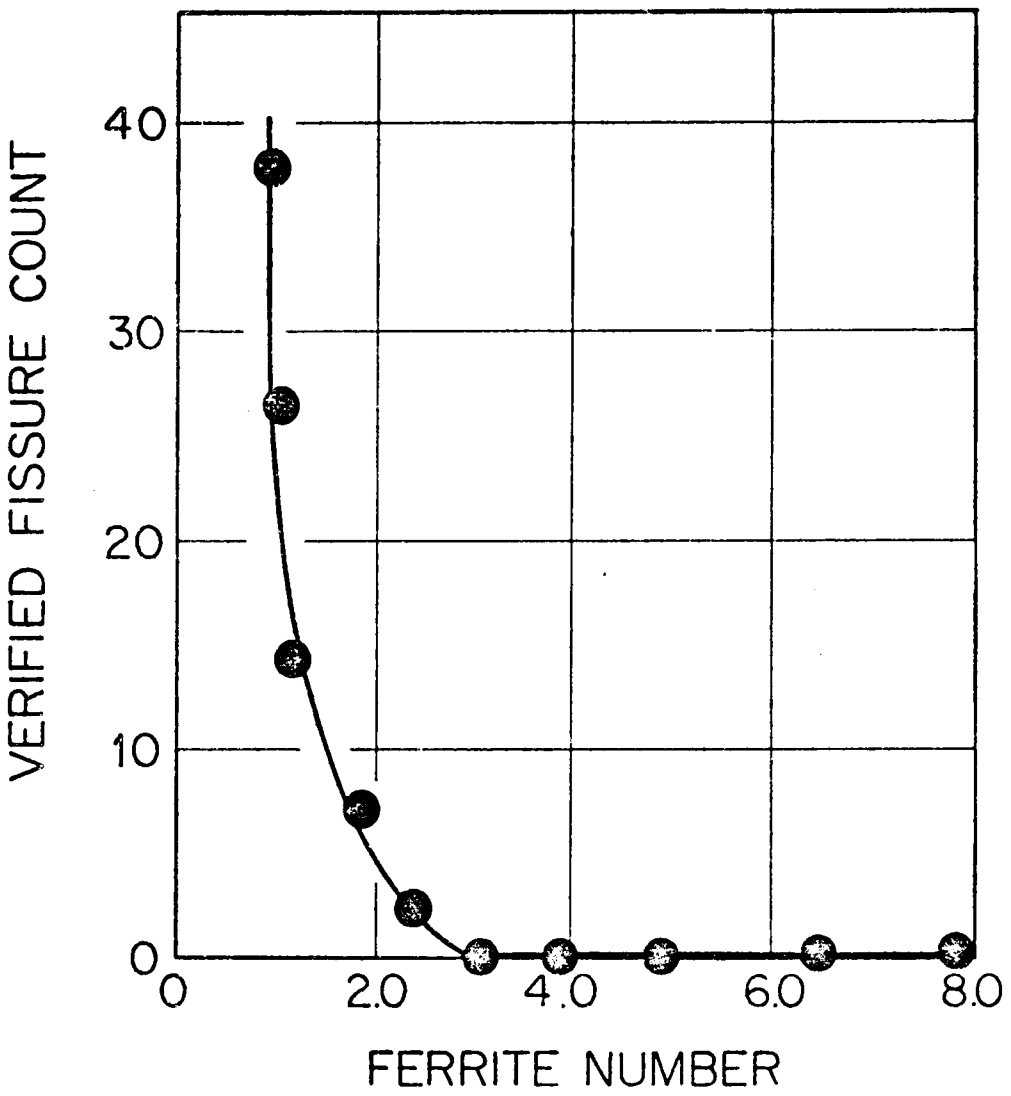

Figure 46. Data presentation method. Verified fissure count vs. Ferrite Number, typical for austenitic stainless steel weld metals.

Investigation and Evaluation of the Test Variables

Weld pad. The weld pad width should be maintained within the limits for the 1/8" electrode welding conditions given previously. This will ensure that the pads investigated will have the same amount of surface area on which the examination for fissuring will be performed. Furthermore, if the pad width is held constant, the pad height will be nearly identical for each specimen (approximately 1/4") and thus the amount of strain from bending on the outer surface of the pad will be the same for all specimens. In like manner, a uniform pad height of approximately 1/4" will provide dilution control and minimize dilution in the top layer of weld beads. When fissuring is evaluated in a relatively undiluted top layer, the base plate used in the test is not a significant variable and either type 304 or 304L stainless steel is recommended.

If welding conditions resulting in significant dilution are to be used, it is suggested that the first layer of weld beads be deposited with a low dilution technique such as that recommended for the 1/8" electrodes. The second layer of weld beads can then be deposited in the manner desired thus minimizing the overall dilution effect.

The number of fissures found on the pad surface examined is considered to be a function of the area evaluated (4 sq. inches in the initial testing) and the length of the interpass boundaries in the center 4 inch evaluation section. With six beads there will be five interpass boundaries and thus 20 linear inches of interpass boundary across the 4 inch evaluation section. If the pad width and the number of passes vary with the welding conditions or techniques used, the essential

variables in the data evaluation will likewise be altered. It is suggested that two procedures be used to normalize the data. Divide the fissure count by: (1) the ratio of the pad width used in a specific test scheme to the standard 1" pad width; and (2) the ratio of the total linear interpass boundary length utilized to the 20 linear inches of interpass boundary in the standard. A double normalization may be used if both the width and number of beads are varied in the same testing scheme.

This normalization technique has not been verified in the current work but it is anticipated that it will help to provide comparative data evaluation. Regardless of whether a normalization procedure is attempted, the minimum ferrite level to eliminate fissuring should not be altered to any great extent by slight variations from the standard weld pad configuration.

Bead sequence. The sequence of weld beads deposited on the base plate is of prime importance in the conduct of the Fissure Bend Test. The recommended sequence is that which was shown previously in Figure 38A, page 97, in which the beads of the top layer are deposited only after all beads of the bottom layer have been deposited. Thus each bead in the top layer (specifically 7-11) experiences essentially only one high peak temperature HAZ thermal cycle, that produced by the immediately succeeding bead. Altering the bead sequence can result in a bead of the top layer receiving multiple HAZ thermal cycles from succeeding weld beads. Test specimens deposited with altered bead sequences showed that fissuring in a bead subjected to multiple HAZ thermal cycles can be increased several fold. This aspect of enhanced fissuring tendency

resulting from multiple thermal cycles has been explained in great detail in Chapter III.

If one wishes to incorporate the influence of multiple thermal cycles in a single test specimen, a bead sequence such as was shown in Figure 38B, page 97, may be used. In this sequence bead 2 will receive double, overlapping HAZ thermal cycles with relatively high peak temperatures from beads 3 and 8. Other sequences can be devised to provide a double thermal cycle on each weld bead or on every other weld bead. When techniques such as these are utilized, the fissure count on the pad surface should be made to reflect the location of the fissures as well as the number of fissures. This separation may be used to evaluate production multipass sequences where double or multiple HAZ thermal cycling is known to occur.

Another aspect of the pad height control and surface roughness control of the top layer is that when pad preparation is undertaken, the final pad surface is a plane passing through the top layer beads only (see Figure 47). However, if excessive material is removed in pad preparation, the plane of evaluation will pass into the first layer of beads and will reflect multiple HAZ thermal cycling as well as dilution effects. In such a circumstance, the ferrite potential of the base plate would have to be considered, and thus the base plate would become an important variable in the test. Careful control is the key to a successful testing program which will truly reveal phenomena of interest.

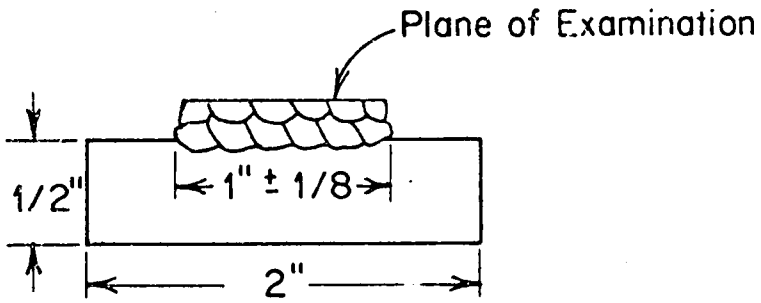

Figure 47. Weld pad cross-section showing recommended plane of examination.

Weld pad restraint. In the Fissure Bend Test the weld pad is deposited directly onto the surface of the restrained base plate and not into a groove, and the level of restraint on the weld metal would be expected to be fairly low. However, two methods of base plate fixturing were utilized and evaluated with regard to their possible effect on fissuring tendency: (1) clamping the base plates on the ends to a heavy backup (the recommended procedure), and (2) 1/4" fillet welding the base plates all-around to a heavy backup. The results of this evaluation indicate that there is no significant difference in weld metal fissuring tendency between the two types of base plate restraint, and thus restraint technique is not an important test variable. An investigator, therefore, has the option to choose either method of base plate restraint, be it clamping or welding the base plates on the ends or all-around. For convenience it is recommended that the base plates be notched on the ends and then clamped in a fixture as shown in Figure 42, page 111. This fixture can accommodate three test specimens and has proven its utility in the testing of over 40 specimens.

Surface preparation. In the Fissure Bend Test the top surface of the weld pads is prepared to provide a smooth surface to allow the detection of fissures. The weld pads are ground while they are still in the restraining fixture. Three different surface preparation techniques were used and evaluated with regard to detection of fissures. These three techniques were discussed in Chapter III, but for the reader's convenience they are again presented at this point: (1) "Milled"--milling the surface and finishing with a 0.002" milling cut, (2) "Surface

ground"--milling the surface followed by grinding with eight passes of 0.001" and finishing with four passes of 0.0005", (3) "Metallographically polished"--milling followed by grinding with eight passes of 0.001" and four passes of 0.0005" and finished by metallographically polishing the surface.

It was shown in Chapter III that when comparing these three methods on 308 and 316 weld pads, there is a significant difference in the number of fissures detected for both weld metal types (see Table II, page 95). For example, in the 308 weld metal an average of 151 fissures were found in the "metallographically polished" pads, an average of 44 fissures were found in the "surface ground" pads, and an average of only 6 fissures were found in the "milled" pads. Similar results are shown for the 316 weld pads. It was also shown that using quantitative metallographic techniques (95), the true average fissure dimension, based on the disc assumption, could be calculated. These calculated sizes are shown for both 308 and 316 weld metal as a function of pad preparation technique in Table II. It is clear from these data that the detectability of each fissure depends on the size of the fissure and on the degree of weld pad surface roughness. On the metallographically polished surfaces it is possible to detect most, if not all, of the fissures present in the plane of examination including the small fissures and short segments of larger fissures. However, relatively few of the smaller fissures are revealed on the surface of ground pads, and furthermore, only the larger fissures can be detected on the milled pads.

This detectability limit is also a function of the resolution of the type of microscope used. In the case of the polished samples, examination

was carried out at 200X since surface roughness did not preclude a high magnification being employed. The ground and milled examination was conducted at 50X magnification. It is also of interest to note that fluorescent penetrant examination of the polished samples readily revealed approximately 70 percent of the fissures. The remaining 30 percent apparently are beyond the resolution of the penetrant technique.

While the "milled" surface preparation does not reveal very many of the fissures present in the weld metal, it is felt that enough fissures are revealed to assess a ferrite-fissuring relationship on a go-no-go basis.

Plane of examination. Only those fissures intersecting the prepared surface are subject to penetrant revelation. Therefore, only a fraction of the fissures present are actually counted. The test is thus predicated on the assumption that a representative fraction (fixed in proportion to the total number) of fissures is exposed to the plane of examination both before and after bending. This assumption must not be a function of the weld metal type and composition.

The amount of weld metal milled and ground from the weld pad surface should be just sufficient to remove most of the irregularities from the pad surface in the center 4 inches (see Figure 47, page 123). Occasionally, there are a few irregularities of such a depth that to remove them would require an excessive amount of weld metal removal. These irregularities should be left on the pad surface, and their location should be documented so as not to confuse them with fissures. Also any surface irregularities on the outlying ends where fissuring evaluation

is not performed can be readily tolerated. The recommended procedure will result in the prepared plane for examination being in the top layer of weld beads where the weld metal has been relatively undiluted by the base plate. Also the interpass boundaries exposed will be those between the top layer weld beads and not those between the top and bottom layers beads, and therefore, the extent of interpass boundaries examined for fissuring will be constant from specimen to specimen. (Virtually all fissures will lie along grain boundaries near interpass boundaries.)

Etching of the prepared surface. Microetching of the milled or ground weld pad surfaces for removal of disturbed surface metal in anticipation of enhanced fissure detection is not recommended. Spurious effects are often produced by macroetching and cracks of unusual morphology (unrelated to fissuring) may occur. However, if the weld pads are metallographically polished, microetching may be desirable for revealing the bead interpass boundaries, the microstructure, fissure morphology, and the relationship of the fissures to the microstructural features.

The following etchant has been found to be highly suitable for revealing the microstructure without producing undesirable side effects and is recommended for use after metallographic polishing is accomplished:

25 gm CrO_3

133 ml Acetic Acid

7 ml H_2O

Use electrolytically with a stainless steel cathode at 7-10 volts for approximately 30 to 60 seconds.

Bending the test specimen. In the majority of weld metals tested in this study (308, 308L, 316, 316L, 309, 16-8-2), fissures are seldom detected on a ground, unbent weld pad. Even with complete metallographic preparation and observation at 200X magnification, few fissures can be found. Thus, to facilitate detection of fissures on the prepared pad surface, the weld pad surface is bent in tension to an included angle of 120° as is shown in Figure 41, page 110. Through careful examination of the surfaces of many specimens in the optical and scanning electron microscopes, it has been determined that the bending does not cause rupture of the weld metal but merely opens up fissures already present in the weld metal. Also the fissures present do not have any tendency to propagate during bending. (For a more complete discussion about the effect the bending operation has on fissure appearance, see Chapter III.)

The bend fixture shown in Figure 45, page 118, is designed with positive stops to consistently provide a reproducible bend angle of 120° included. The use of this fixture is recommended to those who undertake to employ the Fissure Bend Test. The 120° angle of bend is adequate to open for detection a sufficient number of the fissures present across the center 4 inches of the pad surface and provide a basis for evaluation of fissuring tendency. In general, it has been observed that the number of fissures detectable is proportional to the bend angle. It has also been shown that the number of fissures revealed is a function of surface preparation and the resolution of the detection technique.

Fissure determination. To provide accurate fissure detection and identification on the prepared weld pad surface, all specimens should be subjected to a twofold method of inspection: fluorescent penetrant inspection followed by binocular microscopic verification, at 40-50X, of all fluorescent indications. This method proves successful in (1) differentiating fissures from other surface defects, (2) distinguishing the presence of closely spaced fissures that were denoted by a single fluorescent indication, and (3) determining the size of fissures. A fluorescent, self-emulsifying and self-developing liquid penetrant is recommended for use in the test. When the pads are penetrant tested and inspected under a black light, the fissures fluoresce as linear indications on the pad surfaces.

Generally, the greater the magnification, the greater will be the number of fissures found, especially on a metallographically polished, etched, and bent specimen. However, for a ground or milled bent weld pad, 40-50X magnification is sufficient to resolve most of the larger exposed fissures and to provide a ferrite-fissuring relationship or a weld metal-to-weld metal fissuring comparison.

Ferrite. The Ferrite Numbers are recorded on a grid pattern over the center 4 inches of the pad as shown in Figure 44, page 116. The average value of the measurements should be used as the Ferrite Number of the weld pad. A Magne Gage or other magnetic instrument calibrated in accordance with AWS A4.2-74 (59) should be employed to measure the Ferrite Numbers. The Ferrite Numbers measured on prepared pads tend to be slightly higher than those measured on the as-welded surface by

approximately 5 percent. The increase in Ferrite Numbers between the as-welded and prepared pad surface can be the result of: (1) enhanced nitrogen pickup near the weld surface thus reducing ferrite, (2) surface roughness influencing "magnetic linkage" between the Magne Gage magnet and the deposited metal, and (3) the formation of strain-induced martensite due to machining. The total effect may at times be a combination of all three influences.

The Ferrite Numbers measured on the prepared surface where fissuring will be evaluated should be those used in deriving the ferrite-fissuring relationship. Furthermore, because the recommended surface preparation operation does not significantly change the Ferrite Number, this relationship should be accurate.

The bending operation tends to increase the Ferrite Number measured on the center 4 inches of the weld pad. This increase averaged 10-20 percent for all but one of the weld metals tested. The exception was 16-8-2 weld metal for which the average increase was 120 percent. Because bending of the test specimens increases the Ferrite Number substantially (especially for 16-8-2), it is again suggested that the best set of Ferrite Numbers to use in the data presentation is that made on the surface prepared, unbent pads.

The very nature of the bending operation induces both elastic and plastic strains in the weld pad. These strains are of a tensile nature parallel to the pad length and they vary in magnitude from the center toward the ends of the specimen. The transverse strain on the pad surface is compressive and it too varies with location. The extent of

these strains also varies according to pad height and width. To determine the magnitude and extent of these strains, a grid network was scribed on one pad surface. Grid spacing measurements made before and after bending enabled the determination of the extent of strain experienced by the weld pad surface. Figure 48 shows the longitudinal strain as a function of location on a bent specimen. Note that the maximum strain occurs at the center of a span and is approximately equal to 20 percent. Strains of this magnitude would certainly be expected to induce the formation of strain-sensitive martensite in the weld pads. The 16-8-2 material was by far the most prone in reflecting an increase in Ferrite Number as a result of this martensite formation. The Ferrite Numbers plotted on Figure 48 show an increase in ferrite level from 1 FN in the low strain areas to 5 FN in the most highly strained center section of the weld pad. Type 308, 308L, 316, 316L, 309, 318 and 347 weld metals exhibited the same tendency but were far less sensitive to strain-induced martensite formation.

It was discussed previously in Chapter III that plastic strains of this same magnitude (20 percent) have been reported to occur in the center of thick 308, 316, and 16-8-2 stainless steel weldments (91). Thus it appears that the strains experienced by Fissure Bend Test specimens are not necessarily out of line with strains experienced in actual weldments.

Closure

In light of the above discussions which amplify many of the test variables, it is anticipated that the investigator utilizing the Fissure

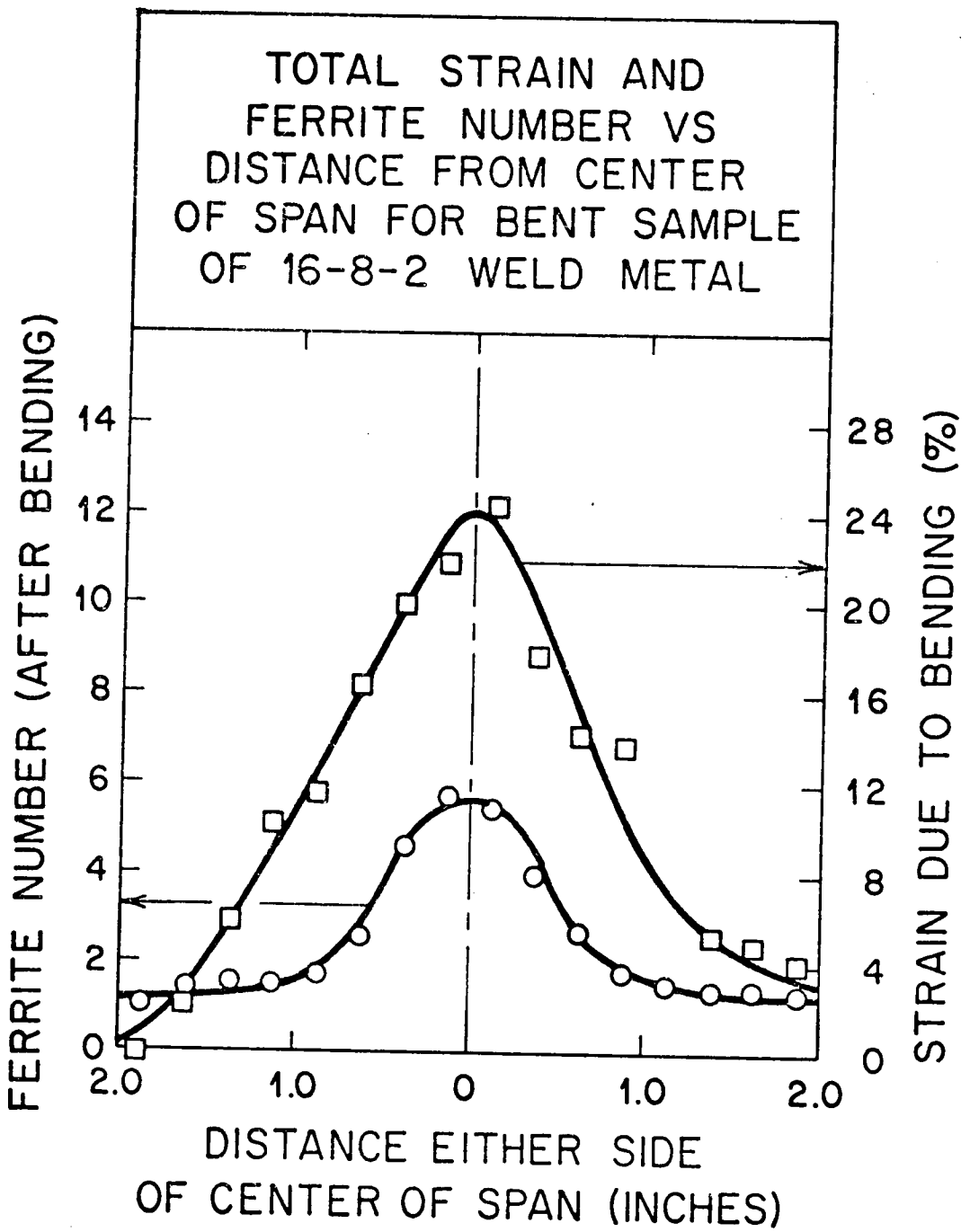

Figure 48. Total strain and Ferrite Number vs. distance from center of span for bent sample of 16-8-2 weld metal.

Bend Test technique will have an adequate basis for starting his evaluation. Undoubtedly, future investigators will uncover more aspects of significance.

The Fissure Bend Test concept should not be considered to be relegated only to the type of usage indicated in this thesis. The test has capabilities of providing both pragmatical and fundamental information. The test method may be extended quite readily to other welding processes such as SA, GTA with filler metal added, and Gas Metal-Arc (GMA). Since the test involves the actual deposition of the weld metal to be evaluated, virtually all the welding process variables can be made a part of the testing scheme and their influence on the fissuring tendency can be determined. Furthermore, while the initial evaluation of the Fissure Bend Test was carried out with austenitic stainless steels weld metals, there is no reason why the test method cannot be applied to other weld metals. It is readily apparent that this extension can be made without modification to the studying of nickel-base, cupro-nickel, aluminum, and other similarly ductile materials. The simplicity of the test lends itself also to the study of the effect of postweld thermal treatments on the fissuring sensitivity and ductility.

CHAPTER V

CONCLUSIONS

The studies of the ferrite-fissuring relationship and of the nature and morphology of fissures in austenitic stainless steel weld metals has yielded conclusions that may be categorized in the following three areas.

Fissure Bend Test Results

1. By utilization of the Fissure Bend Test method, the ferrite-fissuring relationship for austenitic stainless steels can be determined, thus permitting a ranking of these weld metals as to their fissuring tendency. A ranking of the eight weld metals tested is shown in Table I, page 34. At low ferrite levels 16-8-2 weld metal was the least prone to fissuring of all weld metals tested while 347 was the most prone to fissuring.

2. The fissures observed in this study were found along grain boundaries in ferrite-free areas in HAZs.

3. Austenitic stainless steel weld metals when subjected to a significant amount of plastic deformation tend to form a ferromagnetic constituent (strain-induced martensite). Weld metal 16-8-2 was the most prone to this occurrence.

Basic Fissuring Mechanisms

1. Multiple HAZ thermal cycling plays a dominant role in the fissuring of multipass austenitic stainless weldments. The multiple HAZ

thermal cycling increased the fissuring tendency of 308 and 316 weld metals at low ferrite levels (0.4 FN), of 16-8-2 weld metal at a ferrite level of 1.5 FN, and of 316 weld metal at higher ferrite levels (3.0 FN to 3.2 FN). However, 308 weld metal at ferrite levels of 2.5 FN to 3.1 FN appears insensitive to this increased fissuring tendency.

2. The factors leading to the enhanced fissuring propensities in the multiple HAZ experience are the accumulation of strain attendant upon multiple thermal cycling and the continued degradation of the properties in a grain boundary microstructural region either by enhanced segregation or liquation of solidification-induced segregation.

3. The overall fissuring temperature range was defined as extending from the bulk solidus temperature to 1630°F with the majority of the fissures forming in the 2400°F to 1950°F range.

Fissure Size

1. Both the number and size of fissures decreased with increasing ferrite content for all weld metals tested. For 308, 308L, 316, 316L, 309, and 16-8-2 weld metals, the fissures very rarely exceeded 1/16 inch in length and the majority were less than 1/32 inch in length. At lower ferrite levels (0 FN to 2 FN) approximately 5 percent of the fissures in the 318 weld metal and 10 percent of the fissures in the 347 weld metal exceeded 1/16 inch in length.

2. The reason for both the greater fissure size and number found in the columbium-bearing deposits (318 and 347) as opposed to non-columbium deposits (308, 308L, 316, and 316L) at similar ferrite levels is apparently due to the columbium content alone. This conclusion is

fortified by the fact that the core wires were identical for 308, 308L, and 347 and for 316, 316L, and 318 respectively, and thus the residual element levels are virtually identical.

3. The fissures observed on metallographically polished and etched 308 and 316 weld metal pads correlate with those found in production 316 weldments with regard to location and appearance. However, the average fissure size is somewhat smaller, being 0.004 inches to 0.005 inches in length.

4. Fissures do not propagate with applied strain (up to 20 percent plastic strain), but rather the fissure tips become blunted as the bending strain increases.

CHAPTER VI

FUTURE WORK

This initial utilization of the Fissure Bend Test technique in investigating the fissuring technique of austenitic stainless steel weld metals has shown the need for expanded research in related areas. Included are:

1. Applying this technique to other welding processes, such as GTA, GMA, and Plasma Arc. The results of these studies could be compared to those obtained from the SMA deposits.
2. The influence of change in welding technique such as energy input, weave or stringer bead, and preheat.
3. The influence of overlapping HAZ thermal cycling on the minimum amount of ferrite to eliminate fissuring in each of the weld metals tested.
4. The effect of varying selected elements in the electrode and weld metal chemistry to determine their influence on fissuring tendency.
5. Selected electrode lots should be evaluated by other fissuring or cracking tests and the results compared to the Fissure Bend Test results.
6. To evaluate, via hot ductility tests, the effect of multiple thermal cycles on the inherent ductility as a function of weld metal type and Ferrite Number.

LIST OF REFERENCES

LIST OF REFERENCES

1. AEC Regulatory Guide 1.31, "Control of Stainless Steel Welding," June 1973 and Position Statement of April 11, 1974.

2. Bochvar, A. A., and Z. A. Siderskaya, "Failure of Castings Caused by Shrinkage Stresses During Crystallization, as Related to Composition," Izvest. Akad., Nauk SSSR, Otd. Tekhn. Nauk, No. 3 (1947), Brutcher Trans. No. 3806.

3. Pumphrey, W. I., and P. H. Jennings, "A Consideration of the Nature of Brittleness at Temperature above the Solidus in Castings and Welds in Aluminum Alloys," J. Inst. Met., 75 (1948).

4. Pumphrey, W. I., and J. V. Lyons, "Cracking During the Casting and Welding of the More Common Binary Aluminum Alloys," J. Inst. Met., 74 (1948).

5. Medovar, B. I., "On the Nature of Weld Hot Cracking," Avtom. Svarka, 7 (4) (1954), Brutcher Trans. No. 3400.

6. Medovar, B. I., "Effect of Solubility of Alloying Elements Upon Weld Hot Cracking," Avtom. Svarka, 8 (2) (1955), Brutcher Trans. No. 3554.

7. Medovar, B. I., "Influence of Hydrogen, Oxygen and Nitrogen Upon Formation of Hot Cracks in 18-8 Steel Welds," Pts. I, II and III, Avtom. Svarka, 6 (4) (1953), Brutcher Trans. Nos. 3369, 3370, 3371.

8. Pellini, W. S., "Strain Theory of Hot Tearing," Foundry, 80 (11) (1952).

9. Apblett, W. R., and W. S. Pellini, "Factors Which Influence Weld Hot Cracking," Welding J., 33 (2) (1954).

10. Borland, J. C., "Generalized Theory of Super-Solidus Cracking in Welds (and Castings)," Brit. Welding J., 7 (8) (1960).

11. Borland, J. C., "Hot Cracking in Welds," Brit. Welding J., 7 (9), (1960).

12. Borland, J. C., and R. N. Younger, "Some Aspects of Cracking in Welded Cr-Ni Austenitic Steels," Brit. Welding J., 7 (1) (1960).

13. Borland, J. C., "Suggested Explanation of Hot Cracking in Mild and Low Alloy Steel Welds," Brit. Welding J., 8 (11) (1961).

14. Movchan, B. A., and L. A. Poznyak, "On the Nature of Intergranular Cracking of Welds at High Temperatures," Avtom. Svarka, 7 (6) (1954), Brutcher Trans. No. 3572.

15. Movchan, B. A., "Development, Structure and Some Properties of the Crystallite Boundaries in Cast Metals and Alloys," Izvest. Akad. Nauk SSSR, OTN, Met i toplivo, 5 (1959), Brutcher Trans. No. 5663.

16. Movchan, B. A., "The Relationship Between Physical Microhetrogeneity and Hot Cracking in Welds," Svar. Proiz, No. 4 (1962).

17. Prokhorov, N. N., "Weld Hot Cracking," Mashgiz (1952).

18. Baikov, A. A., "Temperature Range in Which Hot Cracks Developed When Single Phase Nickel Alloys Are Fusion Welded," Svar. Proiz, No. 4 (1962).

19. Toropov, V. A., "On the Mechanism of Hot Cracking of Welds," Metallovedenie I Obrabotka Metallov, 7 (1957), Brutcher Trans. No. 3982.

20. Toropov, V. A., "Role of the Grain Boundary Substance in the Hot Cracking of Welds," Metallovedenie I Obrabotka Metallov, 2 (4) (1956), Brutcher Trans. No. 3809.

21. Erokhin, A. A., and O. M. Kuznetsov, "Improving the Capacity of Weld Metal for Resisting Hot Cracking," Avtom. Svarka, 7 (5) (1964).

22. Gavrllyuk, V. S., and M. M. Popova, "Error in the Theory of the Technological Strength of Metals While Crystallizing," Svar. Proiz, No. 4 (1962).

23. Sopher, R. P., "Effects of Chemical Composition on Cracking Resistance of High-Strength-Steel Weld Metals," Welding J., 37 (11) (1958).

24. Terry, C. A., and W. T. Tyler, "Inert-Gas Tungsten-Arc Welding SAE 4130 Steel Sheet," Welding and Metal Fabrication, 26 (3) (1958).

25. Savage, W. F., et al., "Weld-Metal Solidification Mechanics," Welding J., 44 (4) (1965).

26. Savage, W. F., and B. M. Krantz, "An Investigation of Hot Cracking in Hastelloy X," Welding J., 45 (1) (1966).

27. Dudley, R. H., "An Investigation of the Constitutional Liquation Hypothesis," Ph.D. Thesis, Rensselaer Polytechnic Institute, January 1962.

28. Aronson, A. H., "Constitutional Liquation in the Iron-Iron Carbide System," Master's Thesis, Rensselaer Polytechnic Institute, May 1963.

29. Owczarski, W. A., and C. P. Sullivan, "A Microstructure Study in a Welded Superalloy," Welding J., 43 (9) (1964).

30. Russiyan, A. V., and A. A. Sakharnov, "Investigation into the Resistance of Alloys to Hot Cracking in the Heat-Affected Zone," Avtom. Svarka, 17 (9) (1964).

31. Younger, R. N., et al., "Heat Affected Zone Cracking of Two Austenitic Steels During Welding," Brit. Welding J., 8 (12) (1961).

32. Younger, R. N., and R. G. Baker, "Heat-Affected Zone Cracking in Welded Austenitic Steels During Heat Treatment," Brit. Welding J., 8 (12) (1961).

33. Jones, P. W., "Hot Cracking of Mild Steel Welds," Brit. Welding J., 6 (6) (1959).

34. Jones, P. W., "An Investigation of the Hot Ductility of High-Temperature Alloys," Welding J., 34 (4) (1955).

35. Nippes, E. F., et al., "An Investigation of the Hot Ductility of High-Temperature Alloys," Welding J., 34 (4) (1955).

36. Medovar, B. I., et al., "Intergranular Cracks in the Heat-Affected Zone When Welding Austenitic Steels and Alloys," Svar. Proiz, No. 4 (1962).

37. Yakushin, B. F., "Development of Hot Cracks in the Heat-Affected Zone During Welding," Svar. Proiz, No. 4 (1962).

38. Medovar, B. I., "The Mechanism of Formation of Intercrystalline Cracks in the Heat-Affected Zone in Fusion Welding," Zhur. Takh. Fiz., 27 (1957).

39. Scherer, R., G. Riedrich, and H. Hougardy, U. S. Patent 2,240,872, May 6, 1941, "Welding Rod."

40. Pugh, J. W., and J. D. Nisbet, "A Study of the Iron-Chromium-Nickel System," Trans. Metals Branch, American Inst. Mining and Metallurgical Engineers, 50 (2) (1950).

41. Masumoto, I., K. Tamaki, and M. Katsuna, "Hot Cracking of Austenitic Stainless Steel Weld Metal," J. Japanese Welding Society, 41 (11) (1972), Brutcher Trans. No. 8965.

42. Gunia, R., and G. Ratz, "The Measurement of Delta Ferrite in Austenitic Stainless Steels," WRC Bulletin No. 132, August 1968.

43. Goodwin, G., N. Cole, and G. Slaughter, "A Study of Ferrite Morphology in Austenitic Stainless Steel Weldments," Welding J., 51 (9) (1972).

44. DeLong, W. T., "Ferrite in Austenitic Stainless Steel Weld Metal," Welding J., 53 (7) (1974).

45. Hull, F. C., "Effect of Delta Ferrite on the Hot Cracking of Stainless Steel," Welding J., 46 (9) (1967).

46. Marshall, W. K., "A Note on the Relationship Between Chemical Composition and Hot Cracking in Mild and Alloy Steels," Brit. Welding J., 7 (12) (1960).

47. Curran, R. M., and A. W. Rankin, "Welding Type 347 Stainless Steel for 1100°F Turbine Operation," Welding J., 34 (3) (1955).

48. Rollason, E. C., and M. C. Bystram, "Hot Cracking of Austenitic Welds with Special Reference to 18/3/1 Cr-Ni-Nb Alloy," J. Iron and Steel Institute, 169 (12) (1951).

49. Guessier, A., and R. Castro, "Etude Experimentale des Criques de Solidification dans les Aciers," Revue de Metallurgie, 57 (2) (1960).

50. Kauhausen, E., "The Welding of Steels for High Temperature Purposes," Welding J., 35 (7) (1956).

51. Thielsch, H., "Physical Metallurgy of Austenitic Stainless Steels," Welding J., 29 (11) (1950).

52. Lashko, N. F., and S. V. Lashko, "The Role of Carbide Phases and Primary Ferrite in Formation of Crystallization Cracks in Welded Austenitic Steel," Avtom. Svarka, 11 (9) (1958).

53. Sheddon, J. W., and W. I. Pumphrey, "Recent Developments in the Fusion Welding of Iron and Steel," Metallurgica, 48 (2) (1953).

54. Schaeffler, A. L., "Constitution Diagram for Stainless Steel Weld Metal," Metal Progress, 56 (5) (1949).

55. DeLong, W. T., G. A. Ostrum, and E. R. Szumachowski, "Measurement and Calculation of Ferrite in Stainless Steel Weld Metal," Welding J., 35 (11) (1956).

56. Long, C. J., and W. T. DeLong, "The Ferrite Content of Austenitic Stainless Steel Weld Metal," Welding J., 52 (7) (1973).

57. Stalmasek, E., "Measurement of Ferrite Content in Austenitic Stainless Steel Weld Metal Yielding Internationally Compatible Results," International Institute of Welding--Commission No. 2, "Arc Welding," Summary Report of Work Done by IIW Commission 2 in 1963-1973.

58. DeLong, W. T., "Calibration Procedure for Instruments to Measure the Delta Ferrite Content of Austenitic Stainless Steel Weld Metal," Welding J., 52 (2) (1973).

59. AWS A4.2-74, "Standard Procedures for Calibrating Magnetic Instruments to Measure the Delta Ferrite Content of Austenitic Stainless Steel Weld Metal," April 19, 1974.

60. Welding Research Council Report, "WRC Development Program for Standard Weld Metal Sample Preparation Procedures, Phase I Preliminary Results," September 8, 1973.

61. Edmonds, D. P., Oak Ridge National Laboratory, Private Communications, January 1975.

62. King, B. L., "Weld Metal and Heat Affected Zone Hot Cracking in Wrought Austenitic Stainless Steels," BWRA Report C 139/A/2/65, February 1966.

63. Senda, T., et al., "Fundamental Investigations on Solidification Crack Susceptibility for Weld Metal with Trans-Varestraint Test," Welding Research Abroad, 18 (6) (1972).

64. Arata, Y., et al., "Varestraint Test for Solidification Crack Susceptibility in Weld Metal of Austenitic Stainless Steels," Trans. Japan Welding Research Institute, 3 (1) (1974).

65. Poole, L. K., "The Incidence of Cracking in Weld Type 347 Steels," Welding J., 32 (8) (1953).

66. Puzak, P. P., W. R. Apblett, and W. S. Pellini, "Hot Cracking of Stainless Steel Weldments," Welding J., 35 (1) (1956).

67. Puzak, P. P., and H. Rischall, "Further Studies on Stainless Steel Hot Cracking," Welding J., 36 (2) (1957).

68. Fairchild, F. P., "Eight Years of Experience with Austenitic Steel Piping Materials at Elevated Steam Conditions," Trans. of ASME, 79 (8) (1957).

69. Curran, R. M., and A. W. Rankin, "Austenitic Steels in High Temperature Steam Piping," Trans. of ASME, 79 (8) (1957).

70. Younger, R. N., and R. G. Baker, "Heat Affected Zone Cracking in Welded High-Temperature Austenitic Steels," J. Iron and Steel Institute, 196 (10) (1960).

71. Christoffel, R. J., "Cracking in Type 347 Heat Affected Zone During Stress Relaxation," Welding J., 41 (6) (1962).

72. Shackleton, D. N., "High Temperature Cracking Mechanism in the Heat Affected Zone of 25 Cr:20 Ni Stainless Steel Welds," BWRA Report M/47/69, October 1969.

73. Cordea, J. N., R. M. Evans, and D. C. Martin, "Investigation to Determine Causes of Fissuring in Stainless Steel and Nickel-Base Alloy Weld Metals," Technical Documentary Report No. ASD-TDR-62-317, Battelle Memorial Institute, June 1962.

74. Haddrill, D. M., and R. G. Baker, "Microcracking in Austenitic Weld Metal," Brit. Welding J., 13 (1) (1966).

75. Fredriks, H., and L. J. van der Toorn, "Hot Cracking in Austenitic Stainless Steel Weld Deposits," Brit. Welding J., 15 (4) (1968).

76. Lundin, C. D., "Welding Defects, Their Origin and Effect," II Inter-american Conference on Materials Technology, Mexico City, Mexico, August 1970.

77. Honeycombe, J., and T. G. Gooch, "Microcracking in Fully Austenitic Stainless Steel Weld Metal," Metal Construction and Brit. Welding J., 2 (9) (1970).

78. Honeycombe, J., and T. G. Gooch, "Effect of Manganese on Cracking and Corrosion Behavior of Fully Austenitic Stainless Steel Weld Metals," Metal Construction and Brit. Welding J., 4 (12) (1972).

79. Honeycombe, J., and T. G. Gooch, "Microcracking in Fully Austenitic Stainless Steel Weld Metal," Metal Construction and Brit. Welding J., 7 (3) (1975).

80. Tamura, H., and T. Watanabe, "Mechanism of Liquation Cracking in Weld Heat Affected Zone of Austenitic Stainless Steels," Welding Research Abroad, 20 (6) (1974).

81. Burghard, H. C., et al., "An Investigation of the Properties of Type 316 Stainless Steel Weldments Containing Austenitic Micro-fissures," SWRI Topical Report No. 1, Project 17-3078, August 15, 1971.

82. Buchhoit, R. D., et al., "Laboratory Studies of Type 316 Stainless Steel Weld Metal from Maine Yankee Reactor Coolant System," Battelle Final Report, September 17, 1971.

83. Thielsch, H., "Examination of Type 316 Stainless Steel Weld Deposit for Microfissuring and Delta Ferrite Contents for the Oconee Nuclear Power Station, Duke Power Company," Report No. 1057, December 23, 1972.

84. Truman, R. J., and H. W. Kirkby, "Some Ductility Aspects of 18-12-1 Nb Steel," J. Iron and Steel Institute, 196 (10) (1960).

85. Irvine, K. J., J. D. Murray, and F. B. Pickering, "The Effect of Heat-Treatment and Microstructure on the High Temperature Ductility of 18 Cr-12 Ni-1 Nb Steels," J. Iron and Steel Institute, 196 (10) (1960).

86. Hemsworth, B., et al., "Classification and Definition of High Temperature Welding Cracks in Alloys," Metal Construction and Brit. Welding J., 1 (2) (1969).

87. Lundin, C. D., and R. K. Bennett, "Scanning Electron Microscopy of Fractures in Welded Structures," IMS Proceedings (1971).

88. Williams, N. T., et al., "Stresses and Strains in Thick Austenitic Steel Plates During Welding," Proceedings of the Second Commonwealth Welding Conference, The Welding Institute, London, England, 1965.

89. Zhitnikov, N. P., and V. N. Zemzin, "Brittle Failure Tendency of Chromium-Nickel Steel Welds," Svar. Proiz, No. 10 (1970).

90. Shron, R. Z., "Influence of the Mechanical Heterogeneity of Welded Joints in Austenitic Steels on Their Susceptibility to Local Failure," Svar. Proiz, No. 4 (1965).

91. Brooks, C. R., and J. E. Spruiell, University of Tennessee, Private Communications, August 1974.

92. Honeycombe, J., and T. G. Gooch, "Effect of Microcracks on Mechanical Properties of Austenitic Stainless-Steel Weld Metals," Metal Construction and Brit. Welding J., 5 (4) (1973).

93. Savage, W. F., and C. D. Lundin, "The Varestraint Test," Welding J., 44 (10) (1965).

94. Savage, W. F., and C. D. Lundin, "Application of the Varestraint Technique to the Study of Weldability," Welding J., 45 (11) (1966).

95. DeHoff, R. T., and F. N Rhines, "Quantitative Microscopy," McGraw-Hill, New York (1968).

96. Lundin, C. D., et al., Unpublished research at The University of Tennessee, May 1975.

97. Shorshorov, N. K., and Y. V. Sokolov, "The Temperature Range in Which Hot Cracks Develop When Single Phase Nickel Alloys are Fusion Welded," Avtom. Svarka, 16 (4) (1963).

98. Lundin, C. D., Unpublished research at Rensselaer Polytechnic Institute, 1968.

99. Kammer, P. A., et al., "Cracking in High Strength Steel Weldments--A Critical Review," DMIC Report 197, February 7, 1964.

100. DeLong, W. T., Teledyne McKay Corporation, Private Communications, January 1975.

101. Ramsey, P. W., A. O. Smith Corporation, Private Communications, March 1975.

APPENDIXES

APPENDIX A

1. Chemetron Corporation
2. Teledyne McKay Corporation
3. Westinghouse Electric Corporation
4. Babcock and Wilcox Corporation (Barberton)
5. Arcos Corporation
6. Combustion Engineering, Inc.
7. General Electric Corporation
8. Chicago Bridge and Iron Company
9. Babcock and Wilcox Corporation (Alliance)
10. Oak Ridge National Laboratory
11. Lincoln Electric Company
12. Airco Welding Products Corporation

APPENDIX B

TABLE III

WELD METAL ANALYSES
(Percent)

Weld Metal	C	Mn	Si	P	S	Cr	Ni	Mo	N	Cb	Co	Measured FN	Calculated FN
308-A	0.052	1.64	0.35	--	--	18.18	10.95	--	--	--	--	0.2	--
308-B	0.057	1.66	0.35	--	--	18.04	10.25	--	--	--	--	2.2	--
308-C	0.049	1.70	0.36	--	--	19.15	10.35	--	--	--	--	4.0	--
308-D	0.060	1.65	0.37	--	--	19.30	9.89	--	--	--	--	6.8	--
308L-A	0.020	1.62	0.38	--	--	18.40	10.80	--	--	--	--	0.5	--
308L-B	0.024	1.64	0.37	--	--	18.48	10.97	--	--	--	--	1.9	--
308L-C	0.025	1.55	0.32	--	--	19.05	10.05	--	--	--	--	4.7	--
308L-D	0.022	1.66	0.41	--	--	19.09	10.32	--	--	--	--	6.0	--
316-A	0.065	1.92	0.46	0.016	0.008	17.79	12.30	2.22	0.047[1]	--	--	0.3	0.0
316-B	0.064	1.87	0.46	0.014	0.010	18.28	11.94	2.15	0.047[1]	--	--	1.1	2.0
316-C	0.069	1.92	0.43	0.017	0.008	18.94	12.47	2.10	0.047[1]	--	--	2.2	2.2
316-D	0.069	1.96	0.52	0.014	0.010	19.38	11.78	2.12	0.047[1]	--	--	5.8	6.0
316L-A	0.035	1.85	0.40	0.008	0.015	17.88	13.07	2.15	0.047[1]	--	--	0.2	0.0
316L-B	0.036	1.97	0.42	0.014	0.010	17.45	12.10	2.20	0.047[1]	--	--	0.9	1.0
316L-C	0.036	1.87	0.47	0.016	0.008	18.23	12.15	2.2	0.047[1]	--	--	2.5	3.3
316L-D	0.037	1.87	0.46	0.015	0.010	18.60	11.64	2.12	0.047[1]	--	--	5.7	6.0
309-A	0.095	1.51	0.30	0.012	0.008	22.30	12.75	0.08	0.081	--	0.039	0.0	--
309-B	0.10	1.41	0.27	0.012	0.008	22.60	12.60	0.10	0.071	--	ND	2.8	--
309-C	0.10	1.48	ND	ND	ND	23.40	12.24	ND	0.079	--	ND	5.1	--
309-D	0.10	1.49	ND	ND	ND	23.75	12.05	ND	ND	--	ND	7.3	--
318-A	0.055	2.00	0.49	0.014	0.010	16.88	13.46	2.06	0.047[1]	0.51	--	0.0	0.0
318-B	0.052	1.98	0.52	0.014	0.010	17.11	12.11	2.17	0.047[1]	0.49	--	0.8	--
318-C	0.053	2.02	0.52	0.015	0.008	18.17	11.83	2.11	0.047[1]	0.50	--	4.3	3.6
318-D	0.055	2.01	0.55	0.014	0.010	18.82	11.72	2.17	0.047[1]	0.49	--	6.0	6.4
347-A	0.055	1.75	0.48	--	--	18.00	11.01	--	--	0.58	--	0.5	--
347-B	0.060	1.88	0.47	--	--	18.40	10.66	--	--	0.63	--	2.6	--
347-C	0.057	1.86	0.50	--	--	18.95	10.13	--	--	0.66	--	4.8	--
347-D	0.066	1.90	0.49	--	--	19.57	9.86	--	--	0.62	--	6.5	--
16-8-2 Lot 1	0.055	1.69	0.42	0.028	0.015	15.18	7.95	1.56	--	--	0.066	1.2	--
16-8-2 Lot 2	0.065	1.60	0.38	0.025	0.014	15.20	7.92	1.50	--	--	0.078	0.7	--

[1]Calculated.

TABLE IV

CORE WIRE ANALYSES
(Percent)

	C	Mn	Si	P	S	Cr	Ni	Mo	N	Cu	Co	Al	Sn	Pb	Ag
Core wire for 308, 308L, 347	0.016	1.69	0.29	0.021	0.007	19.66	9.88	0.23	--	--	--	--	--	--	--
Core wire for 316, 316L, 318	0.023	1.15	0.46	0.015	0.015	19.55	12.27	2.33	0.031	0.07	0.11	0.023	0.008	<0.001	<0.001
Core wire for 309	0.020	1.64	0.35	0.009	0.009	24.32	12.72	0.08	0.065	--	0.032	--	--	--	--

APPENDIX C

As a part of the GTA remelt multiple thermal cycling study, specimens were produced with a variety of energy inputs and the Ferrite Numbers were recorded. The initial SMA pad surface had a ferrite level of 0.6 FN. When it was remelted with an energy input and travel speed identical with the SMA conditions (16 KJ/in), the Ferrite Number of the GTA remelt beads was identical. However, when travel speed and energy input were varied to span the range from 6-60 KJ/in, the ferrite level varied from 0.5 FN to 1.4 FN. These data are shown as a function of both energy input and travel speed in Figures 49 and 50. Notice that for both figures, a straight line could be drawn to connect the data. Also a linear equation for the straight line in each figure is shown. However, not enough work was done to separate the travel speed and energy input parameters. The data suggest that the solidification rate is important because the Ferrite Number is a function of $\frac{1}{TS}$, much in the same manner that some solidification modes are ascribed the $G/\sqrt{R}$ parameter. The increase in Ferrite Number with increasing energy input appears in direct contradiction with some investigators but agrees with that presented by others (57).

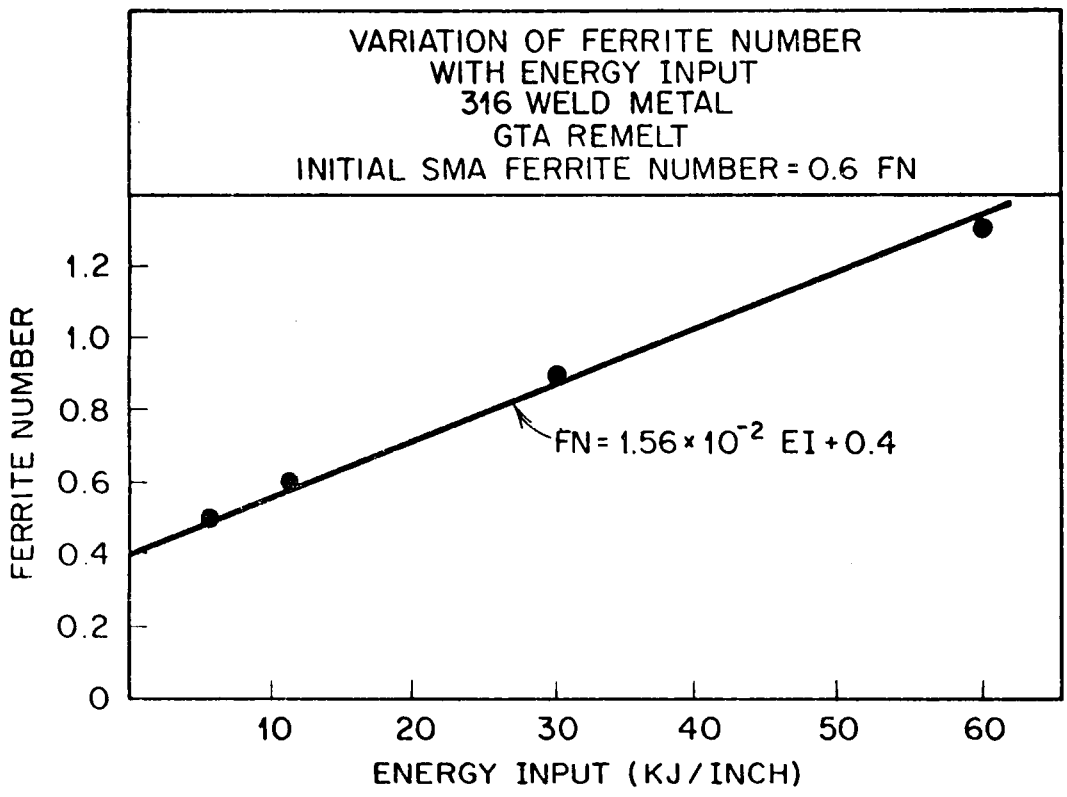

Figure 49. Variation of Ferrite Number with energy input, 316 weld metal, GTA remelt.

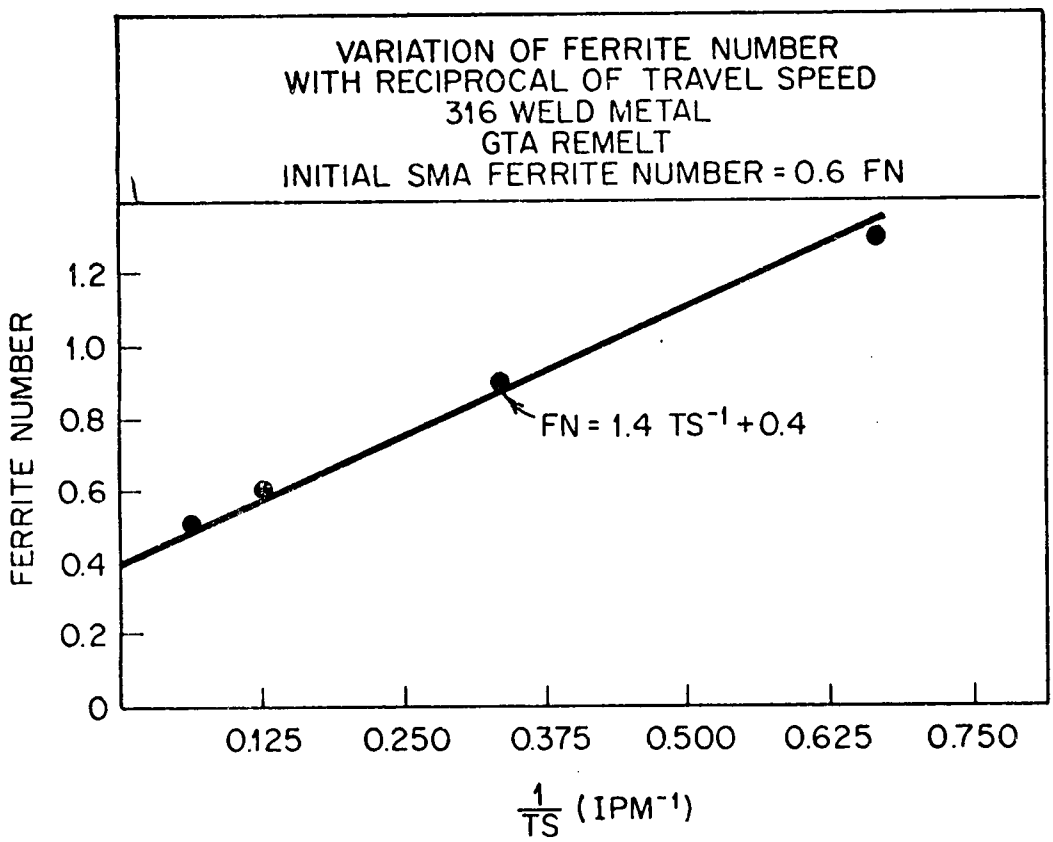

Figure 50. Variation of Ferrite Number with reciprocal of travel speed, 316 weld metal, GTA remelt.

VITA

Daniel Frank Spond was born in Detroit, Michigan, on November 13, 1947. He attended elementary schools in Warren, Michigan, and Valley Center, Michigan, and high school in Nashville, Tennessee. In September 1965 he entered Vanderbilt University and received a Bachelor of Engineering in Material Science Engineering in June 1969. From June 1969 to September 1973, he served as an officer in the U. S. Marine Corps.

In September 1973 Mr. Spond entered The University of Tennessee and began study toward a Master's degree. He accepted a research assistantship in January 1974 and received a Master of Science degree with a major in Metallurgical Engineering in December 1975. He is a member of the American Welding Society, American Society for Metals, and Sigma Xi.

He is married to the former Mary Hart of Little Rock, Arkansas.